On Problems Related To Galaxy Formation

Dissertation
zur
Erlangung des Doktorgrades (Dr. rer. nat.)
der
Mathematisch-Naturwissenschaftlichen Fakultät
der
Rheinischen Friedrich-Wilhelms-Universität Bonn

vorgelegt von
Ahmed Hasan Abdullah
aus
Baghdad

Bonn 2016

Angefertigt mit Genehmigung der Mathematisch-Naturwissenschaftlichen Fakultät der Rheinischen Friedrich-Wilhelms-Universität Bonn

1. Gutachter: Prof. Dr. P. Kroupa
2. Gutachterin: Dr. Maria Massi

Tag der Promotion: 11.04.2016
Erscheinungsjahr: 2016

To My Parents

Erklärung

Hiermit versichere ich, die vorgelegte Arbeit - abgesehen von den ausdrücklich angegebenen Hilfsmitteln -persönlich, selbstständig und ohne die Benutzung anderer als der angegebenen Hilfsmittel angefertigt zu haben. Die aus anderen Quellen direkt und indirekt verwendeten Daten und Konzepte sind unter der Angabe der Quelle kenntlich gemacht. Weder die vorgelegte Arbeit noch eine ähnliche Arbeit sind bereits anderweitig als Dissertation eingereicht worden und von mir wurden zuvor keine Promotionsversuche unternommen. Für die Erstellung der vorgelegten Arbeit wurde keine fremde Hilfe, insbesondere keine entgeltliche Hilfe von Vermittlungs-, Beratungsdiensten oder Ähnlichem, in Anspruch genommen.

Bonn, den _____ _____

Ahmed Abdullah

Acknowledgements

I owe thanks to many people for their support and guidance which gave me a chance to complete this thesis. I am truly indebted and thankful for their support.

First and foremost, I would like to express my deep and sincere gratitude to my advisor, Prof. Dr. Pavel Kroupa, for the continuous support of my study and research, and his motivation, encouragement and patient supervision. It was an honor to have a supervisor who was so patient and willing to help .

I would also like to express my gratitude to Dr. Ole Marggraf, Dr. Andrea Dieball, Dr. Andreas H.W.Kupper, Matthias Kruckow and Lucia Klarmann for support, many useful discussions and suggestions throughout my PhD years.

I want to thank the computer department, specially Dr. Ole Marggraf and Andreas Bödewig for providing me with their kind technical support.

We acknowledge the use of the HyperLeda database available at http://leda.univ-lyon1.fr and the publicly available data from W. E. Harris (http://physwww.mcmaster.ca/harris/Databases.html).

In addition, I would like to give my gratitude to all my friends and colleagues in the the Argelander-Institute for Astronomy (AIfA) at the University of Bonn. In particular, I would like to thank Dr. Andrea Stolte, Behnam Javanmardi, Nicolas Gonzalez Jimenez, Michael Brockamp, Marcel Pawlowski, Christine Schulz, Seungkyung Oh, Yasna Ordenes, Ingo Thies, Fabian Lüghausen, Michael Marks, Armin Rasekh, Joerg Dabringhausen, Sambaran Banerjee, Xufen Wu, Claudia Bruens , Patrick Neunteufel, Patrick Lieberz, Sandra Unruh, Zeinab Shafiee.

A special acknowledgement is due to the Deutscher Akademischer Austauschdienst (DAAD) and Ministry of Higher Education and Scientific Research of Iraq (MoHESR), for financial support during the entire course of study for my PhD.

In addition, I would like to thank Dr. Katja Petereit for supporting Iraqi students, and my host family in Bonn, Maria and Astrid Vochte, who provided me the opportunity to peak into Germany's culture and helped to improve my German language skills

I can not fail to mention, however, my debt to all the members of DAAD-Freundeskreis and the international office, especially Sandra Groeger, M.A.

Last but not the least, my deepest gratitude goes to my family: my father, Hasan Abdullah, for encouragement and supporting me spiritually in every way possible throughout my life.

Abstract

The main idea of the underlying PhD study is to trace the history of the assembly of galaxies and of their subsequent evolution. We approach this issue in two ways: 1) by studying galaxy spin and 2) by studying the oldest stellar population in a given galaxy (i.e. globular clusters).

In the first part of this work, we investigated the relation between the galaxy spin and filaments. The relative orientation of galaxies with respect to their large-scale environment can provide crucial evidence for the formation and evolution of galaxies that follow the various scenarios proposed for the origin of galaxies. To perform our study, we made use of a sample of 1843 spiral galaxies at a redshift z$\approx$ 0.0055 taken from the HYPERLEDA (Hyper-linked Extragalactic Databases and Archives). The ultimate goal for the first part was to calculate the angle θ between the projected spin vector of a spiral galaxy and the projected host filament (long strings of galaxies). The galaxy spin vector is derived from the position angle (PA) of the long axis of a galaxy image. The filaments are represented by the best-fit straight lines using linear regression and various statistical methods to test the fit quality. We found no significant statistical evidence for an alignment of galaxy spin vectors with respect to their hosting filaments. The results are in agreement with hierarchical galaxy formation theory which predicts random directions of galaxy spin vectors.

In the second part of this PhD study, we investigate the properties of globular clusters and of the hosting galaxy. Globular clusters (GC) are important objects for tracing the early evolution of a galaxy. In this thesis, we study the relation between the properties of globular cluster systems -as quantified by the GC specific frequency (S_N)- and the properties of their host galaxies. We support the explanation for the relation between S_N and galaxy mass through tidal erosion.

In order to understand the origin of the relation between the GC specific frequency (S_N) and host galaxy mass, we devise a theoretical model for the specific frequency ($S_{N,th}$). GC erosion is considered to be an important aspect for shaping this relation, since observations show that galaxies with low baryonic densities have a higher S_N, while high density galaxies have a smaller number of GCs. We construct a model depending on the minimum star cluster mass ($M_{ecl,min}$), the slope of the power-law embedded cluster mass function (β), and the relation between the star formation rate (SFR) and the maximum star cluster mass ($M_{ecl,max}$). We find agreement between the primordial value of the specific frequency (S_{Ni}) and our model for β between 1.5 and 2.5 with $M_{ecl,min} \leqslant 10^4 M_\odot$. We also test the relation between the SFR and $M_{ecl,max}$ at higher SFR than previously known.

Zusammenfassung

Der Hauptgedanke dieser Doktorarbeit ist die Geschichte der Galaxienentstehung und ihrer nachfolgenden Entwicklung. Wir betrachten das Thema unter zwei Aspekten: untersuchung 1) des Galaxie-Spin und 2) der ältesten stellaren Populationen in einer Galaxie (z.B. Kugelsternhaufen).
Im ersten Teil dieser Arbeit haben wir die Relation zwischen Galaxie-Spin und -Filamenten betrachtet. Die relative Ausrichtung der Galaxien zu ihren umgebenden großräumigen Strukturen gibt entscheidende Hinweise für die Entstehung and Evolution von Galaxien, die mit verschiedenen Szenarien zum Ursprung der Galaxien beschrieben werden können. Um die Studie durchzuführen haben wir 1.843 Spiralgalaxien mit einer Rotverschiebung von $z \approx 0.0055$ aus der HYPERLEDA-Datenbank (Hyper-linked Extragalactic Databases and Archives) benutzt. Das entscheidende Ziel für den ersten Teil der Arbeit war den Winkel θ zwischen projizierten Spinvektor von Spiralgalaxien und den projizierten umgebendenen Filamenten (längliche Ausläufer der Galaxien) zu berechnen. Der galaktische Spinvektor kann vom Positionswinkel (PA) der langen Achse der Galaxien-abbildung abgeleitet werden. Die Filamente werden von optimal gefitten Geraden repräsentiert, dafür wird eine lineare Regression sowie verschiedene statistische Methoden für die Anpassungsgüte verwendet. Als Resultat konnte kein statistisch signifikanter Nachweis für die Übereinstimmung von Galaxien-Spinvektoren zu ihrem umgebenen Filamenten gefunden werden. Dieses Ergebnis stimmt mit der hierarchischen Galaxienformationstheorie überein, welche zufällige Richtungen des Galaxien-Spinvektors vorhersagt.
Im zweiten Teil dieser Dissertation wurden die Eigenschaften von Kugelsternhaufen und ihren Wirtsgalaxien untersucht. Kugelsternhaufen (GC) sind sehr wichtige Objekte um die frühe Entwicklung von Galaxien zu untersuchen. In dieser Arbeit korrelieren wir Eigenschaften von Systemen aus Kugelsternhaufen – was mit der spezifischen GC-Frequenz (S_N) ermittelt wird – mit den Eigenschaften ihrer Wirtsgalaxien. Wir unterstützen die Erklärung für den Zusammenhang zwischen S_N und Galaxienmasse durch Gezeitenerosion.
Um die Herkunft dieses eben genannten Zusammenhangs zu verstehen, haben wir ein theoretisches Modell für die spezifische Frequenz ($S_{N,th}$) entwickelt. GC-Erosion wird als ein wichtiger Aspekt für die Ausprägung dieses Zusammenhangs betrachtet. Die Annahme basiert auf Beobachtungen von Galaxien kleiner baryonischer Dichten mit großen S_N und Galaxien mit hohen baryonischen Dichten mit kleineren S_N, also weniger Kugelsternhaufen pro Galaxie. Das Modell wird so konstruiert, dass es ausschließlich von einer minimalen Sternhaufenmasse ($M_{ecl,min}$), dem Anstieg des Potenzgesetzes der Haufenmassenfunktion (β) sowie der Relation zwischen Sternentstehungsrate (SFR) und der maximalen Sternhaufenmase ($M_{ecl,max}$) abhängt. Wir finden Übereinstimmungen zwischen primordialen Werten der spezifischen Frequenz (S_{Ni}) und unserem Modell mit $1.5 \leq \beta \leq 2.5$ und $M_{ecl,min} \leqslant 10^4 M_\odot$. Außerdem haben wir den Zusammenhang zwischen SFR und $M_{ecl,max}$ für höhere SFR-Werte als bisher bekannt getestet.

Contents

List of Figures

List of Tables

List of Abbreviations

2dFGRS	2D-Field Galaxy Redshift Survey
PA	Position angle
BCG	Brightest cluster galaxies
ECMF	Embedded cluster mass function
GC	Globular clusters
GCLF	Globular cluster luminosity function
HYPERCAT	Hyperlinked catalogues
HYPERLEDA	Hyper-linked Extragalactic Databases and Archives
IGIMF	Integrated galactic stellar initial mass function
LEDA	Lyon-Meudon Extragalactic Database
LSC	Local Supercluster plane
M_b	Baryonic mass of galaxies
$M_{ecl,max}$	Maximum star cluster mass
$M_{ecl,min}$	Minimum star cluster mass
N_{GC}	Number of globular clusters
RC3	Third Reference Catalogue of Bright Galaxies
S_N	Specific frequency of globular clusters
S_{Ni}	Primordial value of the specific frequency
$S_{N,th}$	Theoretical model for the specific frequency
SDSS	Sloan Digital Sky Survey
SDSS-DR6	6th Sloan Digital Sky Survey data release
SFR	Star formation rate
SVs	Spin vectors
TTT	Tidal-torque theory

CHAPTER 1

Introduction

1.1 Introduction

The morphological classification scheme for galaxies introduced by Hubble in 1936 usually referred to as the "Tuning Fork" diagram, is considered a first step to try and understand the evolutionary sequence of galaxies. The mechanisms and time-scales of these different morphologies were not fully understood, however many studies propose theories for galactic formation and evolution of galaxies and the large-scale structure of the universe.

The origin of galactic angular momentum represents an important role in helping us understand the formation and evolution of galaxies, and also determines the evaluation and final type of galaxy. Since we only know the angular momentum of a few galaxies (von Weizsäcker, 1951; Gamow, 1952), we investigate the alignment of the orientation of the galaxy. Thus, scenarios of galaxy formation predict different spin vector alignments of galaxies with respect to the large-scale environment: e.g. filaments (Figure 1.1).

In this thesis we investigate various scenarios proposed for galaxy formation. We also represent three scenarios for understanding galaxy formation and evolution, for which the parts of qualitative predictions for these models are supported observationally.

1.1.1 Primordial vorticity model

The Monolithic model proposed by Eggen et al. (1962) and Larson (1975) assumes that galaxies are formed by gravitational collapse and fragmentation of super giant gas clumps. According to this classic scenario, galaxies acquire their angular momentum as a result of primordial vortices. It also predicts that early type galaxies formed at a high redshift ($z > 3$) compared to spiral galaxies. In this model, star formation stops shortly after proto-galactic gas clouds collapse and passive stellar evolution governs the galaxy evolution. Additionally, the elliptical galaxies are formed very early and are considered the oldest structures. In this classic scenario, downsizing happens which means that the star formation duration inversely correlates with the mass of the galaxy (see Figure 1.2). Thomas et al. (2005) found higher mean stellar ages and abundance ratios for the most massive galaxies compared to those with less mass, which indicates that they formed stars earlier and over short time-scales. In the Monolithic model, the evolving galaxies depend on initial conditions and effects from the environment. The observed tightness of many scaling relations, such as colour-magnitude relation and the fundamental plane, support the monolithic scenario (e.g. van Dokkum & Stanford, 2003; Peebles, 2003). In elliptical galaxies, the dynamical and light profiles indicate a fast formation process, compared to spiral galaxies that are flat rotating disks which are likely formed by slow accretion.

Two factors determine the morphology of galaxy formation: angular momentum and cooling of the protogalaxy. It is more probable that a disk galaxy forms with a faster rotation (initial angular mo-

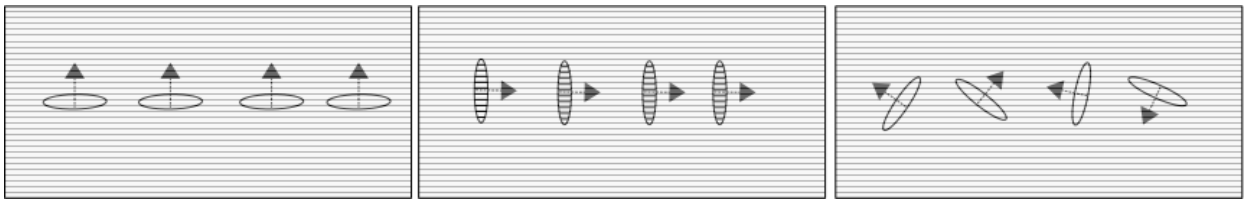

Figure 1.1: Schematic representation of a galaxy spin (black vectors) relative to the host filament in different scenarios of galaxy formation. In the left panel, the spin vector of galaxies is perpendicular to parent filament (primordial vorticity model). In the middle panel, the orientation of galaxies is parallel to the main plane of the filament (pancake model). In the right panel, a random orientation of galaxy results according to the hierarchical scenario.

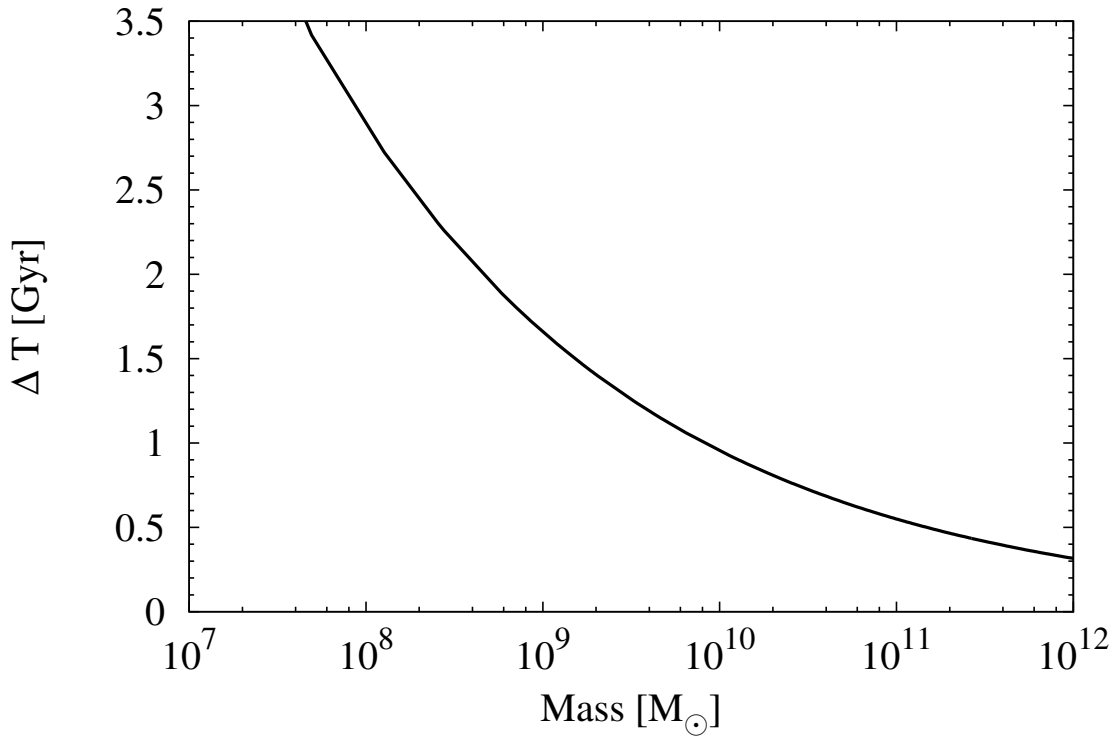

Figure 1.2: Star formation timescales (ΔT) for galaxies as a function of their mass from Recchi et al. (2009) (Fig(18)). Star formation duration is inversely proportional to the stellar mass of the galaxy (downsizing).

mentum aligned) with low-density protogalactic clouds that cool over longer time scales (longer than the dynamical time of clouds), while elliptical galaxies would have formed if the protogalactic clouds would have non-aligned angular momentum and a high-density which would cool faster than the dynamical time scale of the gas cloud (Lynden-Bell, 1967). In contrast to this, through the observation of NGC 3921, Schweizer (1996) found the features of a complex structure in this elliptical galaxy such as ripples, shells, a single nucleus and crossed tidal tails which are interpreted as a merger of two disk galaxies. This theory of galaxy formation proposed various predictions concerning the angular momenta of galaxies and predicts that the spin vector (where the rotation axes are normal to their disk planes) of a galaxy to be perpendicular to the cluster plane (Ozernoi, 1978).

1.1.2 Pancake model

The 'pancake model' predicts the spin vector orientation of galaxies to be parallel to the main plane of the structure. This model, proposed by Zel'dovich (1970), suggested that the clusters first formed and then fragment into galaxies due to adiabatic fluctuations. According to this model, a galaxy acquires angular momentum by a shock wave passing across the protostructure (Godłowski, 2011). In this scenario, gas cools and forms new clouds, while galaxies later form by cloud clusters. This is followed by single clouds clustering to form a cluster of galaxies.

1.1.3 Hierarchical model

In this scenario, the direction of the spin vectors of galaxies should be distributed randomly (Thuan & Gott, 1977). The less massive galaxies form first and then evolve through mergers of protogalaxies or even galaxies to form larger structures. At the time of recombination, the enhancements of densities from self gravity forms structures of the size of dwarf galaxies which later merge to form larger galaxies. During the condensing or collapsing, these merged galaxies would then generate spherical objects. Elliptical galaxies form if most collapses occur before mergers, whereas spiral galaxies form if major collapses occur after mergers.

Searle & Zinn (1978) first proposed that the first objects to form were low mass galaxies at a high redshift, and many mergers at lower redshifts led to the generation of massive galaxies. This also suggests that more massive galaxies have more extended star-formation histories.

The tidal-torque theory (TTT) describes the origin of angular momentum of hierarchical formation (Peebles, 1969). According to this theory, the galactic spin originates via tidal interactions between protogalaxies and their surrounding matter distribution (Peebles, 1969; Thuan & Gott, 1977; White, 1984).

Numerical simulations support the hierarchical model, where mergers of disk galaxies form elliptical galaxies (e.g. Baugh et al., 1998; Cole et al., 2000; Somerville et al., 2001, etc.). Observations of kinematical properties of elliptical galaxies also support the hierarchical model (Whitmore & Schweizer, 1995; Ibata et al., 1995). The galaxy disks formed as a result of gas accreted from intergalactic medium (Katz & Gunn, 1991), while the ellipticals formed by mergers of disk galaxies.

In 1980, Ostriker argued that the observed giant ellipticals, which have a velocity of 300 km s^{-1}, could not form by mergers of spiral galaxy which do not have a rotational velocity higher than 300 of km s^{-1} at the present day. The problems of this model remains with downsizing.

1.2 Spatial orientations of galaxy spin vectors

The spin vector orientations of galaxies in the parent clusters are an important tool to understand the basic physics regarding the origin of the angular momentum of galaxies. The tidal field theory was first proposed by Hoyle (1949) who suggested that a galaxy gains angular momentum through the tidal torques of their neighbours and was applied by Sciama (1955) in his theory of the origin of a galaxy. This idea was refined further by Peebles (1969) who used linear perturbation theory to estimate the angular momentum acquired by a protogalaxy via tidal torques from their neighbours in the early universe.

In addition to discrimination among different scenario of galaxy formation, these models make predictions regarding angular momentum (Peebles, 1969; Doroshkevich, 1973; Lee & Pen, 2002; Trujillo et al., 2006). Many studies have looked of the distribution of galaxy orientation with respect to their surrounding large-scale structures. The study of the alignment of galaxies within various clusters and superclusters suggested that galaxies are aligned with respect to their local large-scale structure (Adams et al., 1980; Flin & Godlowski, 1986; Kashikawa & Okamura, 1992). However, other studies did not find any alignment (Helou & Salpeter, 1982; Dekel, 1985; Garrido et al., 1993).

There are two difficulties related to observational analysis of the orientation of galaxies: firstly, the matter distribution around the galaxies is difficult to determine (Varela et al., 2012). Secondly, the direction of a spin vector of a galaxy requires knowledge of which side of the galaxy is closer to the observer. Some authors have studied galaxy ensembles with different restriction on their disk orientation (Kashikawa & Okamura, 1992), while others used samples with edge-on only or face-on only disk galaxies (Lee & Erdogdu, 2007). There are two main methods of studying the spin vector orientations of galaxies. The first is based on analysing the distribution of position angles (projection of the spin axis on the sky which measured from north to east) which was proposed by Hawley & Peebles (1975). The second method is the position angle -inclination method or simply the 'PA-inclination' method, which was originally proposed by Öpik (1970). This has been applied by Jaaniste & Saar (1978) and significantly modified by Flin & Godlowski (1986) to convert the 2-D projected data of images to 3-D information about the galaxy orientation.

The orientation of galaxies and their surrounding structures have been well studied by many researchers (e.g. Brown, 1964; Reinhardt & Roberts, 1972; Kapranidis & Sullivan, 1983; Flin & Godlowski, 1986). They have aimed to discuss whether or not galaxies are oriented in a random way or if the rotational axes tend to be parallel or perpendicular to the structure's main plane. The studies of the orientation of galactic axes in clusters were quite diverse and sometimes contradictory to one another. For example, Thompson (1976) studied the orientations of galaxies in the Virgo and A2197 clusters and found alignment of galaxy orientations in these clusters. Adams et al. (1980) suggested a bimodal distribution of galaxy orientations by studying the galaxies in seven cluster samples (A76, A179, A194, A195, A999, A1016, and A2197) from the catalogue of Rood & Sastry (1971). It was found that the major axes of these cluster members tend to lie either along the cluster's major axis or perpendicular to it. However, there is no model of galaxy formation that can predict a bimodal distribution of position angle as suggested in this study.

The PA of the major axes of spiral galaxies from the Reference Catalogue of Bright Galaxies (de Vaucouleurs et al., 1964) was investigated by Reinhardt & Roberts (1972). He found that galaxy planes tend to be parallel to the Local Supercluster plane (LSC), i.e.: spin vectors are perpendicular to the LSC plane. Others results (e.g. Jaaniste & Saar, 1978) seem to favour the pancake model by concluding that spin vectors are parallel to the LSC plane. Hoffman et al. (1989) studied samples of 141 spiral galaxies in and around the Virgo Cluster and claimed that there is no strong evidence for the alignment of these galaxies. These inconsistencies arise due to different methods of data sampling, sampling criteria and selection effects. By examining a sample of spiral galaxies in binaries and small groups, Helou (1984)

found that the spin vectors of theses galaxies tend to be antiparallel. MacGillivray & Dodd (1985) found that the presence of a weak non-random effect of galaxies is aligned with, or perpendicular to, the direction towards the cluster's centre. The spatial orientation of spiral galaxies in the Local Supercluster was examined by Flin (1988). He concluded that the rotation axes of galaxies tend to be parallel to the supercluster main plane. Godlowski (1993) analyzed a sample of 2227 galaxies and demonstrated that the orientation of the major axes of galaxies belonging to various substructures of the Local Supercluster show a tendency to the Virgo centre.

The morphological dependence and the anisotropic distribution of galaxy orientation were proposed by Hu et al. (1998) using the orientation of 220 bright isolated field galaxies in the Local Supercluster. The same trend for orientation of spiral galaxies with the plane of the supercluster was found by Flin (2001) when studying 622 spiral galaxies in the Coma cluster. Aryal & Saurer (2004, 2005, 2006) suggested that the galaxy alignments systematically change with galaxy morphology, and found manifest alignment of orientation for late-type galaxies rather than early-type galaxies. The third data release of the Sloan Digital Sky Survey (SDSS-DR3) and the 2dF Galaxy Redshift Survey (2dFGRS) were used by Trujillo et al. (2006), where they found a tendency that the spin vector of spiral galaxies located on the shells of the largest cosmic voids lie preferentially on the void surface. Godłowski & Flin (2010) studied the orientation of galaxy groups in the Local Supercluster and found a strong correlation with the distribution of neighbouring groups up to scales of about 20 Mpc. Aryal (2011) studied the 1621 field galaxies around the LSC and noticed a random alignment in the PA-distribution of spiral galaxies. A random orientation of PA distributions of galaxies in the six rotating clusters is indicated by Aryal et al. (2013).

1.3 Star clusters

Star cluster are considered basic building blocks of a galaxy (Kroupa, 2005). Typical galaxies contain groups of stars (each consisting of 10^2- 10^7 stars) that are gravitationally bound and are known as star clusters. The stars are formed simultaneously from the same cloud of gas, and thus they have approximately the same age and chemical composition. There are two general types of star clusters: open clusters and globular clusters.

1.3.1 Open clusters

Open clusters are irregular systems which contain between one-hundred and several thousand stars with total masses between 10 and $10^6 M_\odot$ and a diameter of less than 10 pc. Open cluster are commonly found in spiral galaxies close to the galactic plane as well as in irregular galaxies. Many clusters may be disrupted by gravitational shocks. Open cluster which originate from gas and dust are similarly short lived, probably less than 1 Gyr old. This is due to disruption by encounters with other interstellar gas clouds (or other clusters), by gravitational interactions and secular gravitational evolution. The first catalogue of open clusters, by Hodge in 1979, listed 403 objects. The best known example of open clusters are the Pleiades, Hyades and the Alpha Persei Cluster. In order to study older stellar systems, we turn to the second type of star clusters, globular cluster, which are considered the key to understanding galaxy formation.

1.3.2 Globular cluster

Globular clusters (GCs) are spherical concentrations of 10^4 to 10^7 stars, with total masses between 10^4 and $10^6 M_\odot$. These spherical collections contain a relatively high density of stars in the centre of up

to $10^6 M_\odot pc^{-3}$ (because of gravitational collapse as a result of gravitational interactions between stars), and with a half-light radius of a few pc. Stars in GCs are approximately made up of the same chemical composition and the same age (typically larger than 10 Gyr) (e.g. Dotter et al., 2010; Cezario et al., 2013). Messier 22 (M22), the first globular cluster to be recorded, was discovered by Abraham Ihle in 1665. In 1782 William Herschel used large telescopes and discovered 37 clusters, and later was the first to coin the term 'globular cluster'. In 1918 Harlow Shapley determined the size of our galaxy and GC system: he also estimated the distance from the Sun to the Galactic centre using GC. Discoveries of GC have continued to increase with time. In 2010 list contains 157 GCs in the Milky Way (Harris, 1996, 2010 edition[1]).

These spherical concentrations of stars can not only be observed in our galaxy but can also be observed in other local galaxies (with the exception of M32) and beyond. There are different numbers of GC found in various types of galaxies: the Milky Way contains fewer in comparison to other galaxies like the giant elliptical galaxy, M87, which contains around 10^4 GCs (Harris, 2009). There are many suggestions for how GC form. Côté et al. (2000) suggested the GCs form in the hierarchical collapse of the halo, or during galaxy mergers due to colliding gas (Schweizer et al., 1996).

GC only host old stars (Population II) and do not contain dust or young stars, and they are generally found in bulges and galactic halos. Most important is the correlation between the properties of GC and the properties of housing galaxies, whereas the properties of GC (mass, age, metallicity, total number and structural parameters) are considered important tools for the formation and evolution of GCs and galaxy star formation episodes. Based on this, we discuss the properties of GC in more detail.

1.3.2.1 The number of globular clusters

The number of globular clusters, N_{GC}, varies between differing morphological types of galaxies, ranging from a few in dwarf galaxies up to a few tens of thousands in giant galaxies. The number of globular clusters discovered was continuously increasing. In 1915 Melotte listed 83 MW GCs, and 97 by 1947. In 1987, Jones'list had 138 in total. The number increased to 147 in 1999 and by 2010, the number had reached 157 (Harris, 1996, 2010 edition[1]). GC discoveries by Balbinot et al. (2013) increased the number of GCs to 160. The number of globular clusters can be calculated from the globular cluster luminosity function (GCLF) peaks at a characteristic turn-over magnitude and then integrating over the whole luminosity function and the surface density, where the GCLF is defined as the relative number of globular clusters per unit magnitude (Harris, 2001). The N_{GC} is determined by doubling the number of GCs brighter than the turnover of the GCLF, when GCLF can accurately be described by a Gaussian distribution. This is much more reasonable since nearly 90% of GC mass occupies the brighter half. Many studies of GCs have confirmed the Gaussian shape of GCLF with a standard dispersion of $\sigma \sim$ 1-1.4 mag (Harris, 2001; Mieske et al., 2012), while the peak of the GCLF in different galaxies typically appears at M_V = -7.4±0.2 was derive from the MW and other galaxies (Ashman & Zepf, 1998; Hanes, 1977). Due to this universality, the GCLF is used as a distance indicator. Figure (1.3) shows the MW GCLF in the V-band with a Gaussian fit. The calculation of N_{GC} for understanding the efficiency of GC formation is affected by many factors, including the physics of the process of cluster formation, the initial cluster mass function, the cluster formation history and the cluster formation efficiency.

1.3.2.2 Specific frequency

A basic parameter representing the globular cluster system of a galaxy is the specific frequency, S_N, which was introduced by Harris & van den Bergh (1981) to measure the richness of a GC system

[1] http://physwww.physics.mcmaster.ca/~harris/mwgc.dat

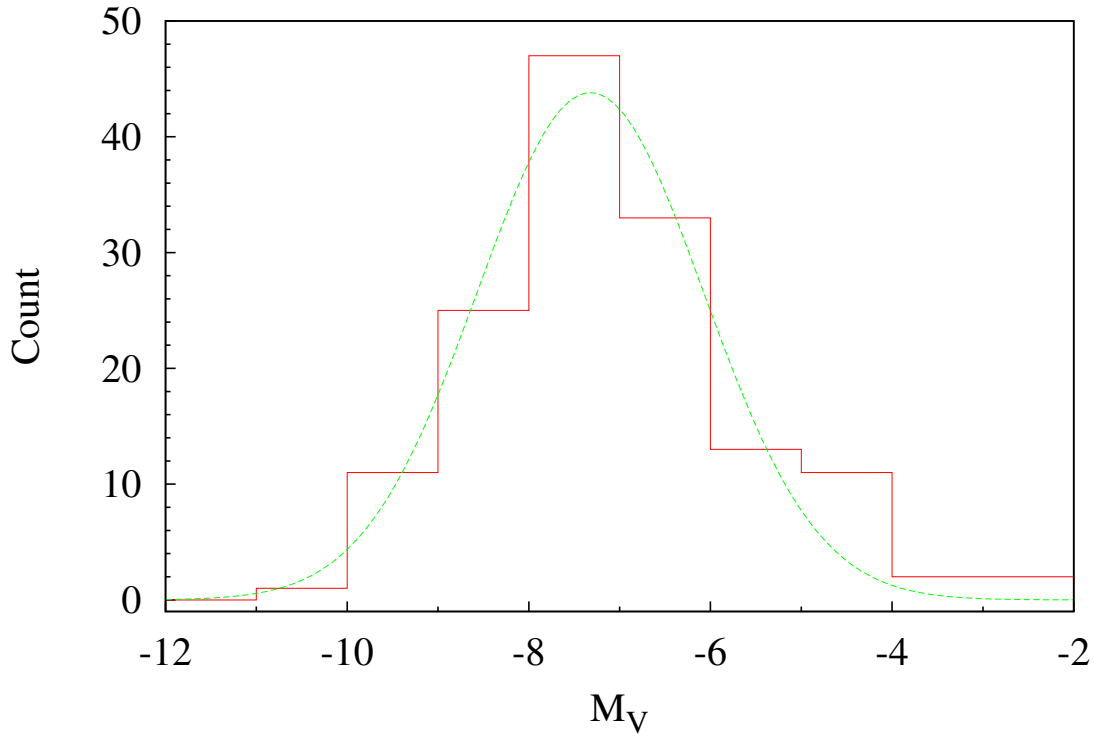

Figure 1.3: Histogram of GC absolute magnitudes for the MW sample from (Harris, 1996, 2010 edition), with a Gaussian fit to this distribution. The luminosity function peaks at M_V = -7.4.

between galaxies. S_N is defined as the number of globular clusters, N_{GC}, divided by the V-band luminosity of the galaxy, normalized at $M_V = -15$ mag,

$$S_N \equiv N_{GC} 10^{0.4(M_V+15)}, \tag{1.1}$$

where M_V is the absolute magnitude of the galaxy in the V-band.

The specific frequency varies between galaxies of different morphological types: S_N is smaller in late-type spiral galaxies than in early-type elliptical (E) galaxies (e.g Miller et al., 1998b). Spiral galaxies have a S_N between 0.5 and 2 (Goudfrooij et al., 2003; Chandar et al., 2004; Rhode et al., 2007). For more luminous elliptical galaxies, S_N ranges from about 2 to 10 and tends to increase with luminosity, while S_N increases from a few to several dozen with decreasing galaxy luminosity for dE galaxies (Miller & Lotz, 2007; Peng et al., 2008; Georgiev et al., 2010).

The disk and spiral galaxies have a smaller value of S_N than elliptical galaxies. The small difference in S_N between spiral galaxies may be due to observational scatter (Harris, 2001). The M_V for disk galaxies includes disk light that is less related to the halo clusters, and thus less representative of S_N directly. The Milky Way galaxy has an $S_N = 0.6 \pm 0.1$ (Ashman & Zepf, 1998), while if only the bulge luminosity is used for the normalization, the mean specific frequencies become equal to four (Côté et al., 2000).

The relation between S_N and mass reveals a 'U'-shape, i.e. higher S_N for dwarfs and supergiants (the low- and high- mass ends of the scale, respectively), and a minimum S_N for galaxies at an intermediate

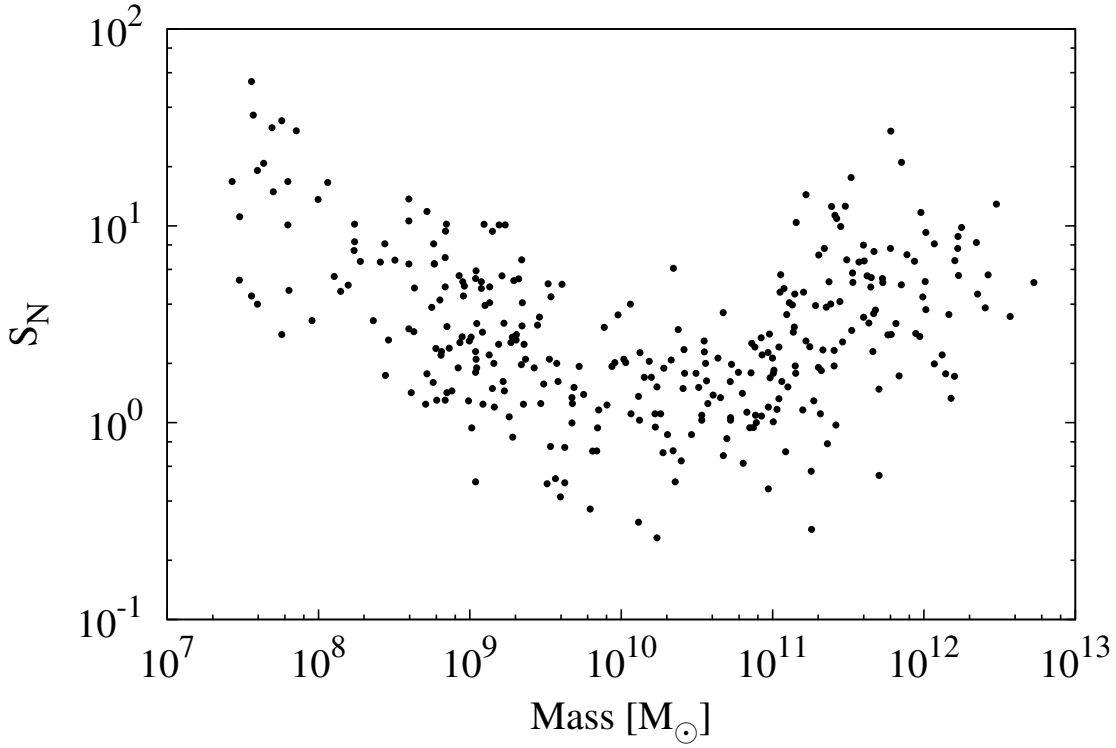

Figure 1.4: Globular cluster specific frequency versus galaxy mass for galaxies form (Harris et al., 2013; Georgiev et al., 2010).

mass (Figure 1.4). We can draw significant conclusions from this figure; one is that the galaxies with intermediate masses, have a number of GCs nearly proportional to the luminosity of the galaxy. Another conclusion is that there is a significant scatter of S_N between giant galaxies and dwarf galaxies. The specific frequencies differ between galaxies with the same luminosity. This difference in S_N between types of galaxies needs to be understood in terms of formation models of galaxies (Wang, 2002). The specific frequencies of GC vary between galaxies of differing type. The reason for this variation is not yet well understood, although many of the solutions suggested seem reasonable. Actually, too many ideas have been generated to explain the observed 'U'-shaped relation between S_N and M_V of the host galaxy. This is also true for understanding the difference of S_N between similar galaxies and the larger range of S_N between different galaxies.

A dependency of S_N on the environment around the host galaxy has been suggested. Galaxies in rich environments contain more clusters than ellipticals in smaller groups (Harris, 1981). The brightest cluster galaxies (BCGs), like cD-type galaxies, have the highest specific frequencies, and can be found near the centres of some rich galaxy clusters. The envelopes surrounding the brightest cD galaxies, which exceed 300 kpc in radius, were clearly visible, since the stellar material of these extended envelopes closely follows the potential of their parent clusters. Kumai et al. (1993) support such a suggestion that there is a significant correlation between specific frequency and local galaxy density around their host galaxy. Blakeslee et al. (1997) proposed the correlation between S_N and environment for 23 galaxies in 19 rich clusters. This trend is also confirmed by Gurzadyan & Mazure (2001) who study a sample

of the subclusters centered on NGC 4874, and suggested S_N decreases with increasing distance from the centre of this group. Later, Peng et al. (2008) showed that the dE in the Virgo galaxies has a higher S_N at closer distances to the central giant M87.

Another ansatz to explain this 'U'-shape is the formation of new GCs during the merging of spiral galaxies. Toomre (1977) proposed the merging spiral galaxies might form elliptical galaxies. Thereafter, Schweizer (1987) proposed that GC form during spiral merging to E galaxies (see also e.g. Ashman & Zepf, 1992). This idea was supported by observations by showing some brighter objects in merging disk galaxies, and by the metallicity distribution among GC of E galaxies (Zepf & Ashman, 1993). However, many objections appear against the idea that elliptical galaxies are formed by merging spiral galaxies (van den Bergh, 1995; Tremaine, 1995). Pahre et al. (1995) interpreted this 'U'-shape as a result of a variation in the mass to light ratio of galaxies, while another interpretation was based on the bimodality in the mass dependence of the M/L of their host galaxies. Forbes (2005) used large surveys to study the properties of the colour bimodality of GCs and suggested a critical stellar mass of the host galaxy ($\sim 3 \times 10^{10} M_{\odot}$): galaxies above these critical masses have two subpopulations of GCs with a narrow range in S_N, while those below these critical masses revealed a single blue GC population with an increasing and spreading out of S_N.

There are differences between the values of S_N for nucleated dE (dE,N) and non-nucleated dE galaxies (Miller et al., 1998b). Their survey revealed that S_N of dE,N was higher than nonnucleated dE by a factor of three. The higher S_N for dE,N is close to value of giant elliptical galaxies, while the value of S_N for nonnucleated dE galaxies are close to dIrr and spiral galaxies. This suggested that these galaxies have a different formation processes of GC (Seth et al., 2004). Strader et al. (2006) found no difference in the S_N of GCs between dE and dE,N by studying 37 Virgo dwarf galaxies. The explanation of higher S_N of globular clusters for dwarf ellipticals and spheroidals, as suggested by van den Bergh (1995), is that most of the gas was swept out the dwarf system by the wind generated from a violent initial burst of cluster formation (at a high value of S_N significant amount of gas was lost). Durrell et al. (1996) investigated the relation between S_N and the absolute magnitude of the galaxy in the V-band, and found similar values for dE and giant elliptical galaxies, and suggested that the higher values of S_N for dE galaxies are a result of gaseous mass loss by supernova. The approximately identical specific frequency of dE and giant ellipticals suggest that these galaxies form clusters as efficiently as giants. Miller et al. (1998a) claimed that E and dE formed at a similar time and with the same efficiencies by studying the luminosity function and colours of the GCs in dE and giant E galaxies. For lower mass galaxies, some mechanisms reduce the stellar mass to explain the higher specific frequencies (Moore et al., 2006). Georgiev et al. (2010) suggested that the dwarf galaxies at low luminosities are more efficient in forming star clusters. Present day starburst activity can have an effect on the luminosity of a galaxy, and the formation and dynamical evolution of GCs can affect N_{GC}. Therefore, both of these criteria affect the specific frequencies.

Mieske et al. (2014) tried to explain the relation between S_N and M_V by GC destruction via tidal erosion and dynamical friction of the stellar component in different galaxies. In this work, we present a model for the S_N of globular clusters, since S_N is reduced through erosion processes.

1.4 Outline of thesis

The thesis is organised in four chapters, and is divided in two parts. The first part contains the study of the orientation of galaxy spin with respect to the large-scale environment. In the second part, we study the relation between the properties of GC systems and the properties of their host galaxies.

After the introduction and problem formulation, we study the relative orientation of galaxies with

respect to their large-scale environment in Chapter 2. We extract a large sample of 4558 galaxies from the Hyper-linked Extragalactic Databases and Archives at z $\approx$ 0.0055 in order to calculate the angle between the spin vectors of spiral galaxies and the host filament in which they are embedded.

In Chapter 3 we study the relation between the properties of GC systems -as quantified through the GC specific frequency- and properties of their host galaxies. We use observations for early-type galaxies, which show that galaxies with low baryonic densities have a higher S_N. These galaxies reduce their S_N values through erosion processes. We derive a theoretical model for the S_N since GC erosion is considered to be an important aspect for shaping the relation between S_N and the baryonic galaxy mass. After correcting GC populations for this erosion, we construct a model depending on the minimum star cluster mass ($M_{ecl,min}$), the slope of the power-law embedded cluster mass function (β), and the relation between the star formation rate (SFR) and the maximum star cluster mass ($M_{ecl,max}$). Finally, the conclusions of this thesis are given in Chapter 4. *The fundamental idea here is that star formation in all galaxies proceeds according to the same physics and thus in star clusters with a universal valid distribution function*.

This thesis has three appendices. Appendix A contains the filaments structures represented by linear regression, spin vector and major axis for spiral galaxy. Appendix B shows the histograms of the computed angles between the spin spiral galaxies and the host filament. Appendix C lists the distance and angles between the spin axis and host structures, in addition to the number, name, right ascension, declination and velocity for each galaxy in the structure.

The content of Chapter 2 is based on the conference proceeding:

Abdullah, A., & Kroupa, P., 2014, "The Alignment of Spin Vectors of Spiral Galaxies in Filaments", ASP Conference Series, Vol. 486, Enrichetta Iodice and Enrico Maria Corsini, eds.

Part of the results of Chapter 3 have already been presented at a conference held in Concepcion, Chile, 2-6 March, 2015, and are also based on the following paper: Abdullah, A., Kroupa, P., & Lieberz, P. 2015, MNRAS, submitted.

During the three years of Ph.D. course, I participated in three conferences:

1. “Multi-Spin Galaxies”, INAF-Astronomical Observatory of Capodimonte, September 30 - October 3, 2013, Naples, Italy.

2. “ Modeling and observing dense stellar systems (MODEST 14) ”, The dance of stars: dense stellar systems from infant to old, June 2 - 6 2014, Bad Honnef, Germany.

3. “ MODEST 15 ”, March 2 - 6, 2015, Concepcion, Chile.

CHAPTER 2

The alignment of spin vectors of spiral galaxies in local filaments

2.1 Introduction

Galaxies are not generally found in isolation, nor are they distributed randomly in space. Many are found in groups and clusters which are themselves part of larger scale structures such as filaments and sheets surrounding cosmic voids (van de Weygaert et al., 2009).

For the purpose of developing an understanding of the formation and evolution of galaxies in large-scale structures, one requires knowledge of how galaxies obtain their angular momentum. This is a relevant question because >75% of all galaxies are late type galaxies (Delgado-Serrano et al., 2010). The orientation of galaxy spin is an important clue for understanding the origin of the angular momenta of galaxies (von Weizsäcker, 1951; Gamow, 1952). The various scenarios proposed for the origin of galaxies predict different spin vector alignments of the galaxies with respect to their large-scale environment. The three proposed scenarios are the pancake model (Doroshkevich, 1973; Doroshkevich et al., 1978), the hierarchy model (Peebles, 1969) and the primordial vorticity theory (Ozernoi, 1978). In the pancake model and the primordial vorticity theory, the spin vectors are predicted to be parallel and perpendicular, respectively, relative to their hosting filaments. The hierarchical model predicts the distribution of spin vectors directions to be random. Within the hierarchical model, the angular momentum is gained through tidal torque. According to this Tidal Torque Theory (TTT), the angular momentum of galaxies is gained through the tidal shear produced by the neighbouring primordial matter distribution (Hoyle, 1951; Peebles, 1969; Doroshkevich, 1970; White, 1984).

Here, we are searching for the alignment of projected spin vectors (hereafter SVs) of spiral galaxies with the projected large-scale structures (filaments) in which they are embedded.

Several studies indicate a correlation between the spin orientation of galaxies and their host structures (Kashikawa & Okamura, 1992; Navarro et al., 2004; Trujillo et al., 2006). Slosar & White (2009), on the other hand, claim to have found contradicting results when studying the spin direction of a large sample of galaxies from the 6th Sloan Digital Sky Survey data release (SDSS - DR6) with regards to the voids in which they are located. More recently, (Jones et al., 2010) found that the spin axes of spiral galaxies are aligned perpendicularly to the parent filament at redshifts of $0.01 < z < 0.11$. Tempel et al. (2013), on the other hand, found only a weak tendency for the spin axis of bright spiral galaxies to be aligned parallel to filaments at $z \approx 0.009$ based on the SDSS.

2.2 HYPERLEDA

Our study is constructed from the HYPERLEDA (Hyper-linked Extragalactic Databases and Archives) which forms a union between the LEDA (Lyon-Meudon Extragalactic Database) and HYPERCAT (Hy-

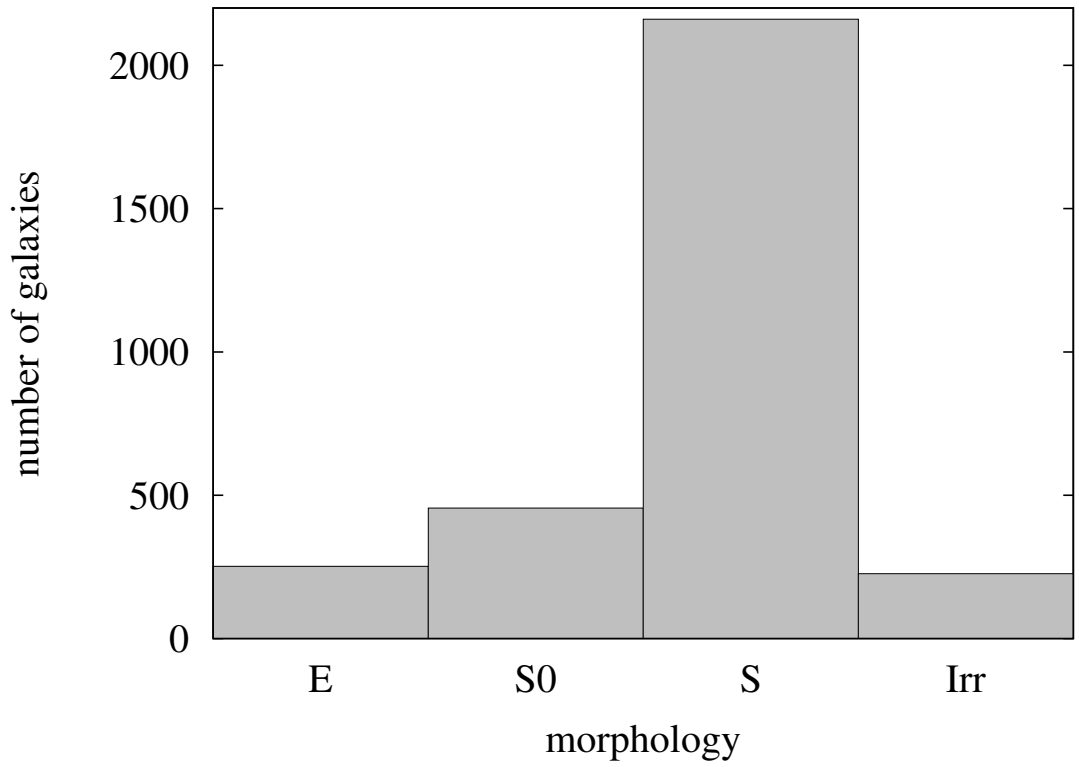

Figure 2.1: Morphology class distribution of our entire galaxy sample.The selection criteria yielded in total 3094 galaxies in our redshift range.

perlinked catalogues) [1]. HYPERLEDA was established as a consequence of a collaboration between the Lyon Observatory, the Paris Observatory, Moscow University and Sofia University, and thus extends the capabilities of LEDA. HYPERLEDA contains a database and the tools to process data according to the user's requirements, and aims to study the physics and evolution of galaxies. The data and all references for data, are available through the HYPERLEDA database (http://leda.univ-lyon1.fr).

Now, HYPERLEDA is integrated in the Virtual Observatory and provides a homogeneous description for a sample of nearly three million galaxies. Data in HYPERLEDA are mainly from measurements in large surveys (ESO surveys) and astronomical literature (i.e. Vauglin et al., 2006).

2.3 Data selection

To build our sample, we used the following selection criteria: (1) the radial velocities are between 1400 and 2200 km s^{-1} (corresponding to a redshift of z ≈ 0.0046 - 0.0073); and (2) spiral galaxies (1 < T < 10), where T is the morphology index defined in the Third Reference Catalogue of Bright Galaxies (RC3) (de Vaucouleurs et al., 1991; Corwin et al., 1994). For each galaxy in our sample, the position angle (PA) and length of the projected major axis of the galaxy at the isophotal level B = 25 mag $arcsec^{-2}$ are extracted.

[1] http://www-obs.univ-lyon1.fr/hypercat/

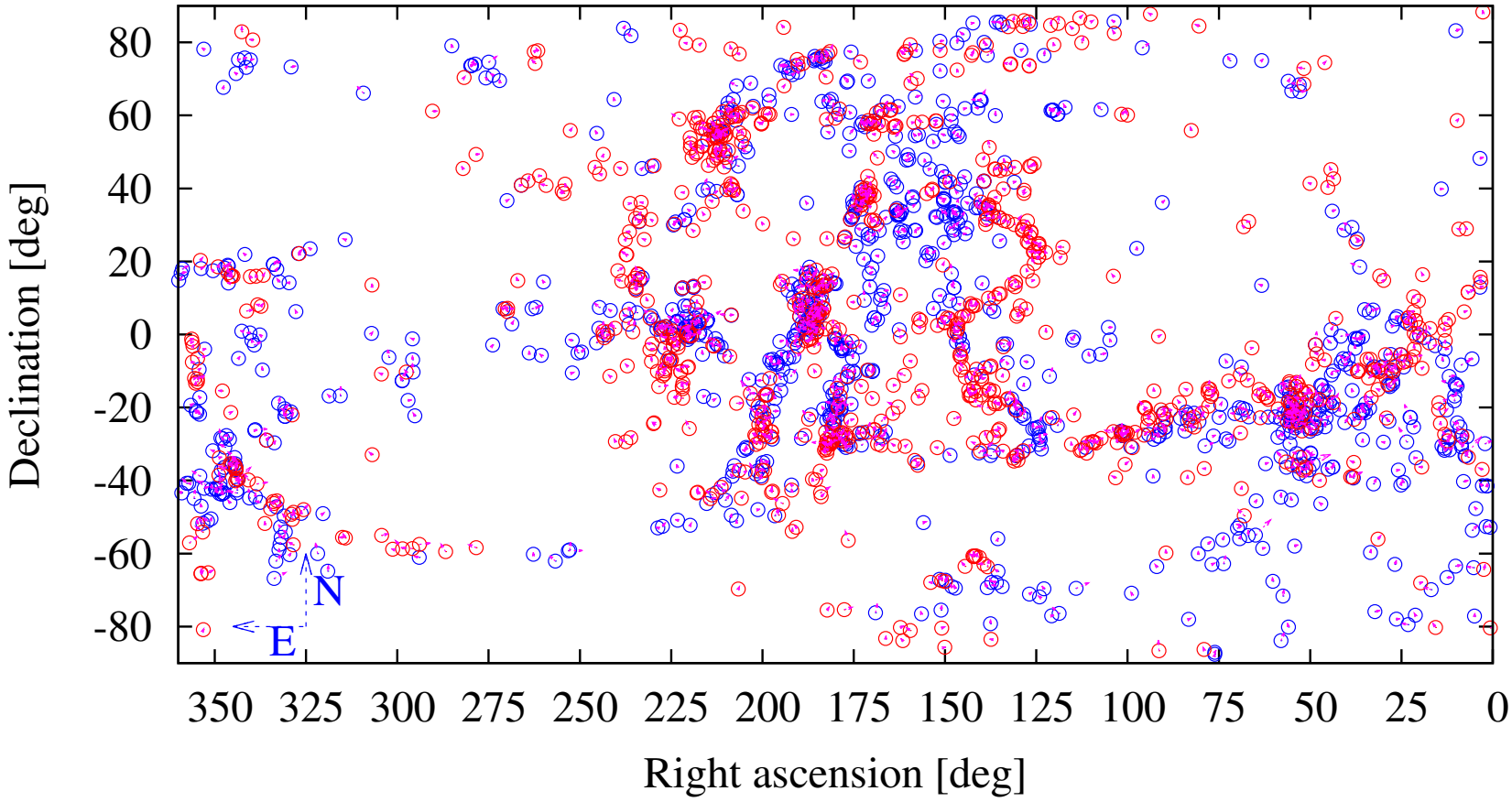

Figure 2.2: The entire sample of 1843 spiral galaxies which have a radial velocity between two ranges 1400-1800 km s^{-1} (blue circles) and 1800-2200 km s^{-1} (red circles).The pink vectors represent the projected spin vector of the galaxies.

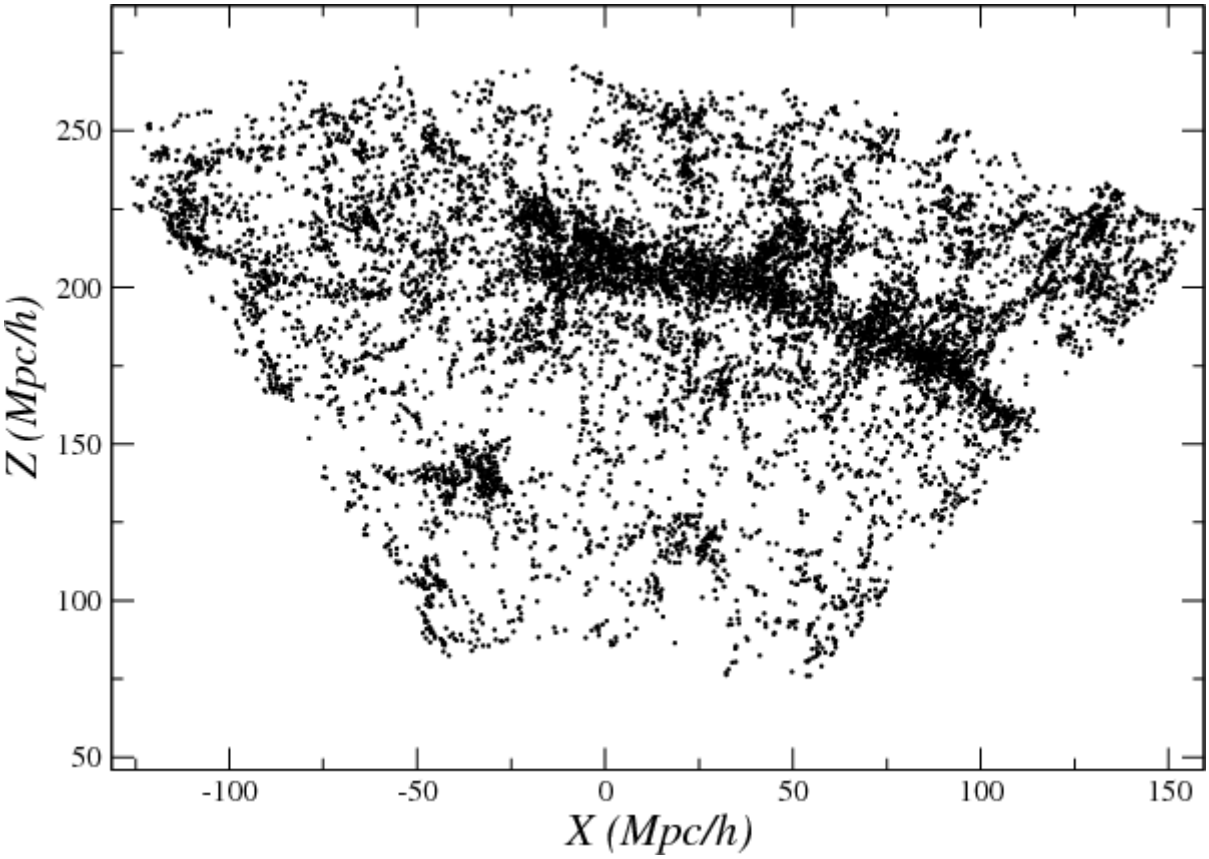

Figure 2.3: The Sloan Digital Sky Survey (SDSS) showing the galaxy distribution from Sylos Labini et al. (2009).

Figure (2.1) shows the distribution of the morphological classifications of our galaxies: 2161 spiral galaxies, 252 elliptical galaxies, 455 lenticular galaxies and 226 irregular galaxies. The distribution of the orientations of the SVs for 1843 spiral galaxies for which the PAs and lengths of the projected major axes are known is shown in Figure (2.2).

2.4 Filaments

Galaxies are distributed in a great cosmic web throughout the universe (Klypin & Shandarin, 1993; Bond et al., 1996). Observation shows the distribution of galaxies at large scales as a complex network of structure elements such as galaxy groups,clusters, superclusters and filaments.

Filaments are most pronounced between clusters of galaxies which are close together and aligned with each other. The cosmic web filaments are visually the most dominant structures in galaxy distribution, since nearly 40% of galaxies are located in filaments (Tempel et al., 2014).

Over the past 50 years, the study of the distribution of galaxies in large-scale structures became an important research subject. Jõeveer et al. (1978) was the first to identify the filaments in galaxy distribution. Many studies have been undertaken to identify the filaments joining neighbouring clusters in observational samples by using different techniques (e.g. Pimbblet, 2005; Bond et al., 2010; Alpaslan et al., 2014).

In 1987, Brent Tully, of the University of Hawaii, identified the Pisces–Cetus Supercluster. This

galaxy filament is estimated to be nearly 300 Mpc long and 50 Mpc wide. The largest filament known so far at a high z (z~ 2.38) is around the galaxy protocluster, J2143-4423 (Palunas et al., 2004; Francis et al., 2004).

Filaments are visible in galaxy surveys, e.g., the 2D-Field Galaxy Redshift Survey (2dFGRS) (Colless et al., 2003), and the Sloan Digital Sky Survey (SDSS)(e.g. Abazajian et al., 2003). More information about these surveys can be found in their web pages: http://www.mso.anu.edu.au/2dFGRS/ for the 2dF survey and http://www.sdss.org/ for the SDSS survey.

For the present purpose a sample of galaxy was extracted from HYPERLEDA using criteria defined in section (2.3). The larger sample provided by the Sloan Digital Sky Survey (SDSS) in Figure (2.3) shows the galaxy distribution with the filament in the middle of the sample (Sylos Labini et al., 2009).

To determine the orientation of the filaments in Figure (2.2), the observed area of the sky was first divided into small rectangular regions using preliminary fits to filaments by linear regression. Nineteen such structures were identified from the galaxy distribution in Figure (2.4). Once the rectangle containing a filament is chosen, the major filament axis is determined by fitting a line to the position of the data points using linear regression. All galaxies in the rectangular box are included in the fit. We extracted 19 filaments structures with 302 disc galaxies, with each structure having at least six or more members, ensuring a reasonable number of galaxies per filament. The thickness of the rectangular region is the root mean square spread of vertical distances between the data and the regression line. Figure (2.5) shows the SVs and the major axes of the spiral galaxies for filaments 5, 8, 11, and 12.

To study the distribution of angles between the SVs of galaxies and host filaments in this work, we resort to the PAs of the galaxies when deriving the orientation of the spin vector of the spiral galaxy, as we know the galaxy spins of only a few galaxies.

2.5 Method of analysis

In order to compute the angle θ between the SVs of a spiral galaxy and its hosting filament, the filament (hereafter Vf) is represented by a linear regression fit. Since the spin axis is perpendicular to the galactic disc, the angle (ω) between a SVs and the north galactic pole can be derived from the position angle (PA) of the major axis of a galaxy, which is counted from north to east in the plane of the sky ranging between 0° and 180° (Figure 2.6). The projected components of the SVs for a galaxy follow from $\omega = 90 - PA$, $SV_x = (D/2) * sin(\omega)$, $SV_y = (D/2) * cos(\omega)$, where D is the length of the projected major axis of a galaxy at the isophotal level of 25 mag/arcsec^2 in the B-band. The absolute value is $|SV| = \sqrt{{SV_x}^2 + {SV_y}^2}$.

Next, we compute the vector of the filament (Vf) and its absolute value$|Vf|$: $Vf_x = x_2 - x_1$ and $Vf_y = y_2 - y_1$ such that $|Vf| = \sqrt{{Vf_x}^2 + {Vf_y}^2}$, where (x_1, y_1) and (x_2, y_2) are two points on the linear fit determined by linear regression. While the absolute value $|SV|$ and $|Vf|$ have no physical relevance, they are needed for our calculations. Having obtained $\overrightarrow{SV}$ and $\overrightarrow{Vf}$, the angle θ between them follows from

$$\theta = \arccos \frac{\overrightarrow{SV}.\overrightarrow{Vf}}{|SV_s||Vf|}. \tag{2.1}$$

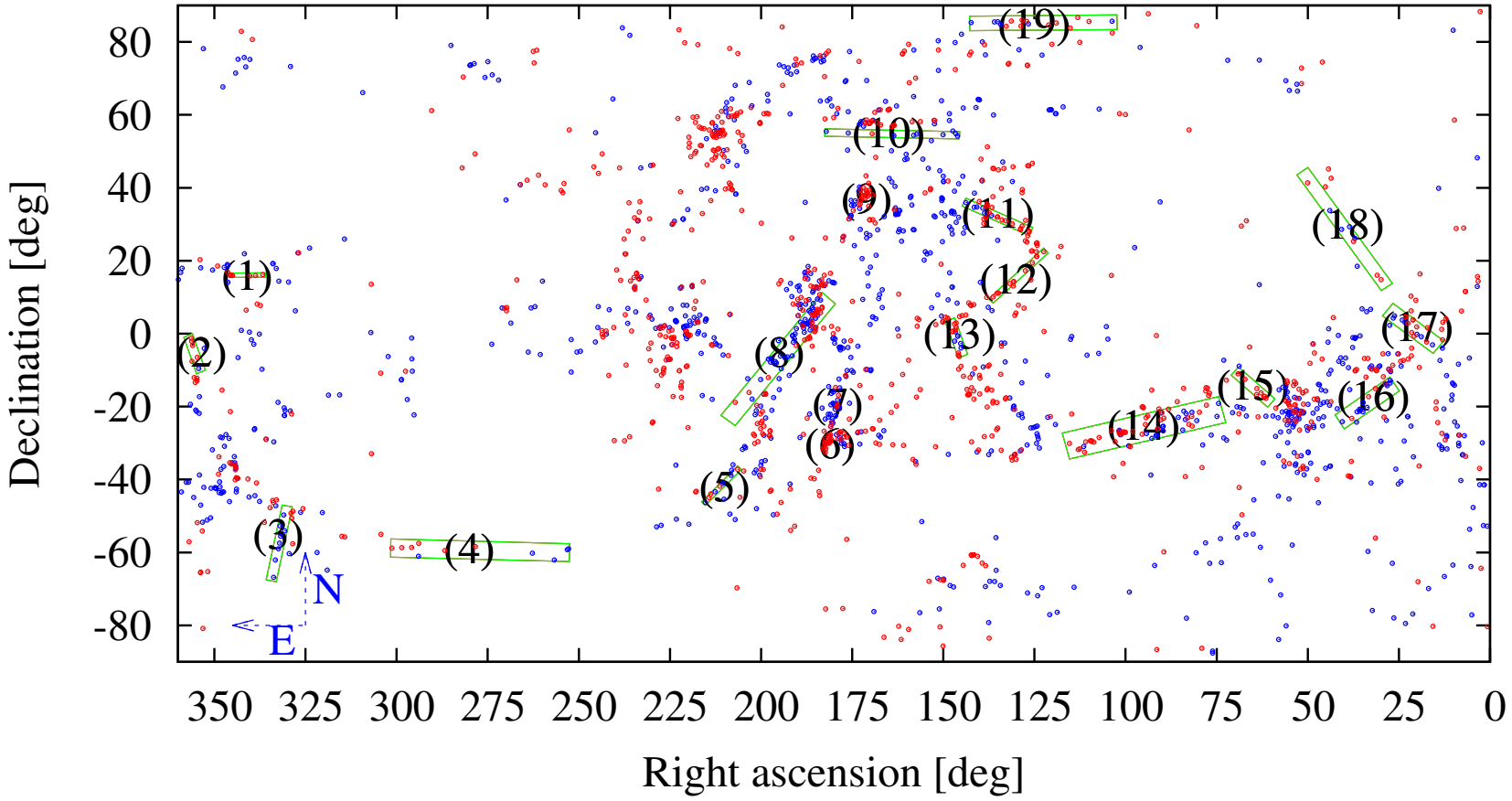

Figure 2.4: Same as Figure (2.2), but showing the 19 filaments and their rectangular regions which all together contain 302 disc galaxies.

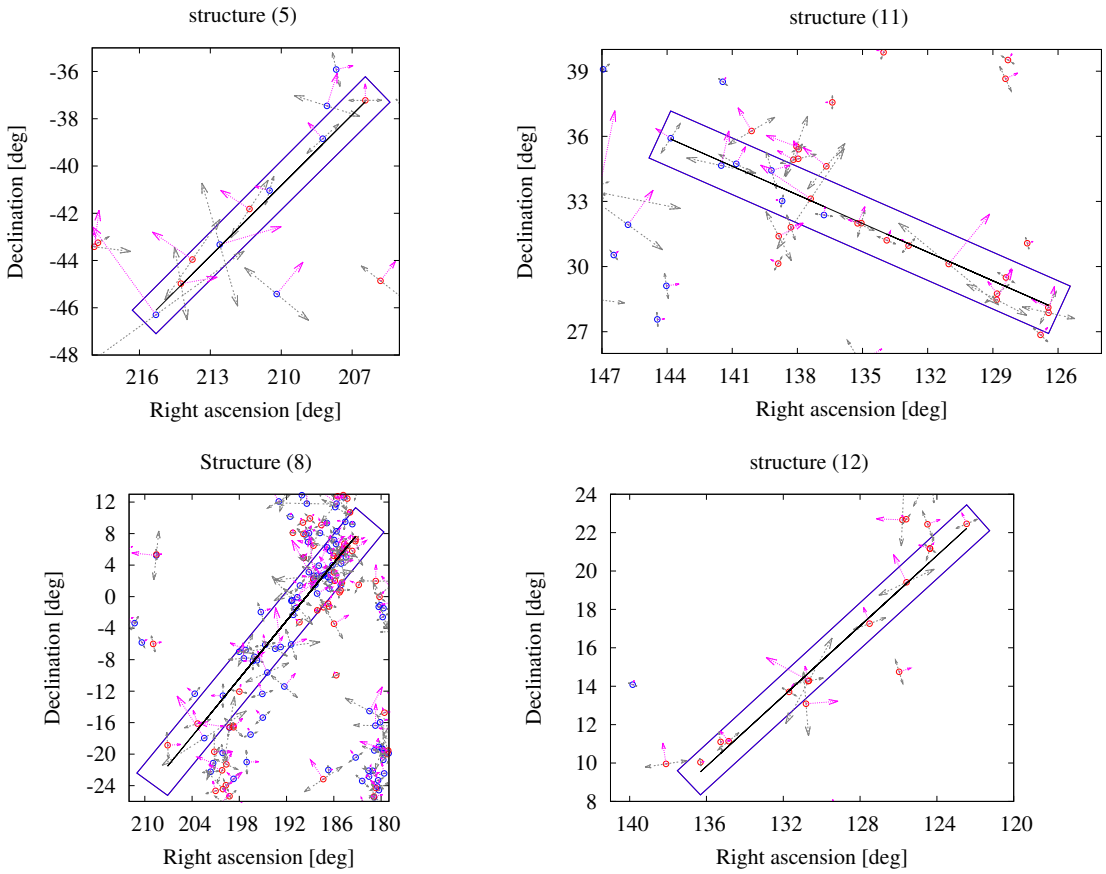

Figure 2.5: The projected spin vectors (pink vectors) and the major axis (gray vectors) for spiral galaxies in two ranges of radial velocity 1400 -1800 km s^{-1} (blue circles) and 1800 - 2200 km s^{-1} (red circles). The black line (filament) shows the linear regression fit to the data points (galaxies) inside the rectangles for structure 5, 8, 11 and 12. The plots for all structures are in Appendix A.

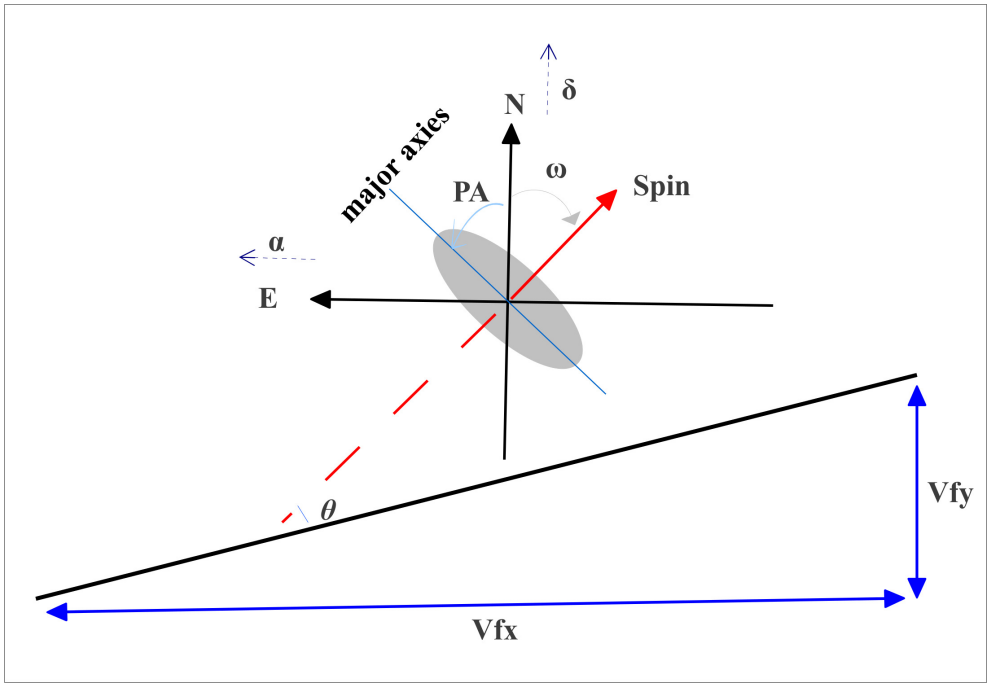

Figure 2.6: Schematic drawing of a sample galaxy, showing the angle θ (angle between the SVs of a spiral galaxy and the filament), and SVs of the spiral galaxy. α and δ are the equatorial coordinates of the galaxy, PA is the position angle, ω is the angle of the SVs. Vf is the filament (represented by the best - fitted straight line)

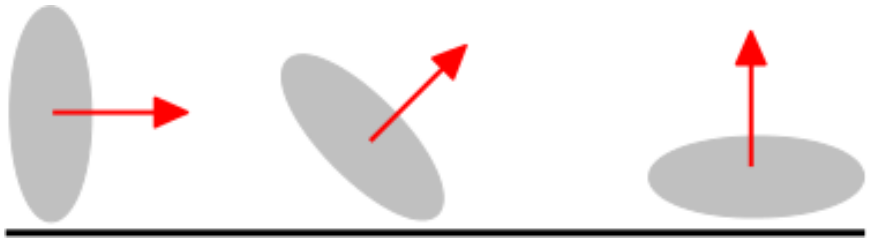

Figure 2.7: Schematic presentation for the orientation of galaxy spin vector (red vectors) relative to their parent filament (black line), where the angle θ between spin vector and filament = 0°, 45° and 90°.

The angles θ for all our galaxies can be found in Appendix C. In our case, θ is limited between 0 and $\pi/2$, where 0 means the SVs of the galaxy is parallel to the filament, and a spin perpendicular to the filament leads to θ=$\pi/2$ (Figure 2.7).

For each galaxy with right ascension α [deg] and declination δ [deg] in the rectangular region considered to represent the structure, we calculate the vertical distance (d) of the galaxy from the regression line given by the equation $a\alpha + b\delta + c = 0$,

$$d = \frac{|a\alpha + b\delta + c|}{\sqrt{a^2 + b^2}}. \tag{2.2}$$

We tested the quality of the fit to the data points by using the root mean square error (S), correlation coefficient and coefficient of determination. The root mean square error provides an important measure of spread or variability of a set of data around the regression line,

$$S = \sqrt{\frac{1}{N-1}\sum_{i=1}^{n} d^2}, \tag{2.3}$$

where d is the vertical distance obtained above and N is the number of galaxies in the structure. The correlation coefficient (R) is

$$R = \frac{\sum(\alpha - \bar{\alpha})(\delta - \bar{\delta})}{\sqrt{\sum(\alpha - \bar{\alpha})^2 \sum(\delta - \bar{\delta})^2}}. \tag{2.4}$$

where $\bar{\alpha}$ and $\bar{\delta}$ are the mean values of right ascension and declination respectively. As a more useful test of the goodness of fit, we used the coefficient of determination R^2. The coefficient of determination is a measure of how close data points fit the regression line, where an R^2 of 1 indicates that the regression line fits the data well, and an R^2 near 0 indicates a regression line that does not fit the data very well. R and R^2 yield an indication of how pronounced a filament is. The statistical parameters for all studied filaments are listed in Table (2.1).

2.6 Results and discussion

We have analyzed a large sample of spiral galaxies with respect to the filaments in which they are embedded for a limited range of galaxies with a radial velocity between 1400 and 2200 km s^{-1}. As can be seen in Table (2.1), the root mean square error for all structures is smaller than 0.6976 Mpc. This means the filament structures are thin and the member galaxies are typically close to the filament. The coefficient of determination was calculated for all 19 structures.

The histogram depicted in Figure (2.8) shows the distribution of angles between the spin vectors and host filaments for 302 spiral galaxies (in Appendix B all histograms per filament can be found) where θ=0 corresponds to a SVs parallel to the filament. No statistically significant evidence for an alignment of the angles with the filaments can be defined for this sample. We found no preferred orientation of the SVs of spiral galaxies with respect to their hosting filaments, which agrees with the hierarchical scenario (Peebles, 1969; Thuan & Gott, 1977) where the directions of galaxy formation spin vectors should be random.

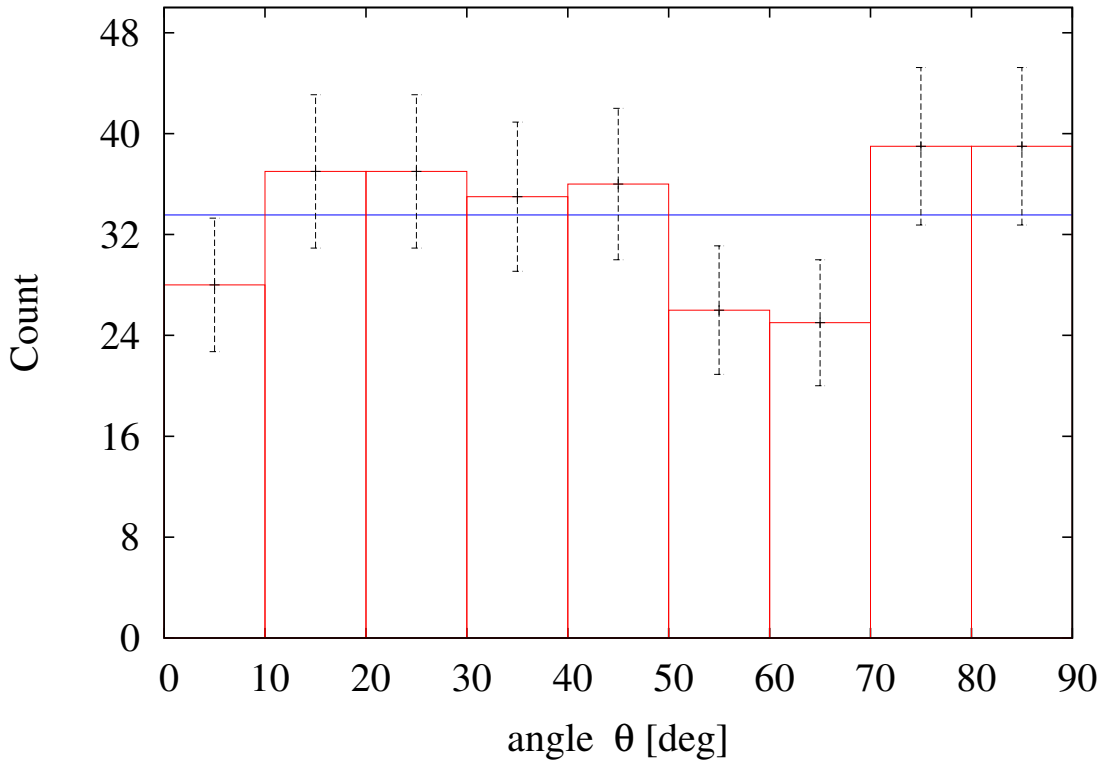

Figure 2.8: The angles θ between spin vectors of all the 302 spiral galaxies and their filaments. Errorbars are Poisson noise, the blue line represents the average value = 33.5

Table 2.1: Statistical parameters for the data analysis. Col. 1: filament designation; Col. 2: length of filament in Mpc; Col. 3: number of galaxies in filament; Col.4 and Col.5: the root mean square error in deg and in Mpc, respectively; Col.6: coefficient of determination.

Filament Nr.	length of filament (Mpc)	Number of galaxies	Root mean square error (deg)	Root mean square error (Mpc)	Coefficient of determination R^2
1	4.36	7	0.107	0.0499	0.823
2	3.96	6	0.639	0.2931	0.753
3	6.98	8	0.456	0.1940	0.812
4	18.97	11	1.128	0.4701	0.701
5	3.86	8	0.206	0.0902	0.994
6	0.72	7	0.148	0.0739	0.768
7	0.75	9	0.173	0.0740	0.783
8	9.62	65	1.155	0.4694	0.927
9	0.98	6	0.109	0.0541	0.986
10	12.94	9	0.264	0.1012	0.688
11	7.86	17	0.334	0.1557	0.982
12	6.94	11	0.326	0.1672	0.991
13	1.39	15	0.664	0.2917	0.723
14	16.94	59	1.613	0.6976	0.735
15	3.43	8	0.387	0.1814	0.950
16	5.15	16	0.985	0.4458	0.947
17	4.96	16	1.058	0.5210	0.741
18	11.26	8	0.703	0.2840	0.981
19	15.95	16	0.701	0.3342	0.618

CHAPTER 3

On the primordial specific frequency of globular clusters in dwarf and major elliptical galaxies

3.1 Introduction

Globular clusters (GCs) are spherical concentrations of $10^4 - 10^7$ stars and among the first stellar systems to form in the early Universe. GCs are found within different morphological types of galaxies, from irregular to spiral and elliptical galaxies. Most of the GCs appear to have formed within a few Gyr after the Big Bang (Gratton et al., 2003) and the global properties of GC systems can be considered as important tracers for the formation and evolution of galaxies.

One of the basic parameters to describe the globular cluster system of a galaxy is the specific frequency, S_N, which is the number of globular clusters, N_{GC}, divided by the V-band luminosity of the galaxy, normalized at an absolute magnitude of the galaxy in the V-band (M_V) of -15 mag (Harris & van den Bergh, 1981):

$$S_N \equiv N_{GC} \times 10^{0.4(M_V+15)}. \tag{3.1}$$

The specific frequency varies between galaxy with different morphology type, whereby S_N increases from late-type spiral galaxies to early-type elliptical galaxies (e.g. Miller et al., 1998b). The mean value of specific frequency for early-type galaxies have on average two times higher than late type galaxies (Georgiev et al., 2010).

The relation between S_N and M_b (the total baryonic mass of a galaxy) reveals a 'U' -shape, i.e., higher S_N for low and high- mass end of the scale while a minimum S_N for galaxies at an intermediate mass, as shown in Figure(3.1) (Harris et al., 2013).

There are many suggestions to explain the observed 'U' -shaped relation between S_N and M_V of the host galaxy. Forte et al. (1982) proposed a tidal stripping model of GCs from smaller galaxies to explain the increasing value of S_N in cD galaxies (central dominant elliptical galaxy) and studies of the GC system around cD galaxies also supported this scenario (Forbes et al., 1997; Neilsen et al., 1997). Schweizer (1987) and Ashman & Zepf (1992) suggested that galactic interactions lead to globular-cluster formation which reflects the low S_N of giant spiral galaxies which merge to form ellipticals.

Georgiev et al. (2010) investigated the trend of increasing S_N above and below the absolute galaxy magnitude of $M_V \simeq -20$ mag and explain this trend by a theoretical model of GC specific frequency as a function of host galaxy dark matter halo mass with a universal specific GC formation efficiency η. This is the total mass of GCs divided by the mass of the host dark matter halo, irrespective of galaxy morphology and which has a mean value of $\eta = 5.5 \times 10^{-5}$. Wu & Kroupa (2013) studied the apparent or phantom virial mass (M_{vir}) of dark matter halos in Milgromian dynamics. They found S_N and η

to be functions of M_{vir}. The number of GCs and η increase for $M_{vir} > 10^{12} M_\odot$ and decreases for $M_{vir} \leq 10^{12} M_\odot$.

Another ansatz to explain this 'U' -shape is for galaxies with a small and large mass to have been very inefficient at forming stars. Harris et al. (2013) suggested these galaxies formed their globular clusters before any other stars, then had a star formation shut off. Star formation is likely regulated by supernova feedback and virial shock-heating of the infalling gas for low and massive galaxies respectively, while intermediate mass galaxies have a maximum star formation efficiency.

Recent studies argue that GC destruction can be important for the relation between S_N and M_V (Mieske et al., 2014). Tidal erosion together with dynamical friction of the stellar component in different galaxies could produce different GC survival fractions at the present day, which may explain the present-day dependence of $S_N(M_V)$.

In this chapter, we present a model for the specific frequency of GCs. It is based on the notion that star formation occurs in correlated star formation events which arise in the density peaks in the molecular clouds that condense from the galaxy's interstellar medium (ISM). These are spatially and temporally correlated with scales < 1 pc and formation durations < 1 Myr and can also be referred to as being embedded clusters.

3.2 The GC populations and tidal erosion

The specific frequency of GCs (S_N) is an important tool to understand the evolution of galaxies (Harris, 1991; Brodie & Strader, 2006).

In this work, the data is taken from the Harris catalogue (Harris et al., 2013). We selected elliptical galaxies with masses ranging between 10^7 and $10^{13} M_\odot$ (with the exception of M32). These masses are dynamical masses of the galaxy, $M_b = 4\sigma_e^2 R_{1/2} G^{-1}$, where σ_e [pc Myr^{-1}] is the velocity dispersion, $R_{1/2}$ [pc] the effective half light radius, and G is the gravitational constant [$G \approx 4.43 \times 10^{-3}$ pc$^3 M_\odot^{-1}$ Myr^{-2}]. We refer to these masses as baryonic masses (M_b) since the putative dark-matter halo has a small contribution to the mass within this radius (e.g. Graves & Faber, 2010; Tiret et al., 2011; Harris et al., 2013; Smith & Lucey, 2013), and stellar remnants from a top-heavy the integrated galactic stellar initial mass function (IGIMF) account for this contribution (Weidner et al., 2013).

Figure (3.1) demonstrates a 'U' -shape relation between S_N (calculated using equation 3.1) and M_b (Harris et al., 2013). Mieske et al. (2014) explained this relation as an effect of tidal erosion. For the purpose of understanding how tidal erosion contributes to this relation, one has to study the relation between the 3D mass density ($\rho_{3D} \equiv M_b / {R_{1/2}}^3$) [$M_\odot$/pc^3] within the half-light radius ($R_{1/2}$)[pc] and M_b [$M_\odot$].

The relation between the 3D mass density and the baryonic mass takes the same trend as the S_N vs. M_b relation as shown by Mieske et al. (2014). Near $M_b = 10^{10} M_\odot$ is the highest mean density, while the density is lower for less and more massive galaxies. Galaxies with different densities appear to generate different cluster evolutions. Mieske et al. (2014) arrived at two equations to calculate the GC survival fraction, f_s, for initially isotropic ($f_{s,iso}$) and radially anisotropic ($f_{s,aniso}$) GC velocity distributions after 10 Gyr of evolution for GCs more massive than $10^5 M_\odot$:

$$f_{s,iso} = -0.160 \times \log_{10}(\rho_{3D}) + 0.315, \tag{3.2}$$

$$f_{s,aniso} = -0.182 \times \log_{10}(\rho_{3D}) + 0.216. \tag{3.3}$$

According to the equations (3.2) and (3.3) more GCs get destroyed at higher densities and also the GC survival fraction is higher for an initially isotropic GC velocity distribution function than for a radially

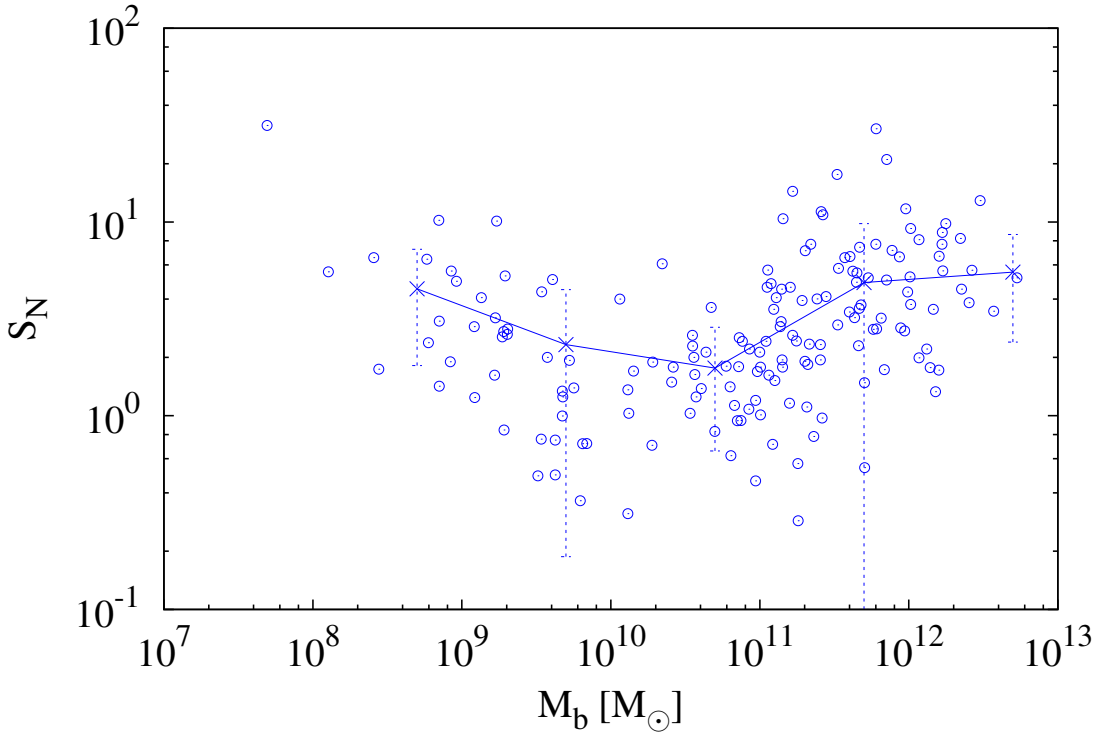

Figure 3.1: The specific frequency of globular clusters versus baryonic galaxy mass for a range of early-type galaxies using the data from Harris et al. (2013). The crosses connected with a line are the average value of S_N per mass bin and the error bars are the standard deviation at the mass bin.

anisotropic one.

The correlation between the S_N and ρ_{3D} has been determined observationally: Figure (3.2) shows the observed present-day GC specific frequency and ρ_{3D} for the same sample as in Figure (3.1), which supports a high erosion of GCs at higher densities. The solid blue line is the bi-variate best fit to the observed data:

$$S_N = (2.77 \pm 0.07) \times (\rho_{3D})^{-0.51 \pm 0.02}, \tag{3.4}$$

This supports the notion that the survival fractions f_s of GCs may be an important aspect of the 'U' -shaped relation between S_N and M_b as suggested by Mieske et al. (2014).

In order to estimate the primordial value of the specific frequency, S_{Ni}, for both cases, isotropic, $S_{Ni,iso}$, and radially anisotropic GC velocity distributions, $S_{Ni,aniso}$, we divide S_N by $f_{s,iso}$ and by $f_{s,aniso}$, respectively,

$$S_{Ni,iso} = \frac{S_N}{f_{s,iso}}, \tag{3.5}$$

$$S_{Ni,aniso} = \frac{S_N}{f_{s,aniso}}. \tag{3.6}$$

The primordial $S_{Ni,iso}$ and the observed present-day specific frequency at different densities are illus-

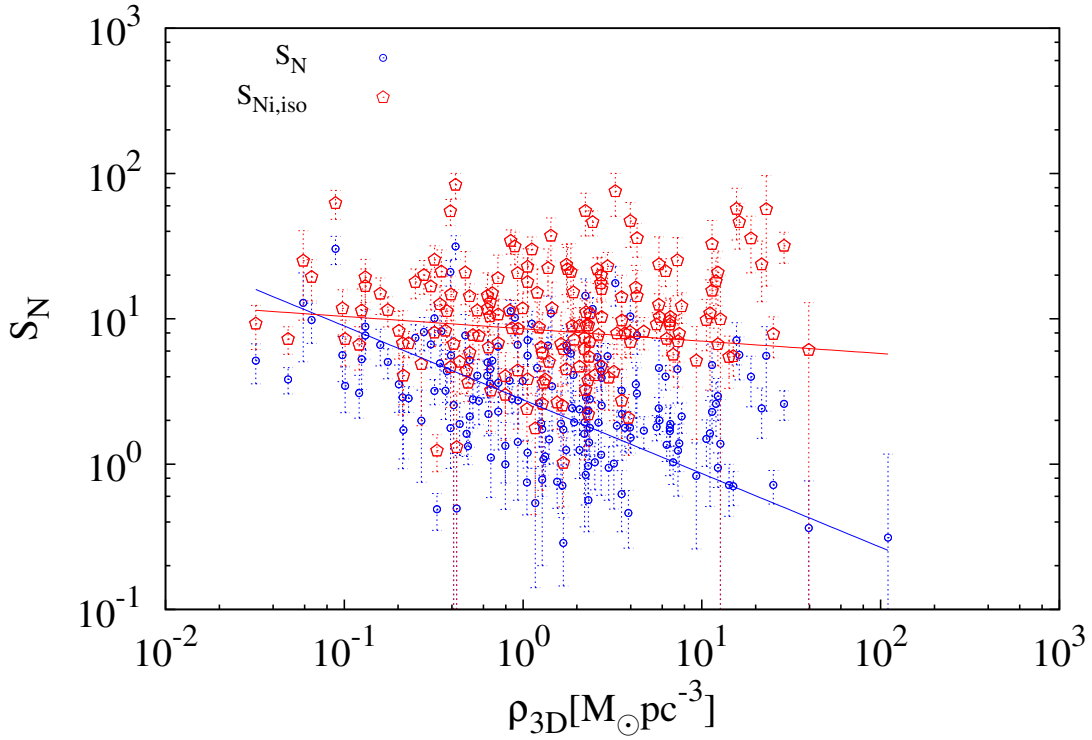

Figure 3.2: The present and primordial values for specific frequencies of globular clusters versus the density (ρ_{3D}) of early-type galaxies. The red open pentagons ($S_{Ni,iso}$) are primordial values for S_N calculated for the isotropic case (equation 3.5). The blue circles are specific frequencies at the present epoch for the same sample as in Figure (3.1). The solid lines are the least square best-fits to the primordial and present cases by weighting with the error (dashed lines) in both directions.

trated in Figure (3.2). As already concluded by Mieske et al. (2014) it emerges that the initial specific frequency (S_{Ni}) has been largely independent of ρ_{3D}. This result has potentially very important implication for our understanding of early galaxy assembly: *S_{Ni} being nearly constant with density, the efficiency of forming young GCs is about the same for all early- type galaxies from dEs to Es, suggesting that the same fundamental principle was active, independent of the mass of the galaxy.*

The primordial values of the number of globular clusters for the isotropic, $N_{GCi,iso}$, and anisotropic, $N_{GCi,aniso}$, cases is calculated by dividing the observed number of globular clusters N_{GC} by the GC survival fractions $f_{s,iso}$ and $f_{s,aniso}$, respectively,

$$N_{GCi,iso} = \frac{N_{GC}}{f_{s,iso}}, \tag{3.7}$$

$$N_{GCi,aniso} = \frac{N_{GC}}{f_{s,aniso}}. \tag{3.8}$$

The primordial number of GCs increases monotonically with host galaxy mass. Figure (3.3) shows this relation for $N_{GCi,iso}$ (red pentagons) and N_{GC} (blue circles) as a function of M_b. Filled symbols are galaxies with a mass smaller than 5×10^9 $M_\odot$ denoted by Branch I (BI), while open symbols are galaxies

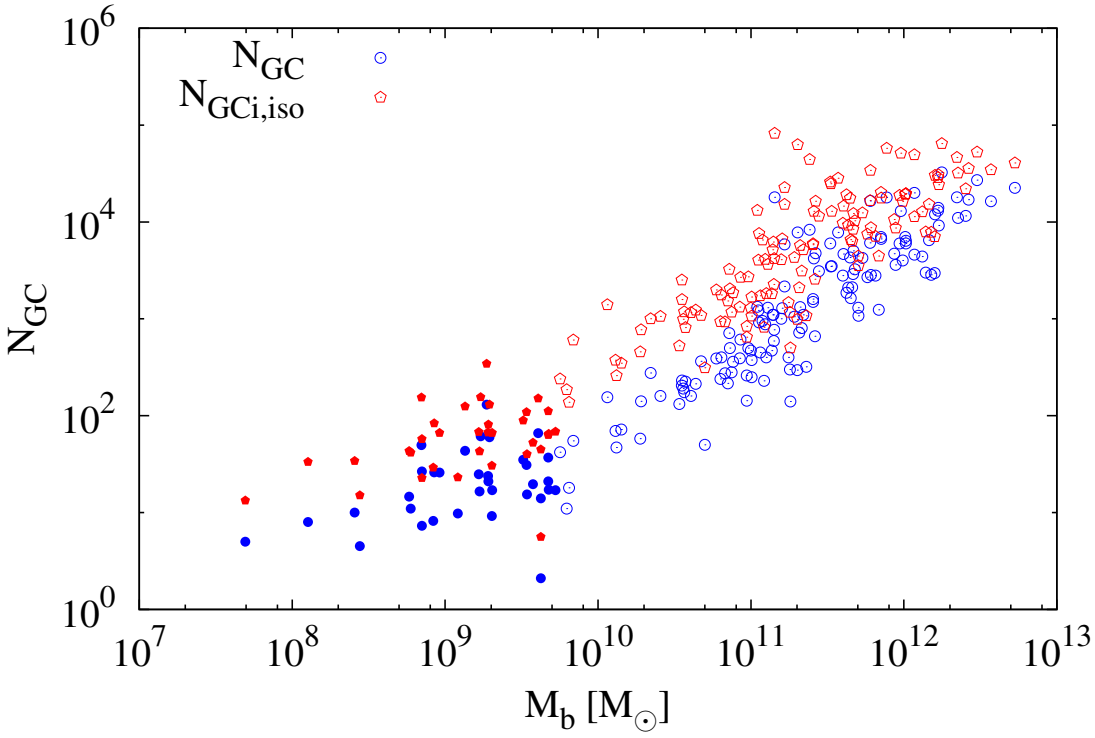

Figure 3.3: The primordial number of GCs (red pentagons) and the present-day number of GCs (in blue, lower points) versus the baryonic mass of a galaxy. The solid symbols are dE galaxies with stellar mass $< 5 \times 10^9 M_\odot$, while open symbols denote more-massive E-type galaxies.

with a mass larger than 5×10^9 $M_\odot$ denoted by Branch II (BII). Galaxies in branch I are dEs, while E galaxies are in branch II. The present-day number of GCs, N_{GC}, is lower than $N_{GCi,iso}$, especially for galaxies at intermediate-mass because of the high destruction rates of GCs. If the fundamental physical processes acting during the assembly of dE and E galaxies were the same, the former formed fewer GCs because their SFRs were much smaller than during the formation of E galaxies (Weidner et al., 2004; Randriamanakoto et al., 2013).

3.3 The $M_{ecl,max}$ - SFR correlation and the star cluster formation time-scale (δt)

An empirical relation has been derived by Recchi et al. (2009) for dE and E galaxies between the central velocity dispersion σ [km/s] that reflects the total stellar mass and the stellar alpha-element abundance [α/Fe]. The implied star formation duration, ΔT [yr], over which the galaxy assembled, inversely correlates with the mass M_b [$M_\odot$] of the galaxy (this is referred to as downsizing),

$$\Delta T = 10^{(11.38 - 0.24 \times \log_{10}(M_b))}. \quad (3.9)$$

Knowing the total baryonic mass of a galaxy, M_b, and ΔT, the star formation rate (SFR) follows as illustrated in Figure (3.4),

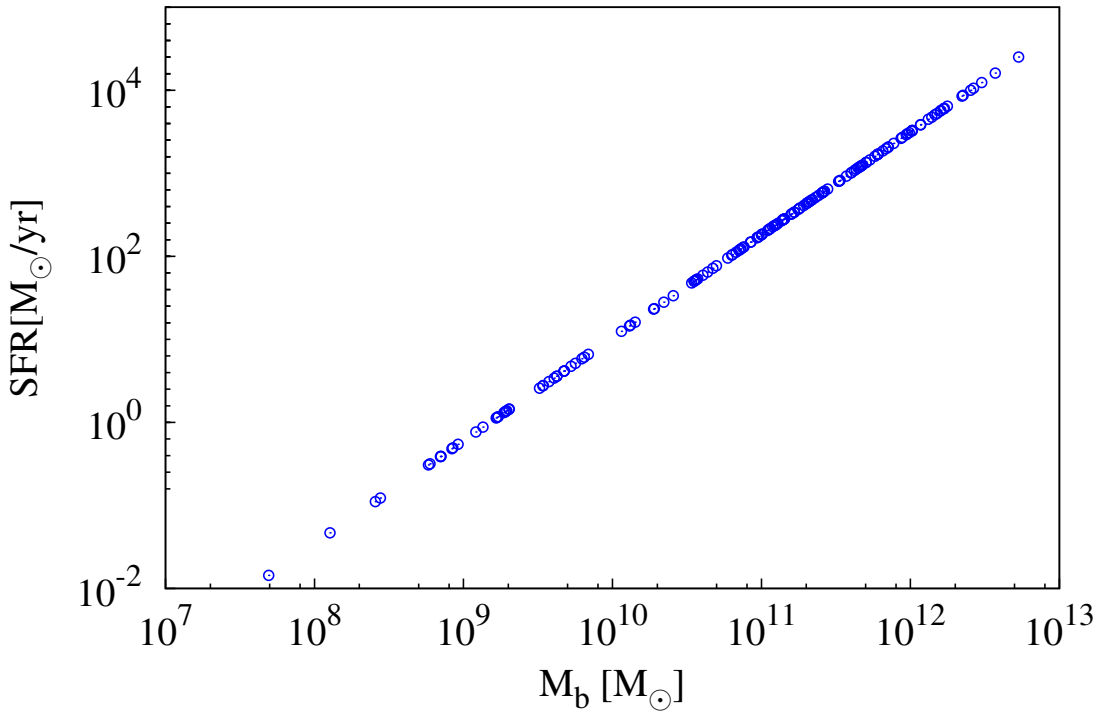

Figure 3.4: The star formation rates (SFR) as a function of M_b, with the SFR from the ΔT-mass relation of Recchi et al. (2009) (their equation (19)). The M_b values are taken from the Harris catalogue (Harris et al., 2013).

$$SFR = \frac{M_b}{\Delta T}. \tag{3.10}$$

The time during which GCs formed (Δt_1) is part of the time scale of star formation in galaxies (ΔT), $\Delta t_1 < \Delta T$ as shown in Figure (3.5). Each part is divided into star cluster formation epochs of equal length δt, which we will calculate later (Figure 3.6). Assuming that all the stars form in star clusters (Lada & Lada, 2003; Kroupa, 2005), the total mass of the star cluster system ($M_{tot,\delta t}$) formed during a characteristic time-scale for star formation, δt, can be calculated using the SFR and δt,

$$M_{tot,\delta t} = SFR \times \delta t. \tag{3.11}$$

Observational studies suggest that the masses and embedded of young star-clusters are distributed as a power law:

$$\xi_{ecl}(M_{ecl}) = K_{ecl}\left(\frac{M_{ecl}}{M_{ecl,max}}\right)^{-\beta} \tag{3.12}$$

where ξ_{ecl} is the mass distribution function of the embedded clusters, K_{ecl} is a normalization constant and M_{ecl} is the stellar mass of the embedded cluster. The power law slope β is found to be between 1.2 and 2.5 (Elmegreen & Efremov, 1997; Lada & Lada, 2003; Kroupa & Weidner, 2003; Weidner et al., 2004; Whitmore et al., 2010; Chandar et al., 2011).

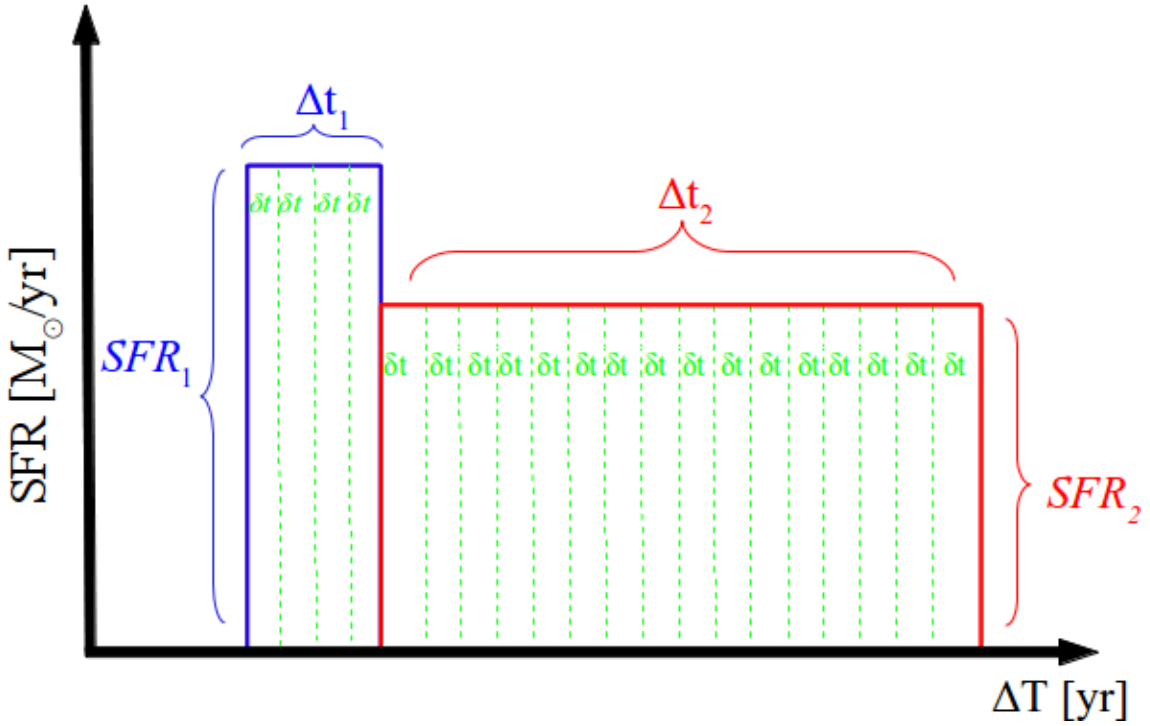

Figure 3.5: Schematic drawing of the duration ΔT from Recchi et al. (2009) (divided into formation epochs of length δt) and the star formation rates (SFR) for the whole galaxy. SFR_1 is the SFR of forming the GC system over time Δt_1 and the rest of galaxy form with SFR $_2$ over time Δt_2. Δt_1 is plotted here as pounding Δt_2 for illustrative purpose only.

The total mass of a population of star clusters, $M_{tot,\delta t}$, assembled within the time span δt can also be expressed as follows

$$M_{tot,\delta t} = \int_{M_{min}}^{M_{ecl,max}(SFR)} \xi_{ecl}(M_{ecl}) M_{ecl} dM_{ecl}, \tag{3.13}$$

where M_{min} is the minimum mass of a star cluster and $M_{ecl,max}$ is the maximum star cluster mass depending on the SFR (Weidner et al., 2004). M_{min} can be assumed to be 5 $M_\odot$, which is about the lowest mass cluster observed to form in the nearby Taurus-Auriga aggregate (Briceño et al., 2002; Kroupa & Bouvier, 2003; Weidner et al., 2004).

In order to determine the normalization constant K_{ecl} in equation (3.12) we use the same assumption as in Weidner et al. (2004) that $M_{ecl,max}$ is the single most massive cluster. For $\beta > 1$ and $\beta \neq 2$ (equation 3.15 undefined) we get

$$K_{ecl} = \frac{\beta - 1}{M_{ecl,max}} \tag{3.14}$$

and equation (3.13) becomes,

$$M_{tot,\delta t} = M_{ecl,max}^{\beta-1} \left(M_{ecl,max}^{2-\beta} - M_{min}^{2-\beta} \right) \frac{\beta - 1}{2 - \beta}. \tag{3.15}$$

In order to determine $M_{ecl,max}$ we correlate the theoretical upper mass limit of the star clusters and the most massive star cluster, using the same criteria as Schulz et al. (2015), which requires only one most

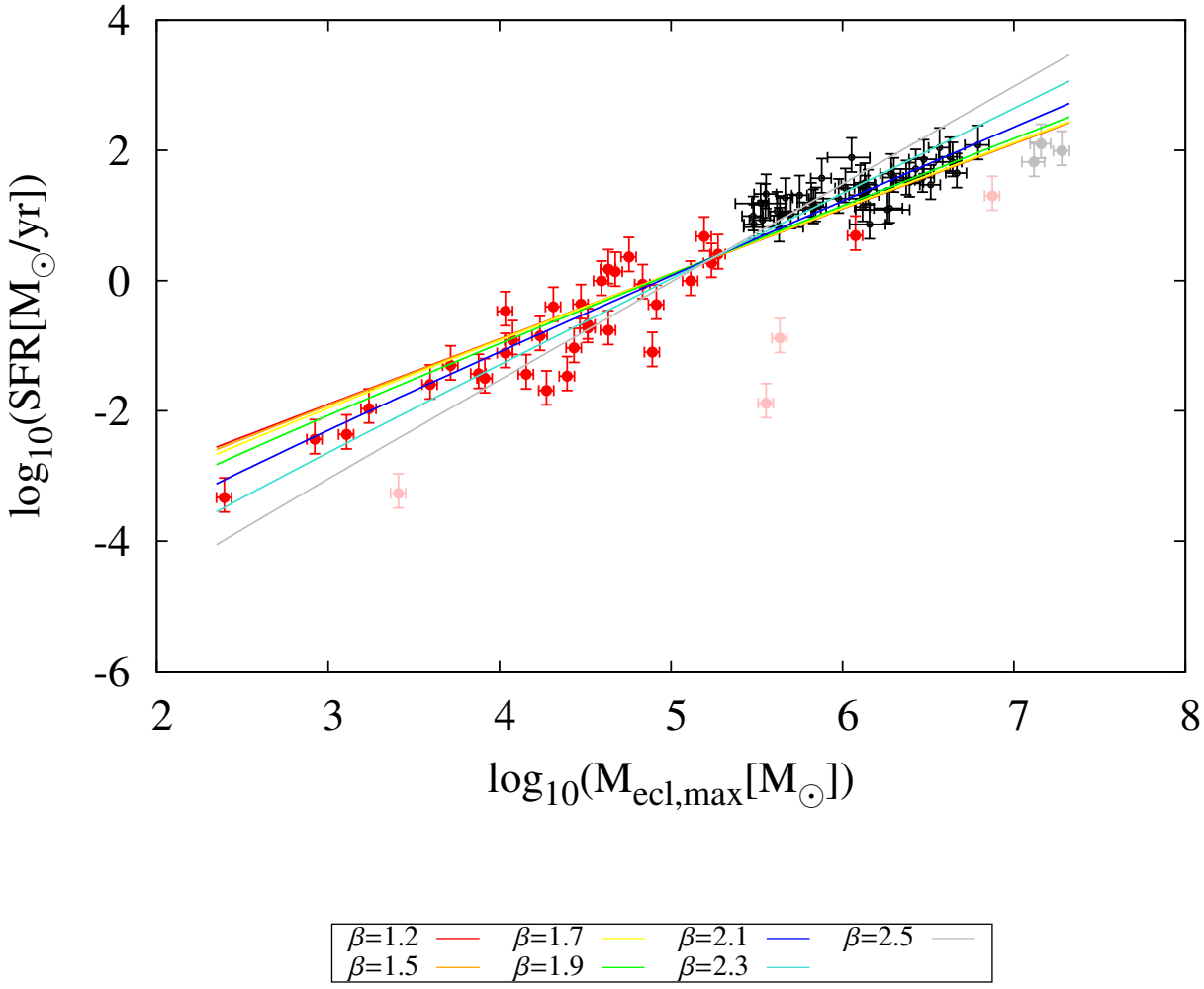

Figure 3.6: The cluster-system formation time-scale, δt, is determined by fitting the SFR - $M_{ecl,max}$ relation from equation (3.16) to all data points using a weighted least-squares method. The δt increases with increasing β (β = 1.2, 1.5, 1.7, 1.9, 2.1, 2.3 and 2.5). The observational data (red circles) are taken from Weidner et al. (2004) with additional recent data points (black circles) from Randriamanakoto et al. (2013). The faded color points are galaxies which were excluded from the least-square fits (see Section 3.3 for details).

massive cluster to exist ($1 = \int_{M_{ecl,max}}^{M_{ecl,max*}} \xi_{ecl}(M_{ecl})dM_{ecl}$, where the theoretical upper mass limit ($M_{ecl,max*}$) $\gg M_{ecl,max}$).

According to the conditions above and by combining equation (3.11) and (3.15) we obtain a relation between the SFR and $M_{ecl,max}$ for $\beta > 1$ and $\beta \neq 2$:

$$SFR = \frac{M_{ecl,max} S^{-1}}{\delta t} \left(1 - \left(\frac{M_{min} S}{M_{ecl,max}} \times \frac{\beta - 1}{2 - \beta}\right)^{2-\beta}\right) \tag{3.16}$$

with $S = (1 - 2^{\frac{2-\beta}{1-\beta}})$.

Table 3.1: Time scale for star formation, δt, for different embedded cluster mass function slopes (β). The χ^2_{red} is extracted from the fits in Figure (3.6).

β	δt [10^6yr]	χ^2_{red}
1.2	0.08	1.78
1.5	0.16	1.76
1.7	0.29	1.69
1.9	0.69	1.53
2.1	2.3	1.33
2.3	11	1.47
2.5	64.2	2.33

Observations indeed indicate that young massive star clusters follow a relation between the visual absolute magnitude of the brightest young cluster and the global SFR of the host galaxy (Larsen, 2002). Based on this evidence Weidner et al. (2004) found a relation between the galaxy-wide SFR and the maximum star-cluster mass. As indicated in equation (3.11) the total mass depends on the current SFR at a certain δt such that $M_{ecl,max}$ depends on the SFR (equation 3.16), which has also been determined observationally (Larsen & Richtler, 2000; Weidner et al., 2004). It follows that galaxies with a high SFR are forming high-mass clusters.

The resulting relation between the SFR and the mass of the most massive cluster is illustrated in Figure (3.6). The data are from Weidner et al. (2004) and Randriamanakoto et al. (2013). We converted the luminosity of the brightest star cluster in the V-band to the most massive star-cluster mass using equation (5) from Weidner et al. (2004). We used these data to determine the length of the formation epoch δt. The uncertainties on SFR were obtained from the uncertainties in conversion of the IR luminosity to a SFR. On the other hand the uncertainties in $M_{ecl,max}$ come from uncertainties in the conversion of luminosities to masses.

We exclude seven galaxies (faded colors) in Figure (3.6) from this population: The first four galaxies are excluded since the SFRs of these dwarf galaxies do not represent the birth of these clusters (further details can be found in Weidner et al. (2004); Schulz et al. (2015)). The last three galaxies (gray) have a luminosity distance from the NED database larger than 150 Mpc. Randriamanakoto et al. (2013) suggested that these brightest super star clusters might be contaminated by other clusters. The cluster-system formation time-scale, or the duration of the star formation 'epoch', δt, is determined by fitting equation (3.16) for β = 1.2, 1.5, 1.7, 1.9, 2.1, 2.3 and 2.5. to the data (Figure 3.6). The best value of δt as a function of β is determined by the reduced chi-squared statistic, χ^2_{red}. As can be seen in Table (3.1) and Figure (3.6), δt increases with β. This result agrees with Schulz et al. (2015), who found by comparison with the literature that β lies between 1.8 and 2.4. Also it is consistent with the analysis by Weidner et al. (2004). The typical star formation time-scale of about 10^7yr has also been deduced from calculations of the Jeans time in molecular clouds (e.g. Egusa et al., 2004). The star formation time-scale can also be determined from examining offsets between $H\alpha$ and CO arms of a spiral galaxy as proposed by Egusa et al. (2009), who found the star formation time to be between 4 - 13 Myr. Thus, every $\delta t \approx 10$ Myr a new population of star clusters hatches from the ISM of a star forming galaxy, which follow the embedded cluster mass function (ECMF).

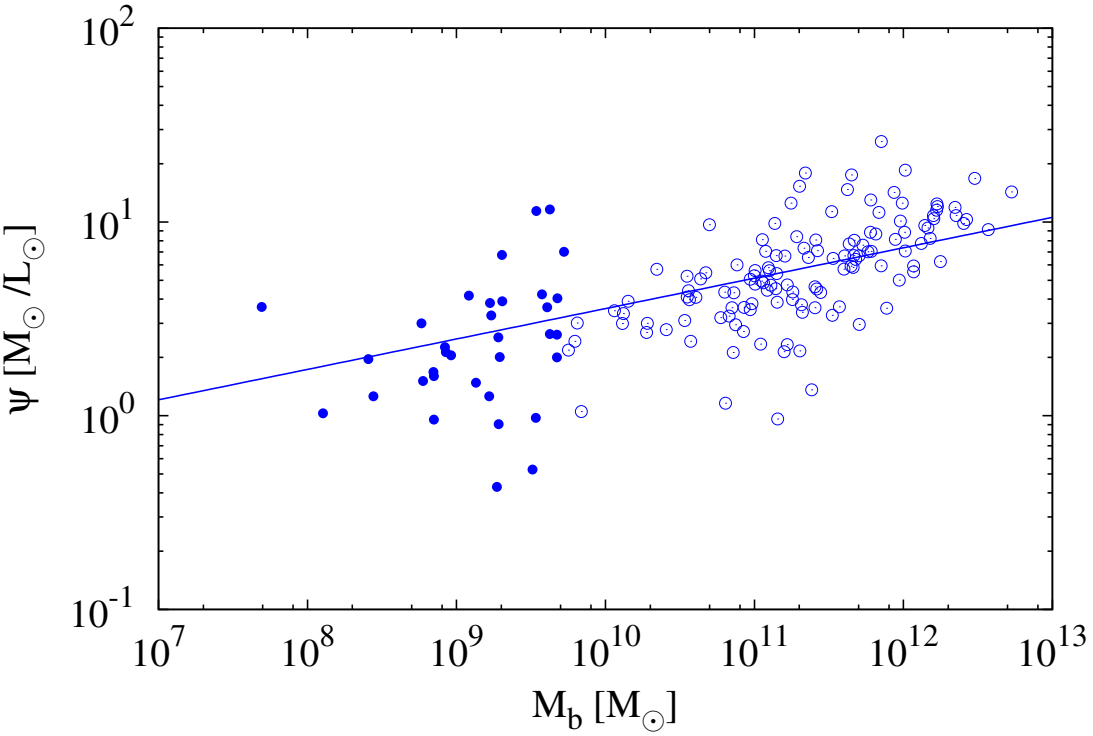

Figure 3.7: The mass-to-light ratio, ψ, of the galaxies in the V- band as a function of M_b, for the same sample as in Figure (3.1).

3.4 Theoretical specific frequency ($S_{N,th}$)

The theoretical model of the specific frequency of globular clusters ($S_{N,th}$) is based on the notion that star clusters are the basic building blocks of a galaxy (Kroupa, 2005). With equation (3.1), we derive an analytical model for $S_{N,th}$, which is the theoretical number of globular clusters, $N_{GC,th}$, per unit galaxy luminosity. The galaxy luminosity can be converted into a mass such that:

$$S_{N,th} = \frac{N_{GC,th}}{M_b} \times \psi 10^{7.9} L_\odot, \tag{3.17}$$

where ψ is the mass-to-light ratio of the galaxy in the appropriate photometric band. Figure (3.7) shows ψ for the photometric band by using the same sample as in Figure (3.1). The best least square fit suggests,

$$\psi = a\left(\frac{M_b}{10^6}\right)^b, \tag{3.18}$$

with a = 0.80 ± 0.13 and b = 0.15 ± 0.01.

In order to estimate $S_{N,th}$ from equation (3.17), the number of globular clusters ($N_{GC,th}$) is required. The number of GCs which formed during δt can be calculated using the ECMF,

$$N_{GC} = \int_{M_{ecl,min}}^{M_{ecl,max}(SFR)} \xi_{ecl}(M_{ecl}) dM_{ecl}, \tag{3.19}$$

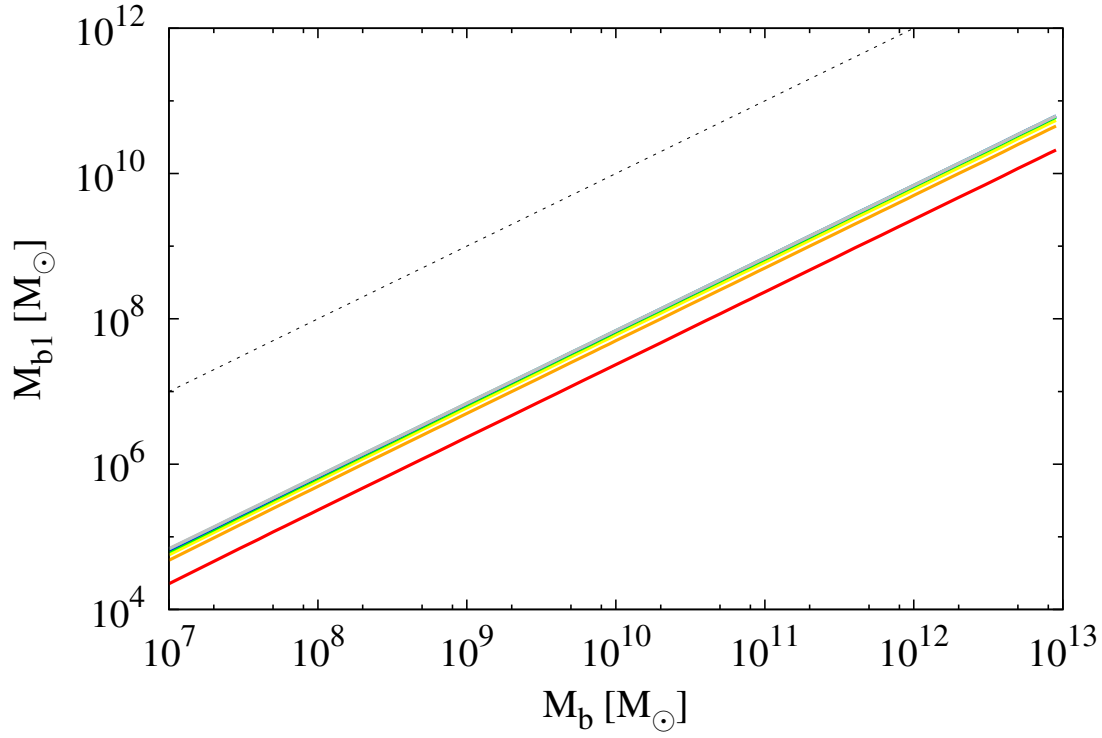

Figure 3.8: The baryonic mass of galaxies (M_b) versus the total masses of GCs (M_{b1}) which form in time Δt_1 (time over which the GC system formed), $M_{b1} = M_{tot,\delta t} \times \frac{\Delta t_1}{\delta t}$. The SFR is assumed to be constant during δt, Δt_1 and Δt_2. The coloured lines are for different β (the same as Figure (3.6)). The dashed line indicates the 1:1 line.

To give

$$N_{GC,th} = \frac{(\beta-1)M_{ecl,max}^{\beta}}{(1-\beta)M_{ecl,max}}\left[M_{ecl,max}^{1-\beta} - {M_{ecl,min}}^{1-\beta}\right] \times \frac{\Delta t_1}{\delta t}. \tag{3.20}$$

From the SFR - $M_{ecl,max}$ relation (Figure 3.6) and to calculate $M_{ecl,max}$ we assume two cases of SFR, in case one the SFR is constant over the time scales δt, Δt_1 and Δt_2, in case two the SFR is not constant over the δt, Δt_1 and Δt_2. The minimum mass of globular clusters ($M_{ecl,min}$) is assumed to be 10^3, 10^4, 10^5 and $10^6 M_\odot$. Note the difference between M_{min} in equation (3.15) and $M_{ecl,min}$ in equation (3.20), since M_{min} is the physical lower limit for the cluster mass (Weidner & Kroupa, 2004).

3.4.1 Constant SFR over δt, Δt_1 and Δt_2

In order to calculate the maximum mass of old cluster systems, we assume that the young and old cluster population formed with the same star-formation time scale, δt, which depends on β. From this assumption we calculate maximum masses of the old cluster system at a given SFR (equation 3.16). In this model the SFR is supposed to be constant over different time scales, i.e., for δt, Δt_1 and Δt_2. After calculating the $M_{ecl,max}$ for an old GC system, we can measure the total mass M_{b1}, which forms within the time scale Δt_1 by using equation (3.15), with $M_{b1} = M_{tot,\delta t} \times \frac{\Delta t_1}{\delta t}$. Figure (3.8) shows M_b versus M_{b1}, which indicates that M_{b1} is smaller than M_b.

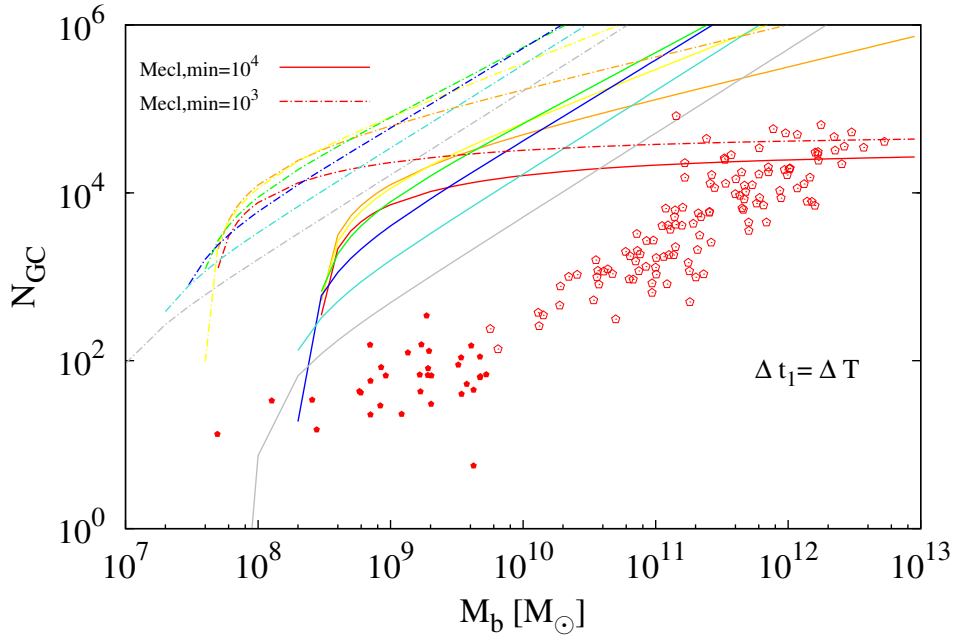

(a)

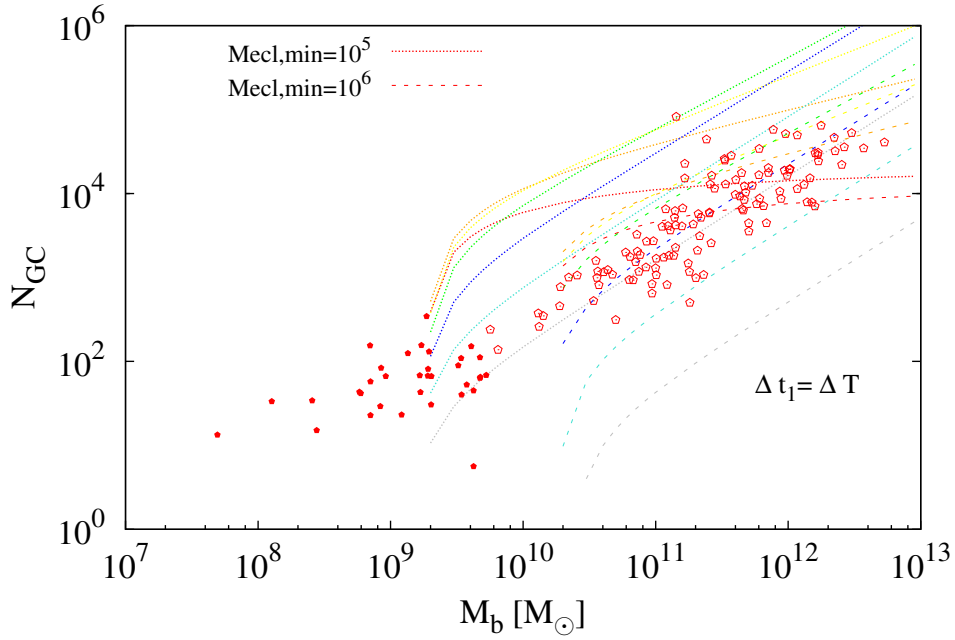

(b)

Figure 3.9: Comparison between the primordial value (red pentagons) of the number of globular clusters, $N_{GCi,iso}$, and the theoretical number ($N_{GC,th}$) of globular clusters (coloured lines). Filled pentagons are dE galaxies with masses $< 5 \times 10^9 M_\odot$ (BI) while open pentagons are E galaxies with masses $> 5 \times 10^9 M_\odot$ (BII). The coloured lines are our models for different β of the ECMF ranging between 1.2 to 2.5 (red to gray as in Figure 3.6). In the upper panel (a), we plot the primordial values for the number of globular clusters, $N_{GCi,iso}$, and the model at $M_{ecl,min} = 10^3 M_\odot$ (dash-dotted lines) and $M_{ecl,min} = 10^4 M_\odot$ (solid lines) for $\Delta t_1 = \Delta T$. In the lower panel (b), we plot $N_{GCi,iso}$ and a model with $M_{ecl,min} = 10^5 M_\odot$ (dotted lines), $M_{ecl,min} = 10^6 M_\odot$ (dashed lines) and for $\Delta t_1 = \Delta T$. Note that the SFRs of dE galaxies are too small to allow the formation of cluster with $M_{ecl,min} \geqslant 10^5 M_\odot$.

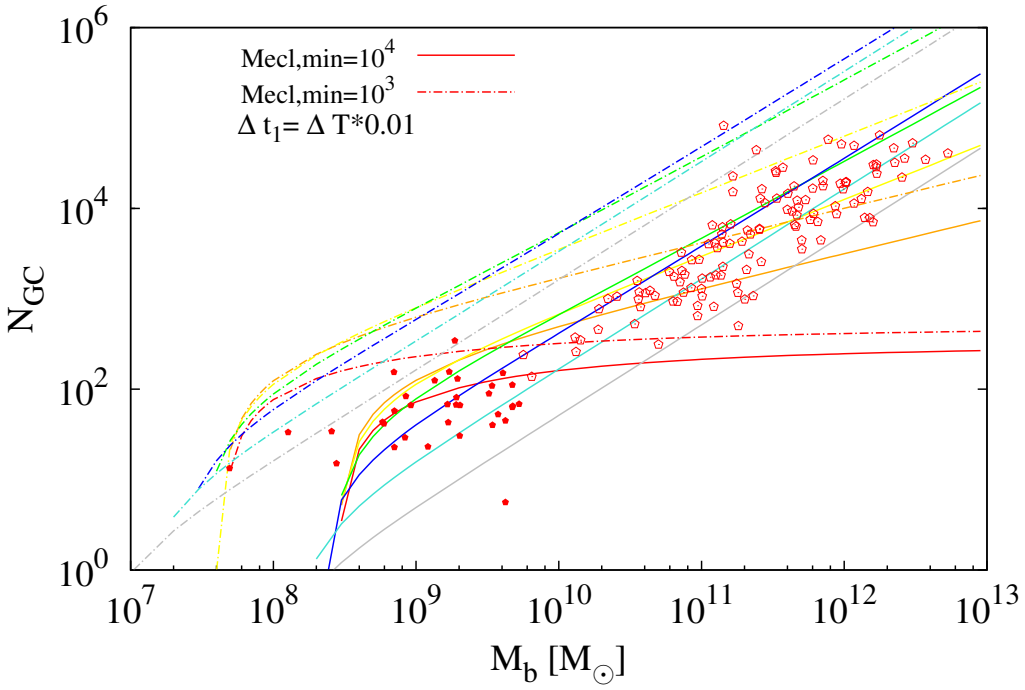

(a)

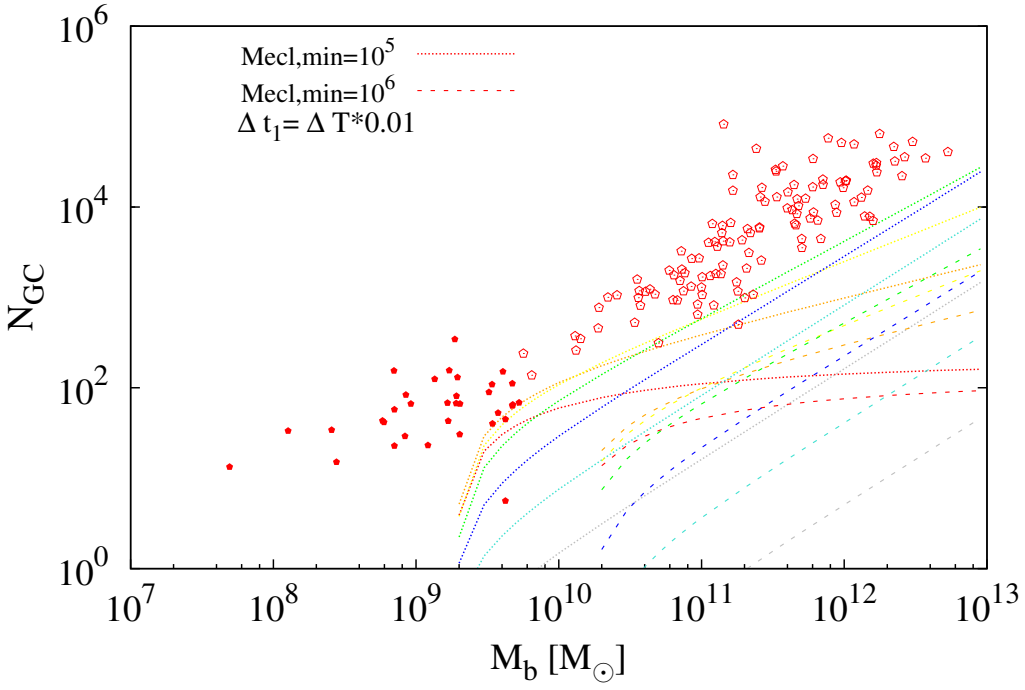

(b)

Figure 3.10: Same as Figure (3.9) but for a model with $\Delta t_1 = \Delta T \times 0.01$.

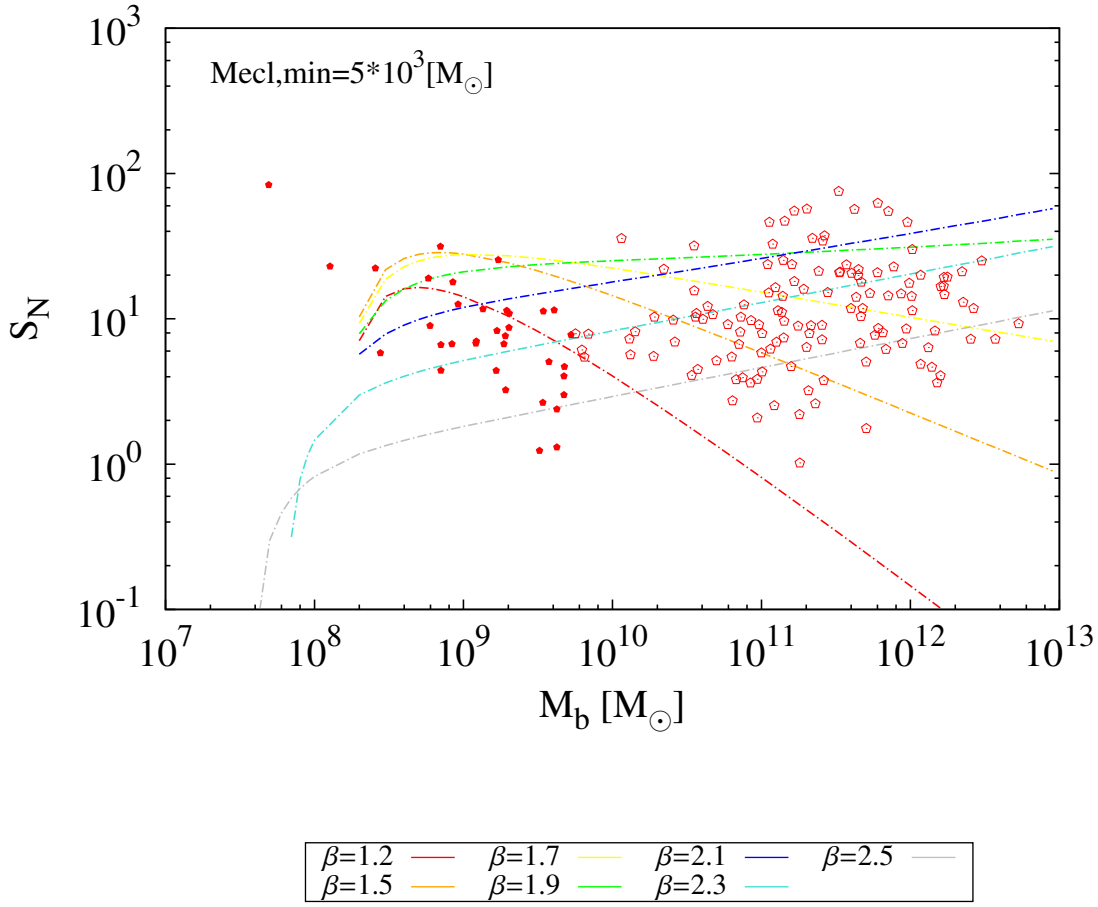

Figure 3.11: Comparison between the primordial value of the specific frequency of globular clusters and the theoretical specific frequency for $M_{ecl,min} = 5 \times 10^3 M_\odot$ at $\Delta t_1 = \Delta T \times 0.005$. The coloured lines indicate our model for different β. The symbols are as in Figure (3.9).

Having obtained $N_{GC,th}$ and M_b and using ψ in the V- band from equation (3.18), we can compute $S_{N,th}$. Due to stellar evolution, dissolution and disruption by dynamical friction or tidal effects, the mass of a star cluster significantly decreases after its birth (e.g. Baumgardt & Makino, 2003; Brockamp et al., 2014). By correcting the observed N_{GC} (equation 3.7) and S_N (equation 3.5) for the erosion of GCs through tidal action or through dynamical friction, we obtain an estimate of the primordial values for each galaxy in our sample (Section 3.2).

3.4.1.1 Comparison between the theoretical model and primordial value of N_{GCi} and S_{Ni}

We investigate the influence of the two parameters β and $M_{ecl,min}$ on N_{GCi} and S_{Ni}. For this purpose, we calculate the model for seven values of β (1.2, 1.5, 1.7, 1.9, 2.1, 2.3 and 2.5), and for four different values of $M_{ecl,min}$ (10^3, 10^4, 10^5 and $10^6 M_\odot$). Since the overall distribution of $S_{Ni,iso}$ and $S_{Ni,aniso}$ is similar (Mieske et al., 2014), we present the model only for the isotropic case.

The E and dE galaxies formed under different physical boundary conditions (Dabringhausen & Kroupa,

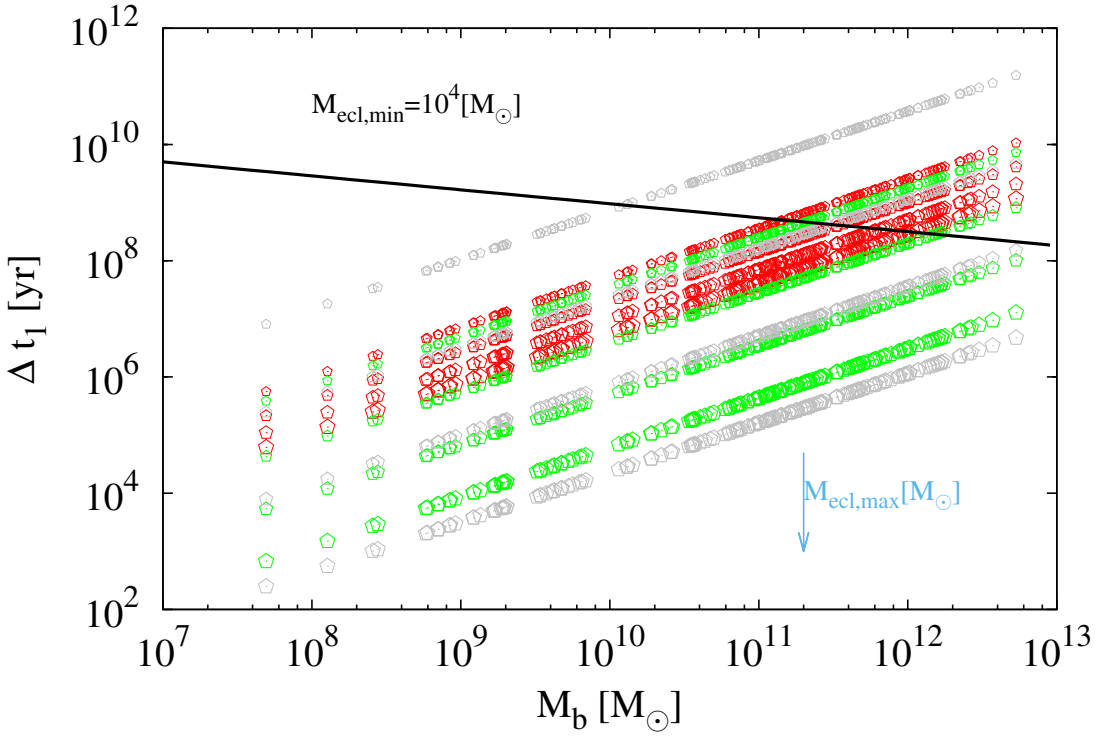

Figure 3.12: The time of GCs formation, Δt_1, versus baryonic mass of a galaxy at $M_{ecl,min}=10^4 M_\odot$. The solid line is the time for forming the whole galaxy, ΔT, from Recchi et al. (2009) (see also Figure 1.2). The colors points are for different β of the ECMF β= 1.2, 1.9 and 2.5 (red, green and gray). Increasing symbol size indicate a higher maximum cluster mass.

2013), which need different formation time-scales. We assume two values for Δt_1: firstly we assume Δt_1 to be equal to ΔT and secondly we assume it to be less than ΔT ($\Delta T \times 10^{-2}$). This is to represent the formation epoch of the GC population which is likely to have been much shorter than the assembly time of the entire galaxy. Figure (3.9) shows the comparison between the primordial number of globular clusters ($N_{GCi,iso}$) and the theoretical number of globular clusters ($N_{GC,th}$) for different β and $M_{ecl,min}$ and for $\Delta t_1 = \Delta T$, Δt_2 =0. The model does not represent the observational data well, unless a larger $M_{ecl,min}$ is chosen. On the other hand, by using a smaller Δt_1, $\Delta t_1 = \Delta T \times 0.01$, we match the observational data in BI and BII at lower $M_{ecl,min}$ (Figure 3.10). Thus, from Figures (3.9) and (3.10) we conclude that solutions are degenerate, the model does not need to be fine-tuned to account for the data.

In Figure (3.11), we present the best model for $S_{N,th}$ to match $S_{N,i}$ by setting $M_{ecl,min}$ to be $5\times10^3 M_\odot$ with $\Delta t_1 = \Delta T \times 0.005$. It follows that dE galaxies are best represented by a model in which their GC population formed on a time scale $\Delta t_1 \approx 0.005\Delta T$ with $M_{ecl,min} \approx 10^3 M_\odot$ and $\beta \approx 1.5$. E galaxies require a similar short time for the formation of their GC population but $M_{ecl,min} \gtrsim 5 \times 10^3 M_\odot$ and $\beta \approx 2.3$. Thus, the dE galaxies may have formed their GC population with a somewhat top-heavy ECMF, while star-bursting galaxies had an approximately Salpeter ECMF. However, this conclusion is not unique, because solution to the dE galaxies with $\beta \approx 2.3$ and also possible by increasing the ratio $\frac{\Delta t_1}{\Delta T}$.

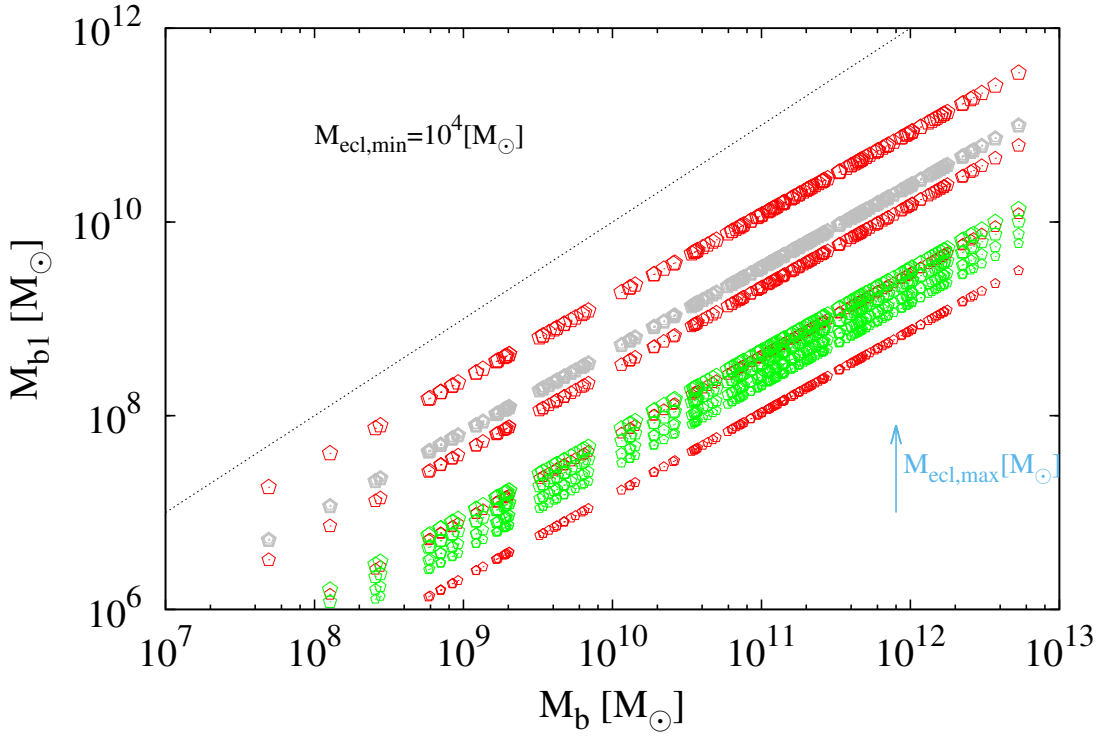

Figure 3.13: The fraction of a galaxy formed during Δt_1 versus baryonic mass of a galaxy at $M_{ecl,min}=10^4 M_\odot$. The dotted line indicates the 1:1 line. The color points and symbol sizes are the same as in Figure (3.12).

3.4.2 SFR not constant over δt, Δt_1 and Δt_2

In the following we compute the primordial value of the number of GCs as a function of galaxy mass. As shown in Figure (3.5), SFRs need not be constant during time, at least over time scales Δt_1 (SFR_1) and Δt_2 (SFR_2). By using equation (3.20) and the observational data (Figure 3.3) for $N_{GCi,iso}$, we can estimate Δt_1. We set the minimum star cluster mass equal to $10^4 M_\odot$, as Baumgardt & Makino (2003) suggested this as the minimum mass remaining which is bound as a cluster after 13 Gyr. We calculate the time scale Δt_1 for $M_{ecl,max}$ ranging between 10^5 and $10^8 M_\odot$ and for different β for clarity, we display only β= 1.2, 1.9 and 2.5, see Figure (3.12). The solid black line indicates the star formation duration, ΔT, as defined by equation (3.9). Above this line, solutions become unphysical. The $M_{ecl,max}$ increases with decreasing Δt_1 and the difference of model data points between different Δt_1 increases with β.

We calculated M_{b1} ($M_{b1} = M_{tot,\delta t} \times \frac{\Delta t_1}{\delta t}$) and compare these results to M_b. In Figure (3.13) we directly compare the total mass which forms in Δt_1 and the total baryonic mass of a galaxy. M_{b1} becomes unphysical above the dotted line, because the fraction of the galaxy M_{b1} can't become larger than the total galaxy mass M_b. As expected M_{b1} (mass of GCs) is smaller than M_b (mass of galaxy) (Figure 3.13).

Weidner et al. (2004) suggested a star-cluster formation time scale of about $10^7 [yr]$. Using this and the galaxy formation time scale ΔT from downsizing (Recchi et al., 2009), we set Δt_1 between 10^7 and 5×10^8 $[yr]$. This is to obtain a physically realistic time scale for GC formation. By using equation (3.20), we obtain $N_{GC,th}$ depending on $M_{ecl,max}$ and Δt_1. In Figure (3.14) we compare the primordial

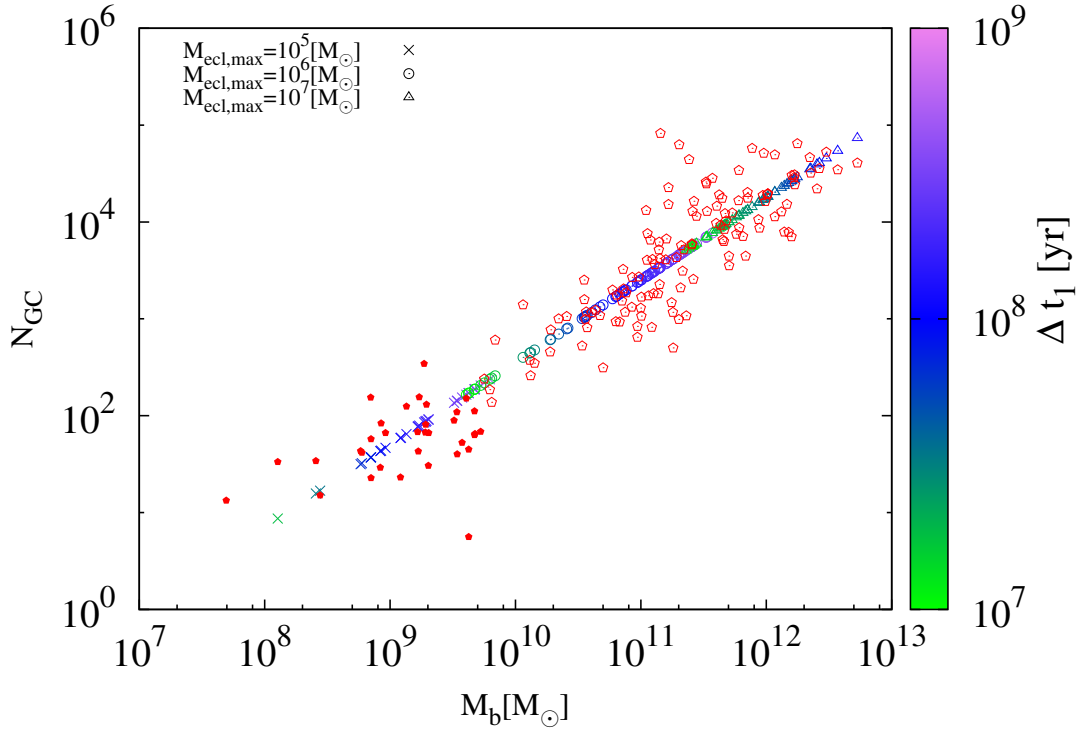

Figure 3.14: Comparison between the observationally derived primordial value of number of globular clusters ($N_{GC,iso}$) and the theoretical number of globular clusters ($N_{GC,th}$) for $M_{ecl,min}=10^4 M_\odot$. The colour scale indicates different Δt_1.

and theoretical values of $N_{GC,th}$ for $M_{ecl,min} = 10^4 M_\odot$ and $\beta = 2.3$ (since only β equal to 2.3 or 2.5 can match $N_{GC,iso}$ at Branch I and II). Figure (3.14) clearly indicates that $M_{ecl,max}$ increases with increasing $N_{GC,iso}$, and $\Delta t_1 \approx 10^8$ $[yr]$ represents most of the $N_{GC,iso}$. The $S_{N,th}$ can be estimated using equation (3.17) after obtaining $N_{GC,th}$ (Figure 3.15).

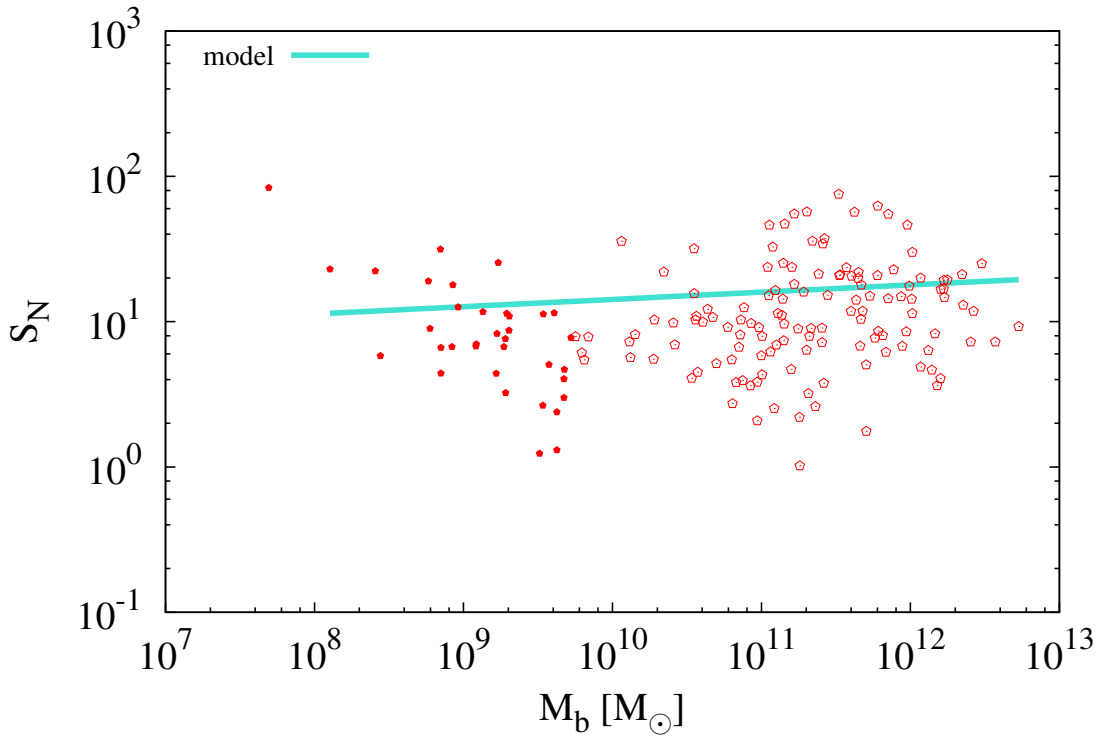

Figure 3.15: Theoretical specific frequency as a function of baryonic galaxy mass (M_b) at β = 2.3. The symbols are as in Figure (3.9).

CHAPTER 4

Conclusion

4.1 Conclusion

The history of galaxy assembly and the subsequent evolution of galaxies has been considered an important issue for a long time. In this thesis, I investigate this subject in Chapter 2 and Chapter 3 by studying the galaxy's spin (angular momentum) with respect to the filament, and by studying the relation between properties of a GC system and the mass of their parent galaxy, respectively.

The first part of this thesis (Chapter 2) examines the correlation between the filaments and rotation axes of galaxies. The origin of galactic angular momentum is considered an important indicator to understand the formation and evolution of galaxies. Different scenarios of galaxy formation predict different spin vector alignments of galaxies. To this aim, we studied the spatial orientations of the spin vector (SVs) of galaxies in their hosting filament. The angle θ between the projected SVs of galaxies and their host filaments are measured for 302 spiral galaxies in 19 filaments using the data from the Hyper-linked Extragalactic Database (HYPERLEDA). Using *linear regression* to define the filaments we divided the whole sample into 19 structures that contained 302 spiral galaxies, and used the position angle (PA) to derive the spin angle relative to the hosting filament. Two statistical methods are applied to describe the thickness of the filaments and the goodness of fit: the root mean square error and coefficient of determination. We found no preferred orientation of the SVs of spiral galaxies with respect to their hosting filaments. This result supports the hierarchical scenario (Peebles, 1969; Thuan & Gott, 1977) where the directions of the galaxy formation spin vectors should be random. We constructed a catalogue of filaments containing the distance and angles between the SVs of spiral galaxies and host filaments.

The second part of this thesis (Chapter 3) aims to study and construct a model for the GC specific frequency.
The properties of GC systems are considered to be tracers for the formation and evolution of galaxies in this work. The specific frequency of GCs is a basic parameter to describe the GC system of a galaxy. The overall trend indicates high values of S_N at opposite ends of the galaxy mass scale, while for a galaxy baryonic mass of around $10^{10}\mathrm{M}_{\odot}$, S_N approaches one. This thesis studied the 'U'-shaped relation between S_N and $\mathrm{M_b}$. The idea followed here extends the notion raised by Mieske et al. (2014) who explained this 'U'-shaped relation through tidal erosion. The most important driver of the erosion process is a tidal field. This idea is supported by showing the correlation between S_N and 3D mass density (ρ_{3D}). For this analysis, we used the Harris catalogue (Harris et al., 2013).

The GC survival fraction depends linearly on $\log_{10}(\rho_{3D})$, i.e., more GCs get destroyed in galaxies with a higher density which then have a smaller value of S_N. It emerges that the primordial value of the specific frequency, S_{Ni}, started approximately independently of the baryonic galaxy mass, $\mathrm{M_b}$, but later changed to a 'U'-shape as a result of tidal erosion, which suggests that all early type galaxies had nearly the same efficiency of forming young GCs.

The primordial number of clusters for the radially anisotropic ($f_{s,aniso}$) GC velocity distribution case is

higher than that of initially isotropic ($f_{s,iso}$) velocity distribution because the erosion rate of GCs depends on the degree of radial velocity anisotropy of the GC system (Brockamp et al., 2014). It follows that the efficiency of massive star cluster formation is approximately constant with the baryonic mass of the galaxy. A significant amount of massive clusters were able to form due to high star formation rates (SFR) (e.g. Weidner et al., 2004). We determined the star cluster formation time-scale (δt) by fitting the SFR-$M_{ecl,max}$ (maximum star cluster mass) relation at higher SFR than previously known.

The work presented in this thesis provides a first approach towards a better understanding S_{Ni} by presenting a new theoretical model of S_{Ni}. We constructed a model to explain the primordial specific frequency of GCs in galaxies at constant SFR over different time scales, Δt_1 and Δt_2, where Δt_1 is the time for GC formation and Δt_2 is the time for the formation of the rest of the galaxy, since the star formation duration (ΔT)= Δt_1+ Δt_2.

We suggested a model in which a population of young clusters is formed following a cluster mass function that depends on the SFR. The theoretical specific frequency of the GC model ($S_{N,th} = \frac{N_{GC,th}}{M_b} \times \psi 10^{7.9} L_\odot$, where $N_{GC,th}$ is the theoretical number of globular clusters and ψ is mass-to-light ratio of the galaxies in the V- band) explains the primordial value of S_{Ni} depending on the minimum star cluster mass ($M_{ecl,min}$) and the power-law index of the cluster mass function (β). The models fit best to S_{Ni} for $M_{ecl,min} = 5 \times 10^3 M_\odot$ and $\Delta t_1 = \Delta T \times 0.005$. From this model, we infer that for a low SFR (at low galaxy masses), we need a lower minimum cluster mass and lower Δt_1, while for a larger SFR (large galaxy masses), we need a higher minimum cluster mass to represent S_{Ni}.

For the model where Δt_1 is shorter than Δt_2, i.e. essentially $SFR_1 > SFR_2$ (where SFR_1 is the SFR of forming the GC system over time Δt_1 and SFR_2 is the SFR of forming the rest of galaxy form over time Δt_2), we can match the primordial S_{Ni} for $\Delta t_1 \approx 10^8\ yr$ and $M_{ecl,min} = 10^4 M_\odot$. The best explanation for dE galaxies is a model with $M_{ecl,max} = 10^5 M_\odot$, and β between 2.3 and 2.5. The best model for E galaxies is where $M_{ecl,max}$ is between 10^6 and 10^7 $M_\odot$ and β is between 1.5 and 2.5. The existence of this difference may indicate a different formation mechanism for dE and E galaxies (Dabringhausen & Kroupa, 2013).

Thus, by accounting for all star formation occurring in correlated star formation events (i.e. embedded clusters) it is naturally possible to account for the observed dependency of S_N on galaxy mass M_b. The large spread of S_N values at a given M_b, and the difference of N_{GC} with M_b for dE and E galaxies, suggest that the detailed star-formation events varied between these systems. However, the overall S_N can be understood in terms of the above assumption, that is, in terms of universal purely baryonic matter playing the same role with all systems.

4.2 Future Work

The work presented in this thesis can serve as a powerful tool to understand galaxy formation and evolution, in particular examining the spin vector alignments of galaxies with respect to the filaments. We extracted a sample of galaxies by using the data from the HYPERLEDA. Using wide-area surveys such as the SDSS will likely classify the measurement of the spin and filament more robustly. We intend to study the distribution of the spin vector galaxies for a larger sample of galaxies. A comprehensive description of the filamentary network needs to be investigated and analysed in more depth. The catalogue presented in Appendix (C) needs to be continuously updated and complemented with additional data.

The other major part of this thesis studied the GC destruction via tidal erosion which reflects the observed present-day GC specific frequency. This contributes to the continuing understanding the formation and evolution of a galaxy. The research described in this thesis suggests further investigation and improvement. On the observational side, our model can reach a full potential if parameters such as

$M_{ecl,max}$, $M_{ecl,min}$ and Δt_1 can be constrained better and independently.

The work presented here has the potential to shed light on studying the primordial value of the specific frequency. Still important questions about the observed 'U' -shape relation between S_N and galaxy mass remain open and need to be investigated in more detail.

Thus, further investigation and in-depth studies of the variation of the ECMF and GC systems in different environments are very important to refine the models studied here.

APPENDIX A

The filament structures.

Here we show all filament structures represented by lines gained by linear regression and the spin vectors (pink vectors) and the major axis (gray vectors) for spiral galaxies inside the rectangular region of each filament.

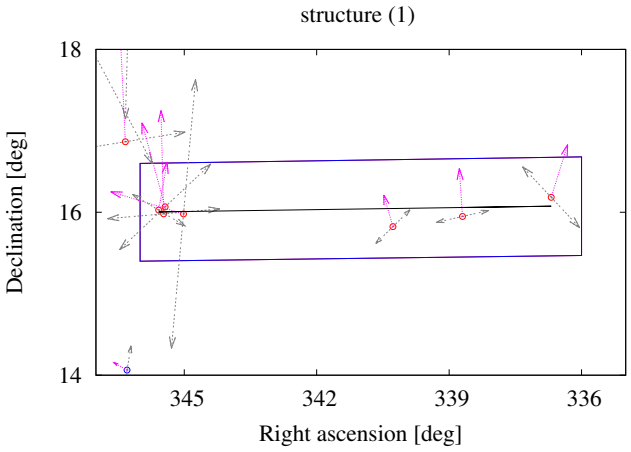

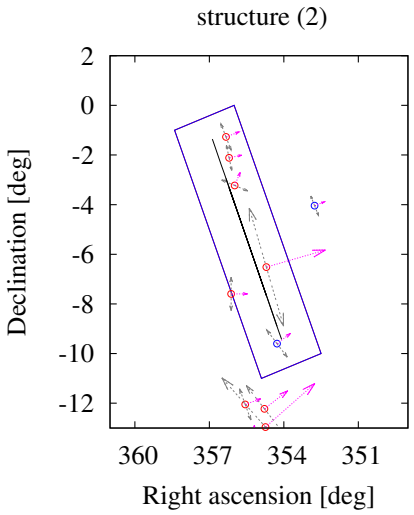

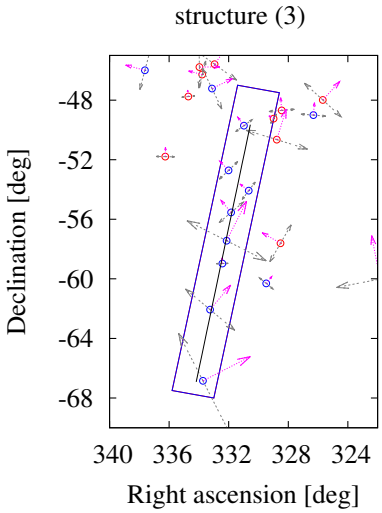
structure (3)
Declination [deg]
-48
-52
-56
-60
-64
-68
340
336
332
328
324
Right ascension [deg]

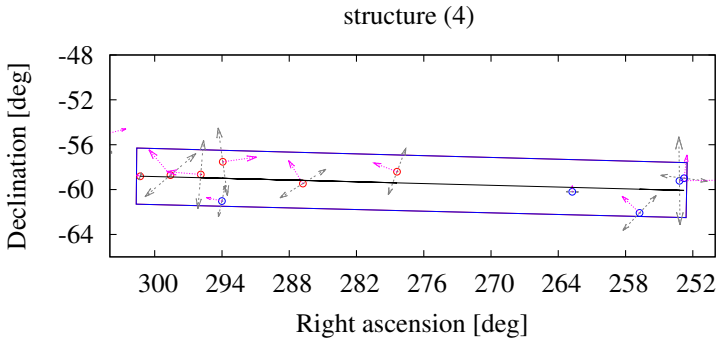
structure (4)
Declination [deg]
-48
-52
-56
-60
-64
300
294
288
282
276
270
264
258
252
Right ascension [deg]

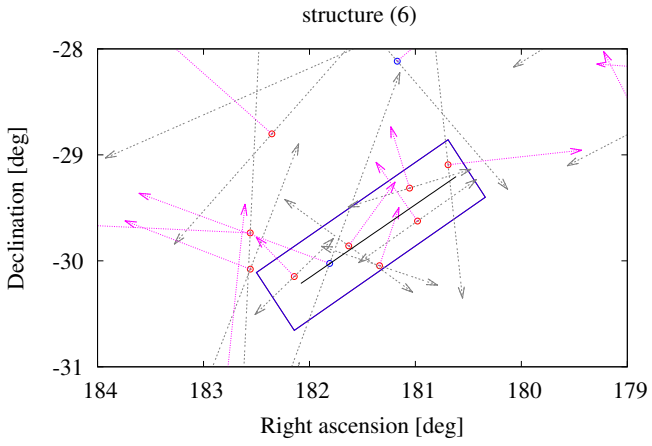
structure (6)
Declination [deg]
-28
-29
-30
-31
184
183
182
181
180
179
Right ascension [deg]

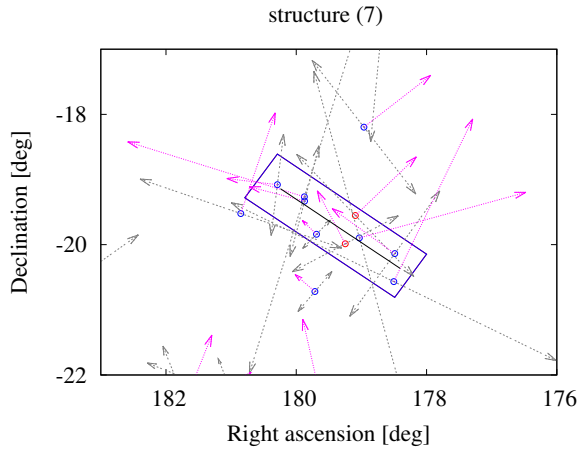
structure (7)
Declination [deg]
-18
-20
-22
182
180
178
176
Right ascension [deg]

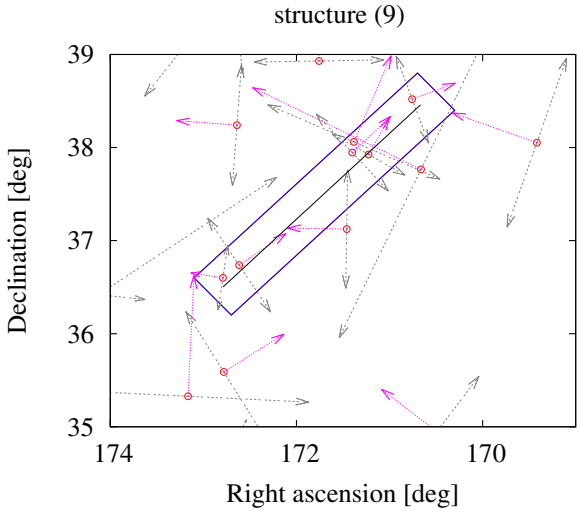
structure (9)
Declination [deg]
39
38
37
36
35
174
172
170
Right ascension [deg]

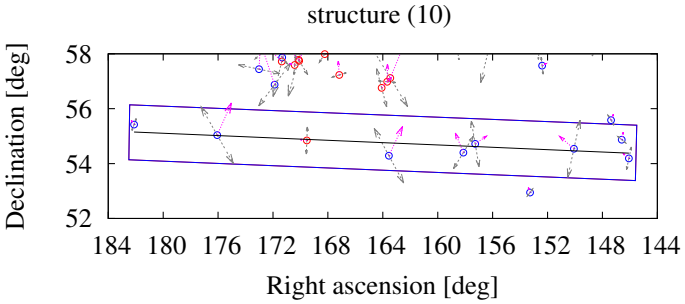
structure (10)
Declination [deg]
58
56
54
52
184 180 176 172 168 164 160 156 152 148 144
Right ascension [deg]

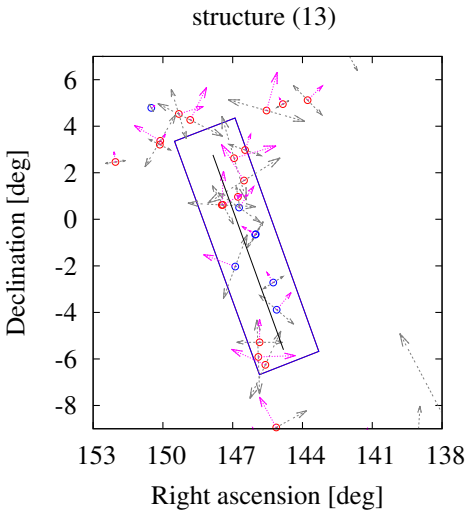
structure (13)
Declination [deg]
6
4
2
0
-2
-4
-6
-8
153
150
147
144
141
138
Right ascension [deg]

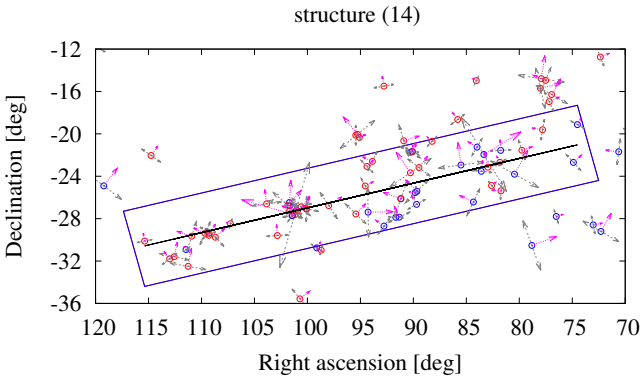
structure (14)
Declination [deg]
-12
-16
-20
-24
-28
-32
-36
120
115
110
105
100
95
90
85
80
75
70
Right ascension [deg]

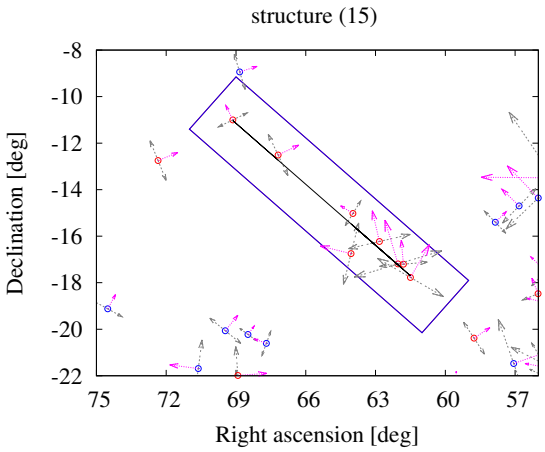
structure (15)
Declination [deg]
-8
-10
-12
-14
-16
-18
-20
-22
75
72
69
66
63
60
57
Right ascension [deg]

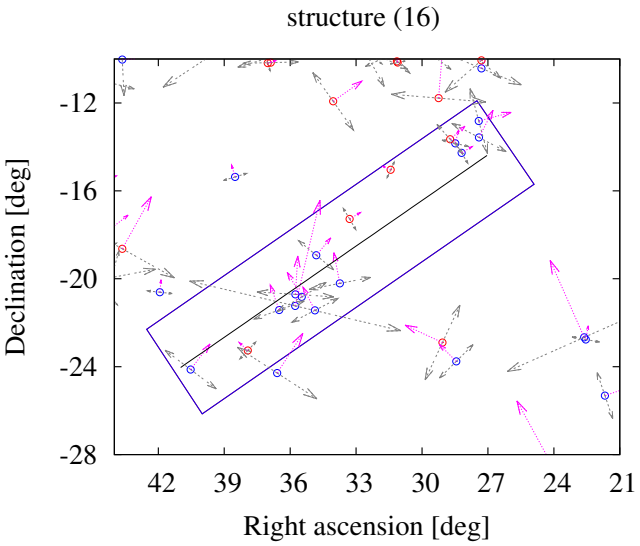
structure (16)
Declination [deg]
-12
-16
-20
-24
-28
42
39
36
33
30
27
24
21
Right ascension [deg]

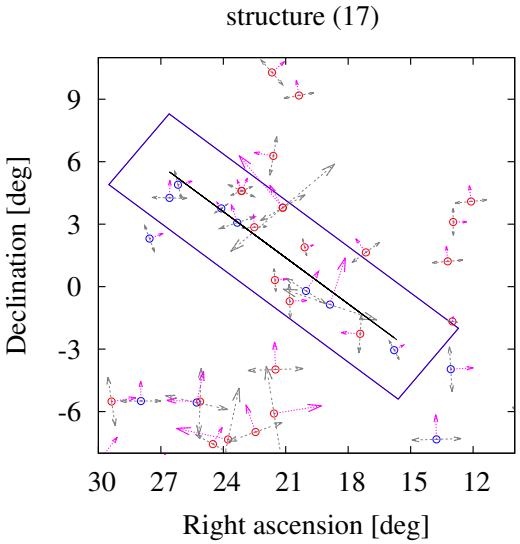
structure (17)
Declination [deg]
9
6
3
0
-3
-6
30
27
24
21
18
15
12
Right ascension [deg]

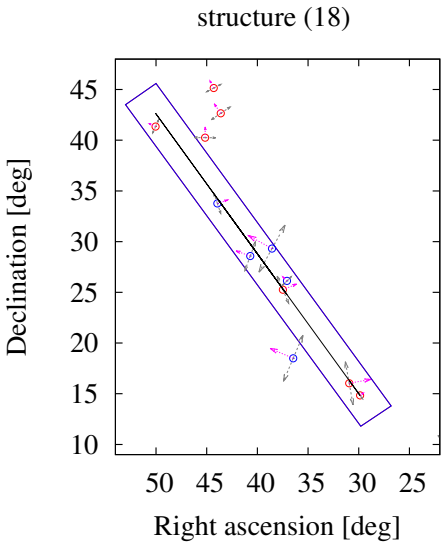
structure (18)
Declination [deg]
45
40
35
30
25
20
15
10
50 45 40 35 30 25
Right ascension [deg]

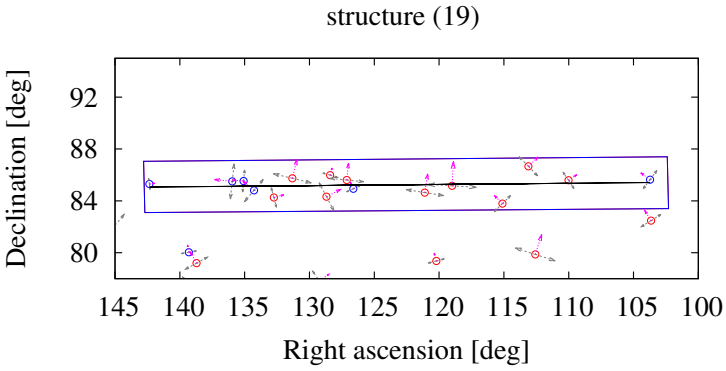
structure (19)
Declination [deg]
92
88
84
80
145 140 135 130 125 120 115 110 105 100
Right ascension [deg]

APPENDIX B

Angles θ between the spin vectors and the filaments for all structures individually.

The histograms here count all angles between the spin vectors of spiral galaxies and the host filament in which they are embedded for all structures.

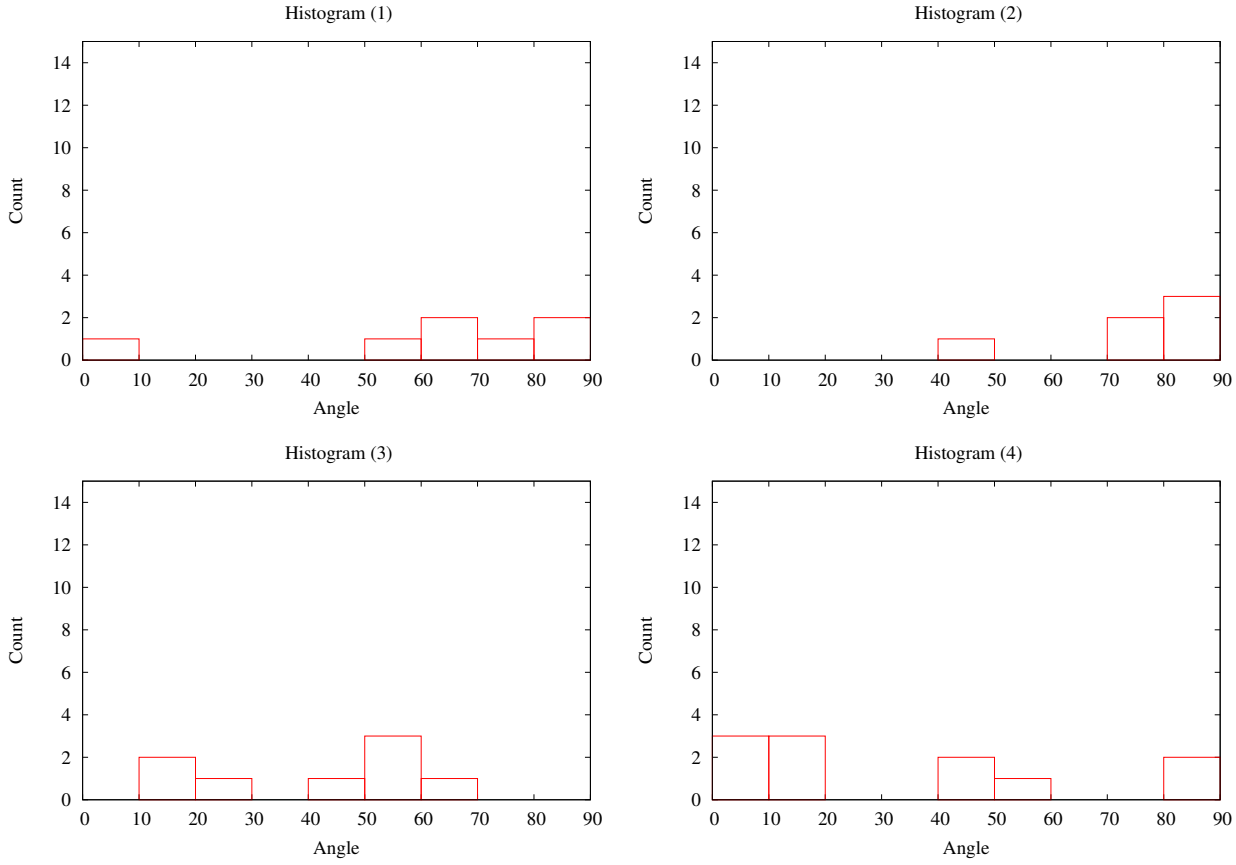

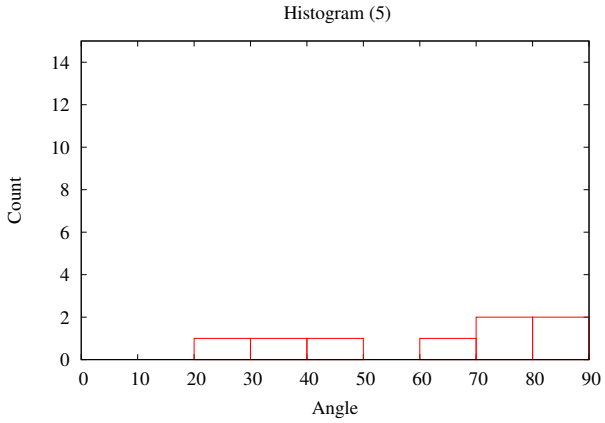
Histogram (5)
Count
Angle
0
2
4
6
8
10
12
14
0
10
20
30
40
50
60
70
80
90

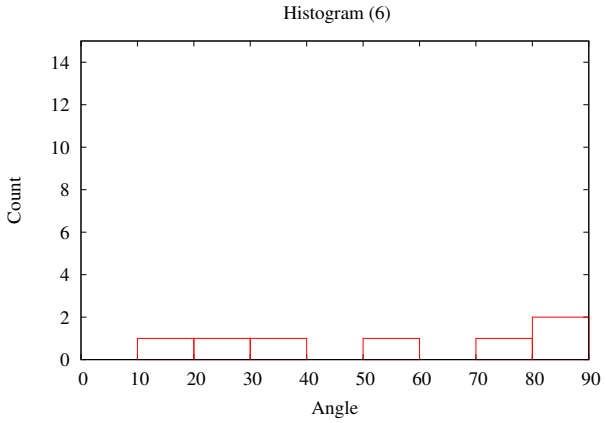
Histogram (6)
Count
Angle
0
2
4
6
8
10
12
14
0
10
20
30
40
50
60
70
80
90

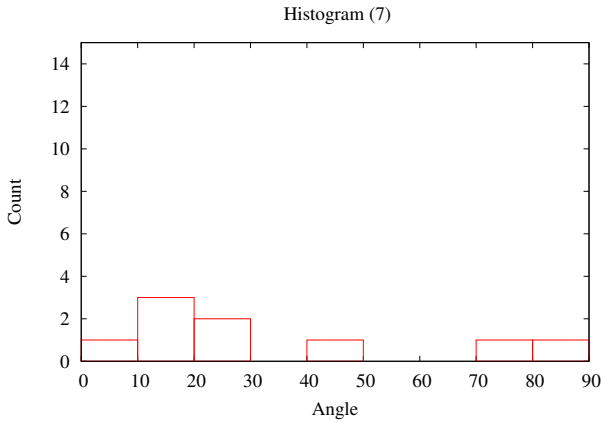
Histogram (7)
Count
Angle
0
2
4
6
8
10
12
14
0
10
20
30
40
50
60
70
80
90

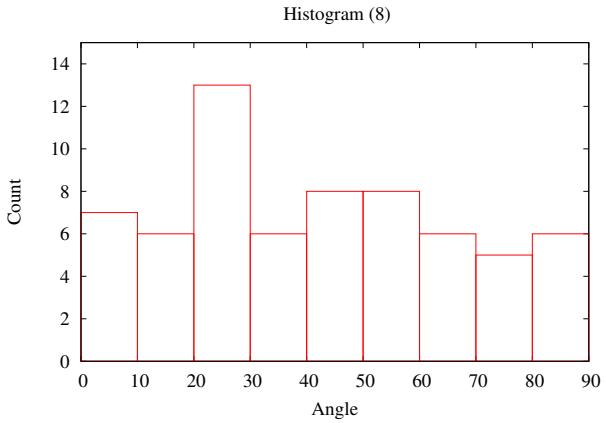
Histogram (8)
Count
Angle
0
2
4
6
8
10
12
14
0
10
20
30
40
50
60
70
80
90

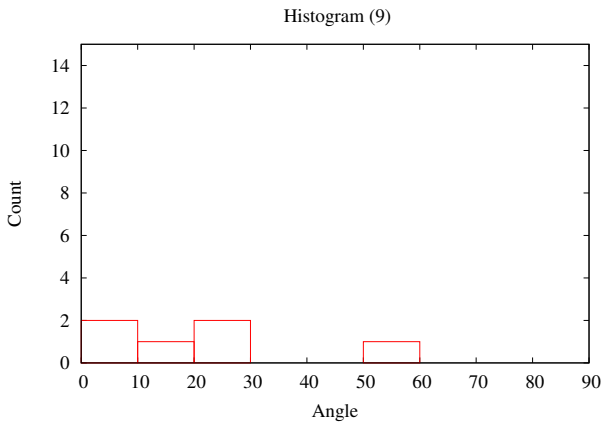
Histogram (9)
Count
Angle
0
2
4
6
8
10
12
14
0
10
20
30
40
50
60
70
80
90

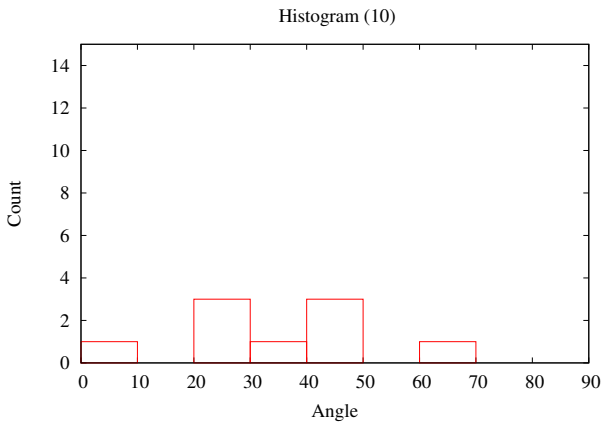
Histogram (10)
Count
Angle
0
2
4
6
8
10
12
14
0
10
20
30
40
50
60
70
80
90

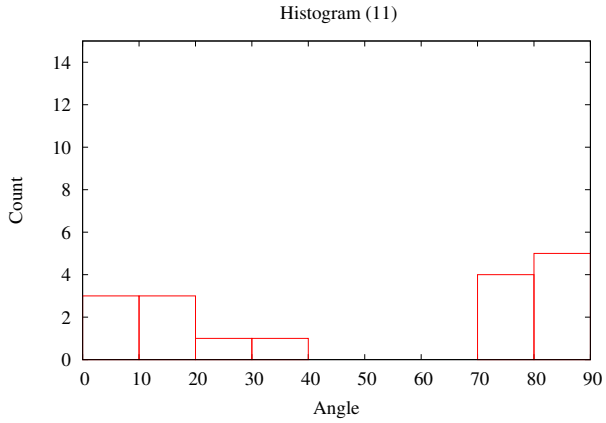
Histogram (11)
Count
Angle
0
2
4
6
8
10
12
14
0
10
20
30
40
50
60
70
80
90

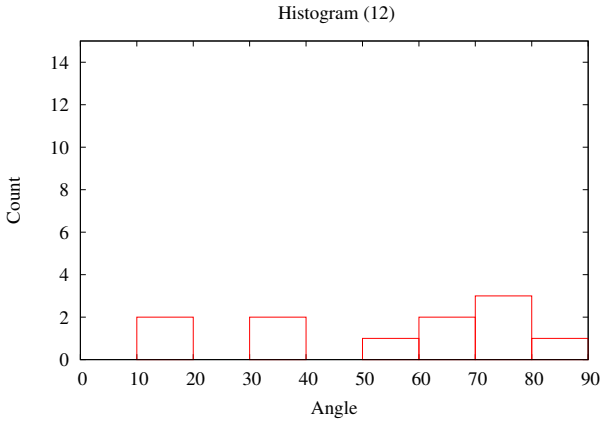
Histogram (12)
Count
Angle
0
2
4
6
8
10
12
14
0
10
20
30
40
50
60
70
80
90

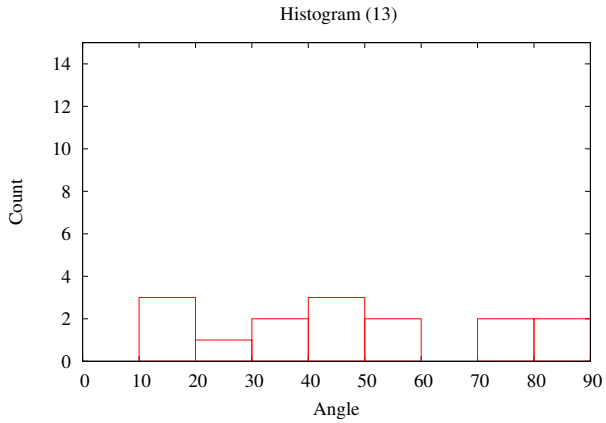
Histogram (13)
Count
Angle
0
2
4
6
8
10
12
14
0
10
20
30
40
50
60
70
80
90

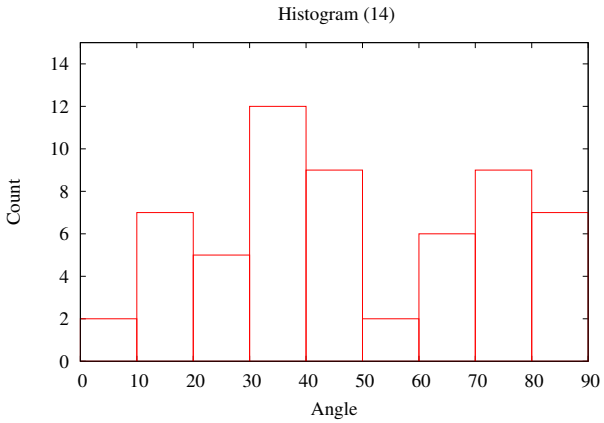
Histogram (14)
Count
Angle
0
2
4
6
8
10
12
14
0
10
20
30
40
50
60
70
80
90

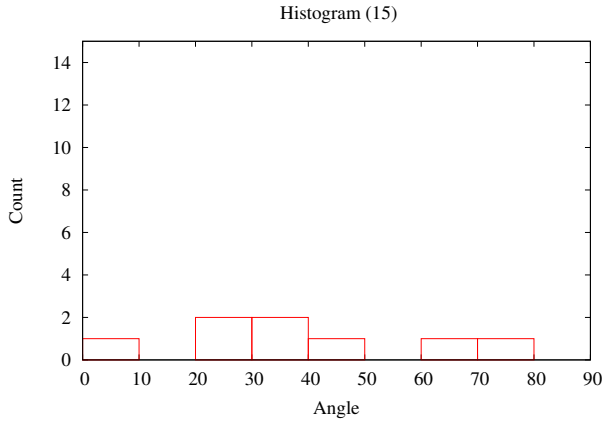
Histogram (15)
Count
Angle
0
2
4
6
8
10
12
14
0
10
20
30
40
50
60
70
80
90

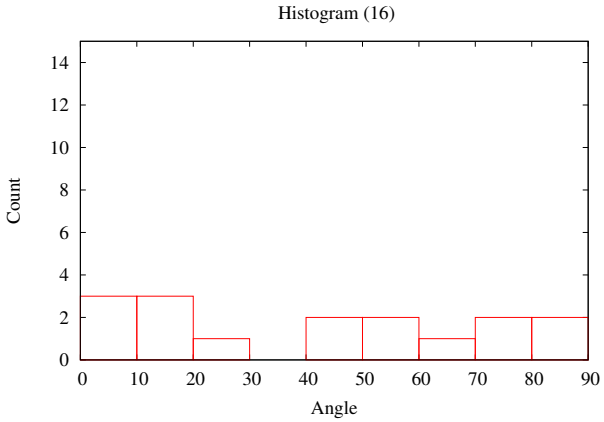
Histogram (16)
Count
Angle
0
2
4
6
8
10
12
14
0
10
20
30
40
50
60
70
80
90

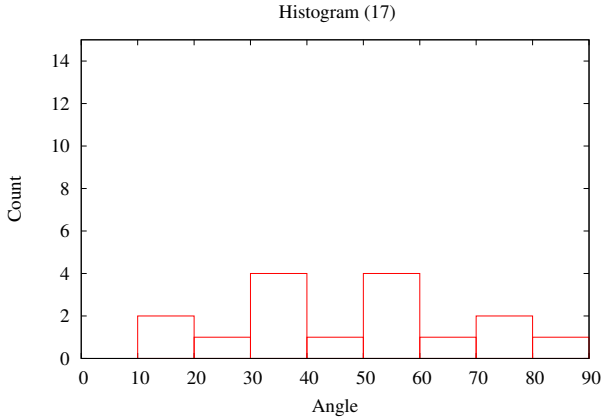
Histogram (17)
Count
Angle
0
2
4
6
8
10
12
14
0
10
20
30
40
50
60
70
80
90

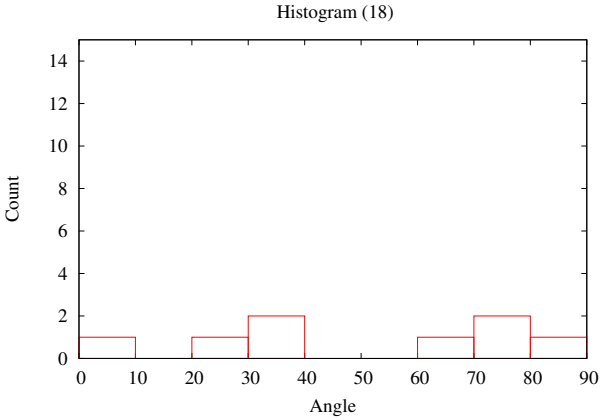
Histogram (18)
Count
Angle
0
2
4
6
8
10
12
14
0
10
20
30
40
50
60
70
80
90

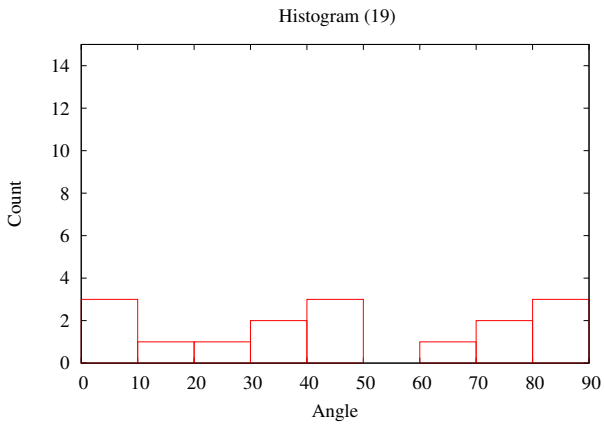
Histogram (19)
Count
Angle
0
2
4
6
8
10
12
14
0
10
20
30
40
50
60
70
80
90

APPENDIX C

The distance and the angles θ between the spin vectors and the filaments for all structures.

The Table shows the number, name, right ascension, declination and velocity for each galaxy in the structure, and also the vertical distance between the galaxy and hosting filament as well as the angles θ for 302 galaxies.

The number of galaxies in the structure	Name of galaxy	Right ascension (deg)	Declination (deg)	Radial Velocity (km s^{-1})	The distance between the galaxy and filament (deg)	The angle θ between galaxy spin and filament (deg)
			Plot (1)			
1	UGC12090	338.70	15.95	1880	0.110	83.45
2	PGC068878	336.69	16.18	1898	0.109	59.55
3	PGC085276	340.27	15.82	1936	0.223	62.45
4	UGC12313	345.43	16.07	1994	0.062	63.45
5	NGC7463	345.47	15.98	2143	0.024	87.75
6	UGC12321	345.58	16.03	2160	0.022	71.55
7	NGC7448	345.02	15.98	2192	0.029	9.85
			Plot (2)			
1	PGC071920	354.27	-9.60	1784	0.229	72.05
2	PGC1016288	356.12	-7.60	1832	1.324	70.95
3	NGC7721	354.70	-6.52	2014	0.372	87.15
4	PGC1101367	356.20	-2.11	2018	0.391	82.95
5	PGC1074374	355.98	-3.23	2080	0.239	42.05
6	UGC12769	356.33	-1.27	2081	0.545	88.05

Plot (3)

1	ESO237-033	330.98	-49.71	1658	0.411	47.69
2	NGC7205	332.14	-57.44	1687	0.043	14.91
3	ESO189-023	331.84	-55.54	1688	0.048	52.09
4	ESO146-014	333.25	-62.07	1700	0.086	28.01
5	ESO189-021	330.65	-54.08	1719	0.807	65.19
6	PGC3083216	332.43	-58.97	1720	0.079	13.89
7	IC5162	332.01	-52.71	1736	0.804	55.79
8	IC5176	333.73	-66.85	1746	0.426	51.01

Plot (4)

1	NGC6221	253.19	-59.22	1484	0.842	2.32
2	ESO138-014	256.75	-62.08	1508	2.118	42.18
3	NGC6215	252.78	-58.99	1560	1.078	84.32
4	PGC365379	262.75	-60.19	1565	0.388	89.48
5	IC4869	294.01	-61.03	1794	2.053	11.18
6	IC4819	286.78	-59.47	1842	0.299	56.58
7	IC4871	293.93	-57.52	1926	1.457	9.32
9	NGC6810	295.89	-58.66	1961	0.268	3.28
10	IC4720	278.39	-58.41	2109	0.983	19.18
11	IC4901	298.60	-58.71	2139	0.138	48.18
12	PGC376121	301.29	-58.82	2178	0.037	16.98

Plot (5)

1	IC4402	215.30	-46.30	1654	0.136	80.91
2	ESO325-034	208.24	-38.84	1655	0.161	87.81
3	PGC049962	210.50	-41.04	1714	0.197	61.39
4	NGC5483	212.60	-43.32	1774	0.065	28.69
5	IC4362	211.34	-41.82	1802	0.241	77.79
6	IC4386	213.76	-43.96	1876	0.430	79.39
7	ESO383-074	206.44	-37.22	1964	0.040	45.31
8	IC4390	214.25	-44.98	2100	0.053	34.89

Plot (6)

1	IC3005	181.81	-30.02	1722	0.002	54.75
2	PGC730818	181.06	-29.31	1981	0.160	72.45
3	PGC722090	181.34	-30.05	2033	0.283	36.95
4	PGC038139	180.98	-29.62	2146	0.139	89.35

5	PGC720820	182.14	-30.15	2150	0.089	80.45
6	PGC157406	181.63	-29.86	2195	0.036	19.45
7	ESO440-044	180.69	-29.09	2200	0.135	28.35

Plot (7)

1	ESO572-045	180.29	-19.08	1510	0.025	26.63
2	PGC037707	179.69	-19.84	1637	0.275	10.57
3	NGC3956	178.50	-20.57	1652	0.223	82.27
4	NGC4027	179.88	-19.27	1670	0.100	16.33
5	ESO572-012	178.49	-20.14	1685	0.143	2.07
6	NGC3981	179.03	-19.90	1715	0.043	48.94
7	NGC4027A	179.87	-19.33	1747	0.046	19.03
8	ESO572-024	179.25	-19.99	1882	0.153	28.57
9	ESO572-022	179.09	-19.55	1914	0.295	77.44

Plot (8)

1	PGC040107	185.66	8.30	1408	2.284	12.71
2	IC3259	185.95	7.19	1421	1.809	31.71
3	UGC07522	186.49	3.43	1423	0.150	78.49
4	NGC5088	200.08	-12.57	1438	0.237	51.11
5	UGC07780	189.18	3.11	1442	1.722	2.51
6	NGC4430	186.86	6.26	1447	1.927	22.79
7	PGC043020	191.42	-6.07	1475	2.352	31.21
8	IC4212	198.01	-6.99	1480	2.167	89.29
9	PGC135801	186.58	1.02	1483	1.609	28.41
10	PGC044358	194.45	-9.63	1484	2.268	63.19
11	PGC040951	187.02	2.91	1484	0.075	29.99
12	NGC4731	192.76	-6.39	1493	1.524	46.49
13	NGC5170	202.45	-17.97	1503	1.346	72.09
14	UGC07512	186.42	2.16	1505	1.011	63.09
15	NGC4666	191.29	-0.46	1518	1.095	10.91
16	NGC4517A	188.12	0.39	1530	0.818	20.61
17	NGC4266	184.93	5.54	1536	0.028	22.99
18	PGC040604	186.47	5.81	1539	1.338	17.01
19	IC3229	185.72	6.68	1539	1.309	9.81
20	NGC4948A	196.27	-8.16	1544	0.080	51.01
21	NGC4775	193.44	-6.62	1567	1.138	7.79
22	UGC07612	187.26	2.72	1574	0.005	88.71
23	UGC07913	191.14	-2.32	1589	0.195	31.99
24	PGC044506	194.70	-6.11	1603	0.161	50.09
25	PGC039639	184.81	5.99	1605	0.163	28.19

26	NGC4668	191.38	-0.54	1623	1.124	47.81
27	UGC07642	187.56	2.62	1637	0.164	78.39
28	PGC041700	188.34	1.52	1642	0.068	51.91
29	NGC4981	197.20	-6.78	1678	1.675	75.41
30	PGC1117977	190.83	-1.47	1682	0.103	20.69
31	NGC4409	186.74	2.49	1690	0.549	41.21
32	UGC07841	190.30	1.41	1703	1.516	86.51
33	NGC4632	190.63	-0.08	1719	0.831	7.79
34	NGC4928	195.75	-8.08	1719	0.275	22.29
35	PGC040408	186.16	4.00	1725	0.047	56.29
36	IC3474	188.15	2.66	1729	0.647	4.01
37	NGC4496A	187.91	3.94	1730	1.271	16.79
38	UGC07387	185.07	4.20	1733	0.761	34.91
39	NGC4527	188.53	2.65	1736	0.937	45.69
40	NGC4995	197.42	-7.83	1743	1.174	43.49
41	NGC4942	196.08	-7.65	1747	0.254	25.81
42	NGC4533	188.59	2.33	1754	0.775	63.01
43	PGC039468	184.47	5.03	1774	0.705	47.81
44	PGC039109	183.65	9.20	1775	1.302	38.29
45	PGC091219	190.37	-3.25	1806	1.382	89.69
46	NGC4536	188.61	2.19	1807	0.704	67.79
47	PGC040285	185.98	3.08	1807	0.769	28.31
48	PGC039532	184.62	5.62	1822	0.218	46.11
49	PGC091195	185.88	2.01	1851	1.529	83.69
50	UGC07422	185.51	5.10	1864	0.143	63.01
51	ESO577-038	207.11	-18.87	1889	1.682	47.11
52	PGC040050	185.55	4.95	1912	0.080	36.71
53	NGC4260	184.84	6.10	1948	0.262	8.39
54	PGC039556	184.66	6.71	1998	0.507	69.41
55	PGC039730	184.97	1.77	1999	2.377	17.21
56	PGC040310	186.01	5.18	2050	0.587	79.29
57	PGC039392	184.29	6.43	2053	0.049	4.41
58	PGC041571	188.10	-1.74	2085	2.182	57.61
59	NGC4180	183.26	7.04	2087	0.366	29.71
60	NGC4197	183.66	5.81	2088	0.839	14.41
61	PGC045824	197.99	-12.06	2112	1.061	28.69
62	NGC4287	185.20	5.64	2138	0.250	20.29
63	PGC047721	203.31	-16.12	2169	0.484	57.19
64	PGC091181	183.25	7.30	2197	0.211	81.29
65	IC3118	184.55	9.50	1733	2.186	59.21
			Plot (9)			
1	PGC034951	170.76	38.52	1836	0.106	22.38
2	PGC035464	172.62	36.74	1961	0.055	8.78
3	PGC035508	172.79	36.60	1968	0.073	51.28
4	UGC06428	171.23	37.93	2016	0.014	17.82
5	PGC035127	171.40	37.95	2094	0.121	0.52
6	UGC06433	171.38	38.06	2111	0.192	23.92

Plot (10)

1	UGC05676	157.27	54.72	1420	0.097	20.22
2	UGC05720	158.13	54.40	1438	0.237	49.48
3	NGC3846A	176.06	55.03	1452	0.015	49.92
4	UGC06016	163.55	54.29	1508	0.467	48.32
5	UGC05369	150.08	54.54	1569	0.072	22.18
6	PGC027886	146.07	54.19	1618	0.190	21.58
7	PGC028037	146.60	54.87	1622	0.476	69.42
8	PGC2501589	182.12	55.42	1740	0.274	33.68
9	PGC034528	169.54	54.84	1897	0.040	3.08

Plot (11)

1	PGC2020885	138.70	33.02	1496	0.542	13.13
2	UGC04988	140.81	34.73	1573	0.178	85.13
3	UGC05105	143.83	35.91	1588	0.043	9.07
4	UGC05020	141.51	34.65	1619	0.175	78.67
5	SDSSJ090706. .25+322219.5	136.78	32.37	1743	0.360	74.57
6	2MASXJ0916 4731+3425471	139.20	34.43	1781	0.550	39.33
7	NGC2770	137.39	33.12	1947	0.081	10.17
8	UGC04725	135.23	31.99	1971	0.085	89.93
9	PGC025273	135.05	32.00	1978	0.009	8.73
10	NGC2604B	128.40	29.50	2021	0.381	82.13
11	UGC04482	128.81	28.75	2039	0.467	29.07
12	PGC025063	133.89	31.21	2039	0.260	88.97
13	PGC1925809	132.88	30.97	2046	0.080	18.27
14	IC2361	126.44	27.87	2072	0.317	78.87
15	UGC04559	131.03	30.12	2085	0.111	74.43
16	NGC2608	128.82	28.47	2148	0.729	86.33
17	UGC04395	126.45	28.12	2192	0.099	2.77

Plot (12)

1	UGC04712	134.85	11.14	2014	0.187	87.06
2	PGC1373747	136.32	10.04	2039	0.371	32.94
3	NGC2648	130.67	14.29	2057	0.311	70.94
4	NGC2725	135.26	11.10	2064	0.440	32.44
5	IC2329	125.58	19.42	2081	0.044	72.76
6	UGC04444	127.51	17.26	2081	0.247	67.76
7	PGC024469	130.70	14.27	2113	0.302	59.56
8	PGC023236	124.37	21.18	2126	0.527	11.96
9	PGC024666	131.70	13.71	2141	0.042	17.96
10	SDSSJ080947. .91+222730.1	122.45	22.46	2152	0.176	70.86
11	PGC023231	124.36	21.16	2158	0.507	60.34

Plot (13)

1	UGC05245	146.89	-2.03	1413	0.778	49.87
2	PGC027864	146.01	-0.64	1449	0.521	42.17
3	PGC027612	145.11	-3.89	1454	0.278	59.63
4	UGC05205	146.03	-0.66	1505	0.494	38.67
5	PGC1084555	145.26	-2.72	1632	0.530	12.37
6	UGC05238	146.72	0.51	1777	0.232	54.53
7	PGC028408	147.93	1.44	1840	0.590	79.57
8	UGC05242	146.77	0.96	1850	0.340	45.77
9	PGC027747	145.60	-6.25	1854	0.976	80.93
10	NGC3018	147.42	0.62	1861	0.387	12.37
11	UGC05228	146.52	1.67	1871	0.819	86.57
12	UGC05249	146.94	2.63	1875	0.742	22.63
13	NGC3023	147.47	0.62	1879	0.432	19.63
14	PGC027817	145.84	-5.28	1881	0.884	39.13
15	PGC027833	145.90	-5.91	2024	1.149	72.37

Plot (14)

1	ESO425-008	91.65	-27.88	1477	2.834	71.82
2	ESO487-030	84.33	-26.43	1486	3.173	39.18
3	ESO425-012	92.78	-28.71	1491	3.370	49.78
4	ESO554-017	83.99	-21.25	1563	1.780	44.58
5	IC2158	91.33	-27.86	1570	2.891	78.38
6	ESO553-045	81.75	-21.56	1619	0.947	79.42
7	ESO488-053	89.83	-25.54	1621	0.996	21.38
8	NGC1964	83.34	-21.95	1660	0.947	17.62
9	ESO552-031	74.51	-19.12	1668	1.586	47.52
10	NGC2131	89.70	-26.65	1671	2.110	74.48
11	ESO427-004	101.42	-27.70	1700	0.333	86.72
12	ESO427-005	101.44	-27.72	1703	0.346	49.38
13	ESO489-029	94.27	-27.39	1705	1.735	12.78
14	ESO490-045	101.69	-26.47	1708	0.921	72.62
15	IC2137	83.59	-23.53	1720	0.535	69.62
16	ESO487-035	85.50	-22.95	1726	0.490	84.02
17	ESO428-033	111.46	-30.92	1728	1.069	69.08
18	NGC1886	80.45	-23.81	1739	1.552	47.12
19	ESO555-022	90.28	-21.74	1748	2.803	46.72
20	ESO490-042	101.66	-26.78	1758	0.615	77.22
21	ESO486-003	74.89	-22.70	1764	1.796	28.32
22	ESO555-020	90.11	-21.67	1787	2.825	71.22
23	ESO488-049	89.66	-25.41	1797	0.915	58.78
24	ESO488-060	91.18	-26.13	1800	1.244	33.38
25	ESO426-001	95.43	-27.56	1806	1.623	32.32
26	NGC2295	101.85	-26.74	1812	0.704	35.02

27	ESO490-010	97.99	-26.77	1824	0.247	19.22
28	ESO555-019	90.09	-21.67	1824	2.828	47.52
29	IC2130	82.96	-23.14	1828	0.307	89.52
30	NGC2139	90.28	-23.67	1839	0.925	69.28
31	ESO553-033	79.76	-21.54	1844	0.485	4.72
32	ESO487-017	82.62	-24.88	1847	2.070	23.32
33	ESO487-010	81.72	-25.37	1853	2.766	17.68
34	ESO487-012	81.83	-22.68	1859	0.130	76.68
35	IC2152	89.47	-23.18	1873	1.209	38.72
36	ESO555-010	88.24	-20.71	1900	3.315	56.58
37	ESO428-031	111.26	-32.50	1916	2.651	66.12
38	NGC2280	101.20	-27.64	1922	0.325	29.58
39	ESO490-036	101.03	-27.18	1936	0.083	14.42
40	ESO553-017	77.80	-19.61	1950	1.893	22.88
41	ESO428-029	110.93	-29.65	1960	0.034	31.88
42	ESO490-031	100.59	-26.89	1992	0.252	32.32
43	ESO428-006	108.69	-29.75	2009	0.595	29.62
44	ESO428-020	109.66	-29.37	2017	0.002	37.98
45	ESO427-014	102.84	-29.59	2019	1.834	80.02
46	ESO489-033	94.54	-24.92	2033	0.727	14.92
47	ESO489-023	93.87	-22.60	2053	2.818	38.58
48	ESO491-009	103.85	-26.61	2054	1.308	84.02
49	ESO428-015	109.28	-29.38	2076	0.094	41.12
50	ESO428-018	109.30	-29.58	2079	0.283	75.58
51	ESO428-037	112.58	-31.60	2085	1.462	63.92
52	ESO489-031	94.38	-23.07	2094	2.484	30.62
53	PGC086068	115.37	-30.11	2108	0.646	87.22
54	ESO429-001	113.00	-31.80	2118	1.554	66.78
55	PGC020249	107.26	-28.49	2127	0.295	30.78
56	ESO490-035	100.94	-27.27	2141	0.028	1.08
57	ESO490-028	100.09	-27.10	2145	0.066	14.98
58	ESO490-029	100.11	-27.04	2147	0.003	62.62
59	ESO490-044	101.68	-27.28	2170	0.139	47.78

Plot (15)

1	PGC015214	67.19	-12.51	1801	0.167	66.64
2	PGC971141	69.14	-11.00	1821	0.021	22.86
3	NGC1519	62.03	-17.19	1830	0.033	32.16
4	PGC014487	61.80	-17.21	1857	0.175	43.86
5	PGC916775	63.97	-15.02	1873	0.390	9.14
6	PGC014626	62.83	-16.23	1879	0.232	35.86
7	ESO550-005	61.50	-17.78	1886	0.056	79.06
8	PGC014768	64.05	-16.75	1954	0.963	27.34

Plot (16)

1	PGC087900	28.20	-14.27	1423	0.755	3.68
2	PGC006703	27.41	-13.57	1446	0.883	27.82
3	PGC087905	28.48	-13.84	1496	1.277	41.62
4	NGC0908	35.77	-21.23	1507	0.661	42.12
5	ESO479-025	40.53	-24.13	1539	0.336	18.22
6	ESO545-016	36.50	-21.42	1550	0.401	75.12
7	NGC0899	35.47	-20.82	1564	0.493	86.02
8	ESO545-003	34.87	-21.44	1596	1.337	82.72
9	ESO545-002	34.81	-18.93	1608	0.687	15.62
10	ESO544-030	33.74	-20.21	1613	0.976	66.32
11	NGC0907	35.76	-20.71	1671	0.236	51.72
12	PGC006706	27.42	-12.82	1707	1.502	19.68
13	PGC916523	31.43	-15.04	1804	1.960	58.68
14	ESO544-025	33.30	-17.28	1812	1.183	4.18
15	PGC142582	37.93	-23.26	1892	1.104	77.68
16	PGC007109	28.72	-13.65	1921	1.561	7.02

Plot (17)

1	PGC006402	26.17	4.90	1619	0.250	50.42
2	UGC01112	23.33	3.07	1709	0.028	35.08
3	UGC00866	20.03	-0.21	1735	0.706	86.48
4	NGC0450	18.88	-0.86	1762	0.549	71.88
5	PGC1077422	15.79	-3.05	1775	0.477	64.42
6	PGC005957	24.10	3.76	1796	0.066	18.58
7	UGC01240	26.59	4.26	1797	1.002	55.08
8	PGC004143	17.42	-2.27	1865	0.817	32.72
9	UGC01011	21.52	0.32	1928	1.172	41.12
10	PGC093081	23.12	4.59	1954	1.321	31.58
11	PGC005744	23.12	4.60	1957	1.326	78.58
12	UGC00931	20.81	-0.70	2008	1.569	38.82
13	UGC01075	22.51	2.85	2099	0.282	50.08
14	NGC0520	21.14	3.79	2162	1.850	13.58
15	PGC004826	20.09	1.89	2167	0.942	50.42
16	PGC093080	21.14	3.79	2171	1.847	23.38

Plot (18)

1	NGC1056	40.70	28.57	1544	0.703	34.05
2	NGC0972	38.56	29.31	1546	1.467	25.05
3	UGC02392	43.94	33.77	1546	0.279	72.75
4	PGC1763621	37.08	26.13	1730	0.791	9.05
5	UGC01970	37.48	25.26	1913	0.038	76.75
6	PGC012468	50.04	41.35	2065	0.763	30.55
7	PGC1468320	29.86	14.83	2090	0.007	89.45
8	NGC0803	30.94	16.03	2099	0.161	64.25

Plot (19)

1	PGC023621	126.62	84.94	1599	0.267	65.52
2	UGC04612	135.08	85.53	1606	0.403	5.52
3	IC0512	135.96	85.50	1614	0.381	6.62
4	UGC03509	103.73	85.64	1645	0.225	37.22
5	UGC04948	142.35	85.30	1730	0.241	7.48
6	UGC04601	134.28	84.81	1752	0.328	40.52
7	UGC04557	132.74	84.26	1810	0.888	14.48
8	UGC03670	110.02	85.59	1861	0.231	33.48
9	UGC04078	121.10	84.64	1861	0.614	80.38
10	PGC023961	128.41	85.98	1872	0.793	73.98
11	IC0499	131.32	85.74	1883	0.577	75.98
12	UGC04396	128.68	84.32	1996	0.867	27.28
13	UGC04297	127.12	85.61	2001	0.407	83.68
14	UGC03890	115.12	83.79	2034	1.518	45.52
15	IC0469	119.00	85.16	2080	0.116	86.18
16	PGC021210	113.11	86.67	2124	1.339	43.48

Bibliography

Abazajian, K., Adelman-McCarthy, J. K., Agüeros, M. A., Allam, S. S., Anderson, S. F., Annis, J., Bahcall, N. A., Baldry, I. K., Bastian, S., Berlind, A., Bernardi, M., Blanton, M. R., Blythe, N., Bochanski, Jr., J. J., Boroski, W. N., Brewington, H., Briggs, J. W., Brinkmann, J., Brunner, R. J., Budavári, T., Carey, L. N., Carr, M. A., Castander, F. J., Chiu, K., Collinge, M. J., Connolly, A. J., Covey, K. R., Csabai, I., Dalcanton, J. J., Dodelson, S., Doi, M., Dong, F., Eisenstein, D. J., Evans, M. L., Fan, X., Feldman, P. D., Finkbeiner, D. P., Friedman, S. D., Frieman, J. A., Fukugita, M., Gal, R. R., Gillespie, B., Glazebrook, K., Gonzalez, C. F., Gray, J., Grebel, E. K., Grodnicki, L., Gunn, J. E., Gurbani, V. K., Hall, P. B., Hao, L., Harbeck, D., Harris, F. H., Harris, H. C., Harvanek, M., Hawley, S. L., Heckman, T. M., Helmboldt, J. F., Hendry, J. S., Hennessy, G. S., Hindsley, R. B., Hogg, D. W., Holmgren, D. J., Holtzman, J. A., Homer, L., Hui, L., Ichikawa, S.-i., Ichikawa, T., Inkmann, J. P., Ivezić, Ž., Jester, S., Johnston, D. E., Jordan, B., Jordan, W. P., Jorgensen, A. M., Jurić, M., Kauffmann, G., Kent, S. M., Kleinman, S. J., Knapp, G. R., Kniazev, A. Y., Kron, R. G., Krzesiński, J., Kunszt, P. Z., Kuropatkin, N., Lamb, D. Q., Lampeitl, H., Laubscher, B. E., Lee, B. C., Leger, R. F., Li, N., Lidz, A., Lin, H., Loh, Y.-S., Long, D. C., Loveday, J., Lupton, R. H., Malik, T., Margon, B., McGehee, P. M., McKay, T. A., Meiksin, A., Miknaitis, G. A., Moorthy, B. K., Munn, J. A., Murphy, T., Nakajima, R., Narayanan, V. K., Nash, T., Neilsen, Jr., E. H., Newberg, H. J., Newman, P. R., Nichol, R. C., Nicinski, T., Nieto-Santisteban, M., Nitta, A., Odenkirchen, M., Okamura, S., Ostriker, J. P., Owen, R., Padmanabhan, N., Peoples, J., Pier, J. R., Pindor, B., Pope, A. C., Quinn, T. R., Rafikov, R. R., Raymond, S. N., Richards, G. T., Richmond, M. W., Rix, H.-W., Rockosi, C. M., Schaye, J., Schlegel, D. J., Schneider, D. P., Schroeder, J., Scranton, R., Sekiguchi, M., Seljak, U., Sergey, G., Sesar, B., Sheldon, E., Shimasaku, K., Siegmund, W. A., Silvestri, N. M., Sinisgalli, A. J., Sirko, E., Smith, J. A., Smolčić, V., Snedden, S. A., Stebbins, A., Steinhardt, C., Stinson, G., Stoughton, C., Strateva, I. V., Strauss, M. A., SubbaRao, M., Szalay, A. S., Szapudi, I., Szkody, P., Tasca, L., Tegmark, M., Thakar, A. R., Tremonti, C., Tucker, D. L., Uomoto, A., Vanden Berk, D. E., Vandenberg, J., Vogeley, M. S., Voges, W., Vogt, N. P., Walkowicz, L. M., Weinberg, D. H., West, A. A., White, S. D. M., Wilhite, B. C., Willman, B., Xu, Y., Yanny, B., Yarger, J., Yasuda, N., Yip, C.-W., Yocum, D. R., York, D. G., Zakamska, N. L., Zehavi, I., Zheng, W., Zibetti, S., & Zucker, D. B. 2003, AJ, 126, 2081

Adams, M. T., Strom, K. M., & Strom, S. E. 1980, ApJ, 238, 445

Alpaslan, M., Robotham, A. S. G., Driver, S., Norberg, P., Baldry, I., Bauer, A. E., Bland-Hawthorn, J., Brown, M., Cluver, M., Colless, M., Foster, C., Hopkins, A., Van Kampen, E., Kelvin, L., Lara-Lopez, M. A., Liske, J., Lopez-Sanchez, A. R., Loveday, J., McNaught-Roberts, T., Merson, A., & Pimbblet, K. 2014, MNRAS, 438, 177

Aryal, B. 2011, Research in Astronomy and Astrophysics, 11, 293

Aryal, B., Bhattarai, H., Dhakal, S., Rajbahak, C., & Saurer, W. 2013, MNRAS, 434, 1939

Aryal, B. & Saurer, W. 2004, A&A, 425, 871

—. 2005, A&A, 432, 431

—. 2006, MNRAS, 366, 438

Ashman, K. M. & Zepf, S. E. 1992, ApJ, 384, 50

—. 1998, Globular Cluster Systems

Balbinot, E., Santiago, B. X., da Costa, L., Maia, M. A. G., Majewski, S. R., Nidever, D., Rocha-Pinto, H. J., Thomas, D., Wechsler, R. H., & Yanny, B. 2013, ApJ, 767, 101

Baugh, C. M., Cole, S., Frenk, C. S., & Lacey, C. G. 1998, ApJ, 498, 504

Baumgardt, H. & Makino, J. 2003, MNRAS, 340, 227

Blakeslee, J. P., Tonry, J. L., & Metzger, M. R. 1997, AJ, 114, 482

Bond, J. R., Kofman, L., & Pogosyan, D. 1996, Nature, 380, 603

Bond, N. A., Strauss, M. A., & Cen, R. 2010, MNRAS, 409, 156

Briceño, C., Luhman, K. L., Hartmann, L., Stauffer, J. R., & Kirkpatrick, J. D. 2002, ApJ, 580, 317

Brockamp, M., Küpper, A. H. W., Thies, I., Baumgardt, H., & Kroupa, P. 2014, MNRAS, 441, 150

Brodie, J. P. & Strader, J. 2006, ARAA, 44, 193

Brown, F. G. 1964, MNRAS, 127, 517

Cezario, E., Coelho, P. R. T., Alves-Brito, A., Forbes, D. A., & Brodie, J. P. 2013, A&A, 549, A60

Chandar, R., Whitmore, B., & Lee, M. G. 2004, ApJ, 611, 220

Chandar, R., Whitmore, B. C., Calzetti, D., Nino, D. D., Kennicutt, R. C., Regan, M., & Schinnerer, E. 2011, The Astrophysical Journal, 727, 88

Cole, S., Lacey, C. G., Baugh, C. M., & Frenk, C. S. 2000, MNRAS, 319, 168

Colless, M., Peterson, B. A., Jackson, C., Peacock, J. A., Cole, S., Norberg, P., Baldry, I. K., Baugh, C. M., Bland-Hawthorn, J., Bridges, T., Cannon, R., Collins, C., Couch, W., Cross, N., Dalton, G., De Propris, R., Driver, S. P., Efstathiou, G., Ellis, R. S., Frenk, C. S., Glazebrook, K., Lahav, O., Lewis, I., Lumsden, S., Maddox, S., Madgwick, D., Sutherland, W., & Taylor, K. 2003, ArXiv Astrophysics e-prints

Corwin, Jr., H. G., Buta, R. J., & de Vaucouleurs, G. 1994, AJ, 108, 2128

Côté, P., Marzke, R. O., West, M. J., & Minniti, D. 2000, ApJ, 533, 869

Dabringhausen, J. & Kroupa, P. 2013, MNRAS, 429, 1858

de Vaucouleurs, G., de Vaucouleurs, A., Corwin, Jr., H. G., Buta, R. J., Paturel, G., & Fouqué, P. 1991, Third Reference Catalogue of Bright Galaxies. Volume I: Explanations and references. Volume II: Data for galaxies between 0^h and 12^h. Volume III: Data for galaxies between 12^h and 24^h.

de Vaucouleurs, G. H., de Vaucouleurs, A., & Shapley, H. 1964, Reference catalogue of bright galaxies

Dekel, A. 1985, ApJ, 298, 461

Delgado-Serrano, R., Hammer, F., Yang, Y. B., Puech, M., Flores, H., & Rodrigues, M. 2010, A&A, 509, A78

Doroshkevich, A. G. 1970, Astrofizika, 6, 581

—. 1973, Astrophys. Lett., 14, 11

Doroshkevich, A. G., Shandarin, S. F., & Saar, E. 1978, MNRAS, 184, 643

Dotter, A., Sarajedini, A., Anderson, J., Aparicio, A., Bedin, L. R., Chaboyer, B., Majewski, S., Marín-Franch, A., Milone, A., Paust, N., Piotto, G., Reid, I. N., Rosenberg, A., & Siegel, M. 2010, ApJ, 708, 698

Durrell, P. R., Harris, W. E., Geisler, D., & Pudritz, R. E. 1996, AJ, 112, 972

Eggen, O. J., Lynden-Bell, D., & Sandage, A. R. 1962, ApJ, 136, 748

Egusa, F., Kohno, K., Sofue, Y., Nakanishi, H., & Komugi, S. 2009, ApJ, 697, 1870

Egusa, F., Sofue, Y., & Nakanishi, H. 2004, PASJ, 56, L45

Elmegreen, B. G. & Efremov, Y. N. 1997, ApJ, 480, 235

Flin, P. 1988, MNRAS, 235, 857

—. 2001, MNRAS, 325, 49

Flin, P. & Godlowski, W. 1986, MNRAS, 222, 525

Forbes, D. A. 2005, ApJL, 635, L137

Forbes, D. A., Brodie, J. P., & Grillmair, C. J. 1997, AJ, 113, 1652

Forte, J. C., Martinez, R. E., & Muzzio, J. C. 1982, AJ, 87, 1465

Francis, P. J., Palunas, P., Teplitz, H. I., Williger, G. M., & Woodgate, B. E. 2004, ApJ, 614, 75

Gamow, G. 1952, Physical Review, 86, 251

Garrido, J. L., Battaner, E., Sanchez-Saavedra, M. L., & Florido, E. 1993, A&A, 271, 84

Georgiev, I. Y., Puzia, T. H., Goudfrooij, P., & Hilker, M. 2010, MNRAS, 406, 1967

Godlowski, W. 1993, MNRAS, 265, 874

Godłowski, W. 2011, International Journal of Modern Physics D, 20, 1643

Godłowski, W. & Flin, P. 2010, ApJ, 708, 920

Goudfrooij, P., Strader, J., Brenneman, L., Kissler-Patig, M., Minniti, D., & Edwin Huizinga, J. 2003, MNRAS, 343, 665

Gratton, R. G., Bragaglia, A., Carretta, E., Clementini, G., Desidera, S., Grundahl, F., & Lucatello, S. 2003, A&A, 408, 529

Graves, G. J. & Faber, S. M. 2010, ApJ, 717, 803

Gurzadyan, V. G. & Mazure, A. 2001, New Astronomy, 6, 43

Hanes, D. A. 1977, MNRAS, 180, 309

Harris, W. E. 1981, ApJ, 251, 497

—. 1991, ARAA, 29, 543

—. 1996, ApJ, 112, 1487

Harris, W. E. 2001, in Saas-Fee Advanced Course 28: Star Clusters, ed. L. Labhardt & B. Binggeli, 223

—. 2009, ApJ, 703, 939

Harris, W. E., Harris, G. L. H., & Alessi, M. 2013, ApJ, 772, 82

Harris, W. E. & van den Bergh, S. 1981, AJ, 86, 1627

Hawley, D. L. & Peebles, P. J. E. 1975, AJ, 80, 477

Helou, G. 1984, ApJ, 284, 471

Helou, G. & Salpeter, E. E. 1982, ApJ, 252, 75

Hodge, P. W. 1979, AJ, 84, 744

Hoffman, G. L., Williams, B. M., Lewis, B. M., Helou, G., & Salpeter, E. E. 1989, ApJS, 69, 65

Hoyle, F. 1949, in Problems of Cosmical Aerodynamics, ed. J. M. Burgers and H. C. van de Hulst (Dayton: Central Air Documents Office), 195

Hoyle, F. 1951, in Problems of Cosmical Aerodynamics, 195

Hu, F. X., Yuan, Q. R., Su, H. J., Wu, G. X., & Liu, Y. Z. 1998, ApJ, 495, 179

Ibata, R. A., Gilmore, G., & Irwin, M. J. 1995, MNRAS, 277, 781

Jõeveer, M., Einasto, J., & Tago, E. 1978, MNRAS, 185, 357

Jaaniste, J. & Saar, E. 1978, in IAU Symposium, Vol. 79, Large Scale Structures in the Universe, ed. M. S. Longair & J. Einasto, 448

Jones, B. J. T., van de Weygaert, R., & Aragón-Calvo, M. A. 2010, MNRAS, 408, 897

Jones, K. G. 1991, Science, 254, 592

Kapranidis, S. & Sullivan, III, W. T. 1983, A&A, 118, 33

Kashikawa, N. & Okamura, S. 1992, PASJ, 44, 493

Katz, N. & Gunn, J. E. 1991, ApJ, 377, 365

Klypin, A. & Shandarin, S. F. 1993, ApJ, 413, 48

Kroupa, P. 2005, in ESA Special Publication, Vol. 576, The Three-Dimensional Universe with Gaia, ed. C. Turon, K. S. O'Flaherty, & M. A. C. Perryman, 629

Kroupa, P. & Bouvier, J. 2003, MNRAS, 346, 369

Kroupa, P. & Weidner, C. 2003, ApJ, 598, 1076

Kumai, Y., Hashi, Y., & Fujimoto, M. 1993, ApJ, 416, 576

Lada, C. J. & Lada, E. A. 2003, ARAA, 41, 57

Larsen, S. S. 2002, AJ, 124, 1393

Larsen, S. S. & Richtler, T. 2000, A&A, 354, 836

Larson, R. B. 1975, MNRAS, 173, 671

Lee, J. & Erdogdu, P. 2007, ApJ, 671, 1248

Lee, J. & Pen, U.-L. 2002, ApJL, 567, L111

Lynden-Bell, D. 1967, MNRAS, 136, 101

MacGillivray, H. T. & Dodd, R. J. 1985, A&A, 145, 269

Melotte, P. J. 1915, MmRAS, 60, 175

Mieske, S., Hilker, M., & Misgeld, I. 2012, A&A, 537, A3

Mieske, S., Küpper, A. H. W., & Brockamp, M. 2014, A&A, 565, L6

Miller, B. W., Ferguson, H. C., Lotz, J., Stiavelli, M., & Whitmore, B. C. 1998a, ArXiv Astrophysics e-prints

Miller, B. W. & Lotz, J. M. 2007, ApJ, 670, 1074

Miller, B. W., Lotz, J. M., Ferguson, H. C., Stiavelli, M., & Whitmore, B. C. 1998b, ApJL, 508, L133

Moore, B., Diemand, J., Madau, P., Zemp, M., & Stadel, J. 2006, MNRAS, 368, 563

Navarro, J. F., Abadi, M. G., & Steinmetz, M. 2004, ApJL, 613, L41

Neilsen, Jr., E. H., Tsvetanov, Z. I., & Ford, H. C. 1997, ApJ, 483, 745

Öpik, E. J. 1970, Irish Astronomical Journal, 9, 211

Ostriker, J. P. 1980, Comments on Astrophysics, 8, 177

Ozernoi, L. M. 1978, in IAU Symposium, Vol. 79, Large Scale Structures in the Universe, ed. M. S. Longair & J. Einasto, 427–437

Pahre, M. A., Djorgovski, S. G., & de Carvalho, R. R. 1995, ApJL, 453, L17

Palunas, P., Teplitz, H. I., Francis, P. J., Williger, G. M., & Woodgate, B. E. 2004, ApJ, 602, 545

Peebles, P. J. E. 1969, ApJ, 155, 393

—. 2003, ArXiv Astrophysics e-prints

Peng, E. W., Jordán, A., Côté, P., Takamiya, M., West, M. J., Blakeslee, J. P., Chen, C.-W., Ferrarese, L., Mei, S., Tonry, J. L., & West, A. A. 2008, ApJ, 681, 197

Pimbblet, K. A. 2005, MNRAS, 358, 256

Randriamanakoto, Z., Escala, A., Väisänen, P., Kankare, E., Kotilainen, J., Mattila, S., & Ryder, S. 2013, ApJL, 775, L38

Recchi, S., Calura, F., & Kroupa, P. 2009, A&A, 499, 711

Reinhardt, M. & Roberts, M. S. 1972, Astrophys. Lett., 12, 201

Rhode, K. L., Zepf, S. E., Kundu, A., & Larner, A. N. 2007, AJ, 134, 1403

Rood, H. J. & Sastry, G. N. 1971, PASP, 83, 313

Schulz, C., Pflamm-Altenburg, J., & Kroupa, P. 2015, A&A, 2015.

Schweizer, F. 1987, in Nearly Normal Galaxies. From the Planck Time to the Present, ed. S. M. Faber, 18–25

Schweizer, F. 1996, AJ, 111, 109

Schweizer, F., Miller, B. W., Whitmore, B. C., & Fall, S. M. 1996, AJ, 112, 1839

Sciama, D. W. 1955, MNRAS, 115, 3

Searle, L. & Zinn, R. 1978, ApJ, 225, 357

Seth, A., Olsen, K., Miller, B., Lotz, J., & Telford, R. 2004, AJ, 127, 798

Slosar, A. & White, M. 2009, JCAP, 6, 9

Smith, R. J. & Lucey, J. R. 2013, MNRAS, 434, 1964

Somerville, R. S., Primack, J. R., & Faber, S. M. 2001, MNRAS, 320, 504

Strader, J., Brodie, J. P., Spitler, L., & Beasley, M. A. 2006, AJ, 132, 2333

Sylos Labini, F., Vasilyev, N. L., & Baryshev, Y. V. 2009, A&A, 508, 17

Tempel, E., Kipper, R., Saar, E., Bussov, M., Hektor, A., & Pelt, J. 2014, A&A, 572, A8

Tempel, E., Stoica, R. S., & Saar, E. 2013, MNRAS, 428, 1827

Thomas, D., Maraston, C., Bender, R., & Mendes de Oliveira, C. 2005, ApJ, 621, 673

Thompson, L. A. 1976, ApJ, 209, 22

Thuan, T. X. & Gott, III, J. R. 1977, ApJ, 216, 194

Tiret, O., Salucci, P., Bernardi, M., Maraston, C., & Pforr, J. 2011, MNRAS, 411, 1435

Toomre, A. 1977, in Evolution of Galaxies and Stellar Populations, ed. B. M. Tinsley & R. B. G. Larson, D. Campbell, 401

Tremaine, S. 1995, AJ, 110, 628

Trujillo, I., Carretero, C., & Patiri, S. G. 2006, ApJL, 640, L111

van de Weygaert, R., Aragon-Calvo, M. A., Jones, B. J. T., & Platen, E. 2009, ArXiv e-prints

van den Bergh, S. 1995, Nature, 374, 215

van den Bergh, S. 1995, Astron.J., 110, 2700

van Dokkum, P. G. & Stanford, S. A. 2003, The Astrophysical Journal, 585, 78

Varela, J., Betancort-Rijo, J., Trujillo, I., & Ricciardelli, E. 2012, ApJ, 744, 82

Vauglin, I., Prugniel, P., & Paturel, G. 2006, in SF2A-2006: Semaine de l'Astrophysique Francaise, ed. D. Barret, F. Casoli, G. Lagache, A. Lecavelier, & L. Pagani, 367

von Weizsäcker, C. F. 1951, ApJ, 114, 165

Wang, J. 2002, Progress in Astronomy, 20, 74

Weidner, C. & Kroupa, P. 2004, MNRAS, 348, 187

Weidner, C., Kroupa, P., & Larsen, S. S. 2004, MNRAS, 350, 1503

Weidner, C., Kroupa, P., Pflamm-Altenburg, J., & Vazdekis, A. 2013, MNRAS, 436, 3309

White, S. D. M. 1984, ApJ, 286, 38

Whitmore, B. C., Chandar, R., Schweizer, F., Rothberg, B., Leitherer, C., Rieke, M., Rieke, G., Blair, W. P., Mengel, S., & Alonso-Herrero, A. 2010, AJ, 140, 75

Whitmore, B. C. & Schweizer, F. 1995, AJ, 109, 960

Wu, X. & Kroupa, P. 2013, MNRAS, 435, 1536

Zel'dovich, Y. B. 1970, A&A, 5, 84

Zepf, S. E. & Ashman, K. M. 1993, MNRAS, 264, 611